Investigating reward systems in the human midbrain with fMRI

Eve H. Limbrick-Oldfield

2012

Neurophysiology and Cognitive Neuroimaging Groups,
MRC Clinical Sciences Centre,
Imperial College, London

This thesis is submitted for the degree of
Doctor of Philosophy

Acknowledgements

Many thanks to both my supervisors; they have given me their time and advice, for which I am extremely grateful. They have allowed me the freedom to make my own decisions, and learn from my own mistakes. I would also like to thank all the members of the Neurophysiology and Cognitive Neuroimaging groups, past and present, who have all provided many hours of useful discussion and good advice. I owe a great deal to Ed for his unconditional support and help throughout the past three years. Finally, I would like to thank all the volunteers who participated in the studies presented here, without them; there would be no data!

Declaration of publications

The work presented in chapters 3 and 4 of this thesis has been published in Neuroimage (Limbrick-Oldfield et al., 2012). The work of chapter 5 is currently being prepared for submission.

Limbrick-Oldfield, E.H., Brooks, J.C., Wise, R.J., Padormo, F., Hajnal, J.V., Beckmann, C.F., and Ungless, M.A. (2012). Identification and characterisation of midbrain nuclei using optimised functional magnetic resonance imaging. NeuroImage 59, 1230-1238.

Declaration of originality

I declare that the work contained within this thesis is my own, and the work of others is appropriately referenced.

Abbreviations

ANOVA:	Analysis of variance
B0:	Static magnetic field
BET:	Brain extraction tool
BOLD:	Blood oxygen level dependent
CBF:	Cerebral blood flow
CP:	Cerebral peduncle
CSF:	Cerebrospinal fluid
CLi:	Caudal linear nucleus
COPE:	Contrast of parameter estimates
dHb:	Deoxyhaemoglobin
ECG:	Electrocardiogram
EPI:	Echo-planar imaging
EFP	Extracellular field potential
EPSP	Excitatory post-synaptic potential
EV:	Explanatory variable
FEAT:	FSL Expert Analysis Tool
FLAME:	FMRIB's local analysis of mixed effects
fMRI:	Functional magnetic resonance imaging
FOV:	Field-of-view
FSL:	FMRIB software library
FNIRT	FMRIBs non-linear registration tool
FWHM:	Full width half maximum
GABA:	Gamma-aminobutyric acid
GLM:	General linear model
HRF:	Haemodynamic response function
IFN:	Interfascicular nucleus
IPSP:	Inhibitory post-synatpic potential
LFP:	Local field potential
LHb:	Lateral habenula
McFLIRT:	Motion Correction FMRIB's Linear Registration Tool

MNI:	Montreal Neurological Institute
MPRAGE:	Magnetisation prepared rapid gradient echo
MR:	Magnetic resonance
MRI:	Magnetic resonance imaging
NM:	Neuromelanin
PAG:	Periaqueductal grey
PBP:	Parabrachial pigmented nucleus
PD:	Proton density
PE:	Prediction error
PIF:	Parainterfascicular nucleus
PN:	Paranigral nucleus
PNM:	Physiological noise model
RETROICOR:	Retrospective image correction
RF:	Radiofrequency
RN:	Red nucleus
ROI:	Region-of-interest
RLi	Rostral linear nucleus
RRF:	Retrorubral field
SENSE:	Sensitivity encoding
SCP:	Superior cerebellar peduncle
SN:	Substantia nigra
SNc:	Substantia nigra pars compacta
SNr:	Substantia nigra pars reticulata
SNR:	Signal to noise ratio
T1:	Longitudinal relaxation
T2:	Transverse relaxation
TE:	Echo time
TH:	Tyrosine hydroxylase
TR:	Repetition time
TSE:	Turbo spin-echo
tVTA:	Tail of the ventral tegmental area
VTA:	Ventral tegmental area

Abstract

Localising activity in the human midbrain with conventional functional MRI (fMRI) is challenging because the midbrain nuclei are small and located in an area that is prone to physiological artefacts. In the first section of this thesis I present a replicable and automated method to improve the detection and localisation of midbrain fMRI signals. I designed a visual fMRI task that was predicted would activate the superior colliculi bilaterally. A novel anatomical registration pathway was used to optimise the localisation of the small midbrain nuclei in stereotactic space. This pathway was compared to conventional registration pathways, and was shown to significantly improve midbrain registration. To reduce the physiological artefacts in the functional data, I estimated and removed structured noise using a modified version of a previously described physiological noise model (PNM). Whereas a conventional analysis revealed only unilateral colliculi activity, the PNM analysis revealed the predicted bilateral activity.

I then used these methods to investigate the role of the midbrain dopaminergic system in reward. Midbrain dopamine neurons play central roles in positive reward prediction errors (PEs). Non-human studies now indicate that dopamine neurons also code for aversive, punishing events, and may code negative PEs. However, our understanding of how such events are coded in the human dopaminergic midbrain is limited, and has been hindered by the technical challenge of using fMRI in this region. Here I show that during a financial reward and punishment task the ventral tegmental area (VTA) codes for both positive and negative PEs. The fMRI data from the midbrain contained a significant amount of physiological noise, but once I applied the PNM responses were also observed in the substantia nigra pars compacta (SNc), with negative PE signals extending more laterally. These findings indicate that both the human VTA and SNc code for both positive and negative PEs.

List of figures

List of tables

Table of contents

1. Introduction

All mammals learn to interact with their environment to optimise their chances of survival. Early in evolution, brainstem systems developed to encourage food-seeking and reproductive behaviour (reward) and avoid harm (punishment). It has become apparent from a large body of research that the modulatory neurotransmitter dopamine is central to these systems.

Current theories of the role of the dopaminergic midbrain in reward have been developed based largely on the findings of non-human experiments. Neurophysiological recordings of activity from single neurons have proved to be an invaluable tool in demonstrating the role of specific neuronal populations in behaviour. However, in order to apply such animal models to the human, it is important to investigate if the predictions of these models can explain human neuronal activity. In the case of the dopaminergic midbrain this has proved challenging. Invasive recordings are not possible for obvious ethical reasons. Functional magnetic resonance imaging (fMRI) is clearly feasible as an indirect measure of neural activity and has been successfully utilised to test animal models in the human (Logothetis, 2008). However there are technical barriers to imaging the human midbrain with fMRI (Düzel et al., 2009). As a result of this, little is known about the role of the human midbrain in reward.

This introduction is organised into three sections. In the first section I will outline the current theories of the role of the dopaminergic midbrain in reward and punishment. In the second section I will describe the anatomy of the midbrain in the human, and how this compares with the non-human anatomy. This is important for understanding how non-human models may translate to the human, and in understanding the likely localisation of these functions in the human brain. In the final section of the introduction I will cover the technical challenges to be overcome when imaging the human dopaminergic midbrain with fMRI. Midbrain optimised fMRI must attempt to reduce the influence of these challenges to successfully and accurately image this region of the brain.

1.1. The role of the midbrain in reward

1.1.1. What is reward, and how does it influence our behaviour?

A stimulus can be defined as rewarding if an animal will work to receive it, and for humans rewarding stimuli include food, sex, and money. The experience of reward is a complex construct that has multiple components that rely on several different brain areas, including the dopaminergic midbrain (Berridge and Robinson, 2003; Schultz et al., 1997), the ventral striatum (O'Doherty et al., 2004), the orbitofrontal cortex (Plassmann et al., 2010; van Duuren et al., 2009), and the anterior cingulate cortex (Amiez et al., 2005; Amiez et al., 2006; Holroyd and Coles, 2008). Reward itself is not an observable behaviour, but can be separated into three components that can be measured. These are liking, wanting and reinforcement learning (Berridge and Kringelbach, 2008). Liking involves an affective response to a stimulus at the time of receipt. Wanting is the subjective desire of a stimulus, and may occur before receipt of a stimulus. Reinforcement learning is the process by which behaviour is optimised to maximise the occurrence of rewarding events and the avoidance of punishment (Sutton and Barto, 1987).

There are two main types of reinforcement learning. Pavlovian conditioning is defined as learning that occurs about the relationship between two stimuli that cannot be controlled by behaviour. The original example is of course the dog that learns to associate the ring of a bell with the delivery of food. The extent to which the dog salivates can be used as a behavioural a measure of learning, and learning in this instance is expressed through activity within the autonomic nervous system. Instrumental conditioning, on the other hand, involves the selection of willed (voluntary) actions that lead to a desired goal. This goal can be the receipt of reward or the avoidance of punishment. The association learned here is between the action and the outcome, at least initially, as later there may be a stimulus-response association (habit formation) when the response to a stimulus occurs without conscious processing. Therefore, learning can be measured by observing actions.

By observing such behaviour, models of how optimal learning occurs have been developed, to understand the mechanisms that ensure behaviour maximises rewards and minimises punishments. Temporal difference learning (Sutton and Barto, 1987) is a computational model of reinforcement learning whereby predictions are made about future events based on the experience of past events. Errors in prediction are used to update future predictions, so that these predictions will match the actual experience as closely as possible. By holding accurate predictions about future events, behaviour can be modified to optimise the outcome.

Such theories of reinforcement learning were developed well in advance of the discovery of the neural mechanisms that are involved in these processes. The main focus of the investigation of the neural substrates of reward has been on the neurotransmitter dopamine due to its neuromodulatory role in learning and motivation (Berridge and Kringelbach, 2008; Dayan and Balleine, 2002; Haber and Knutson, 2010; Redgrave et al., 2008; Schultz, 2000). Interest in dopamine has also been maintained by its proposed role in disease. For example, drugs of abuse cause an increase in dopamine release in the striatum (Koob and Volkow, 2009; Lüscher and Ungless, 2006) and schizophrenia has been associated with a maladaptive dopamine system (Moran et al., 2008; Murray et al., 2008).

The dopaminergic midbrain is the major source of dopamine in the brain (Haber and Fudge, 1997; McRitchie et al., 1998; Schultz, 2000; Schultz, 2002). It consists of the substantia nigra pars compacta (SNc) and the ventral tegmental area (VTA). This small population of neurons projects extensively to multiple regions in the brain: the striatum (Fallon, 1981; Prensa and Parent, 2001), limbic and paralimbic regions (Swanson, 1982), and extensive neocortial regions, particularly in the frontal lobes (Fallon, 1981). The extensive projection targets of these midbrain structures allow dopaminergic neurons to modulate the response of multiple regions that control the many aspects of behaviour.

1.1.2. Non-human experiments investigating the role of dopamine in reward

A neural correlate for the error term of the temporal difference model was proposed by Schultz, Dayan and Montague (1997) in the dopaminergic midbrain. Single cell recordings in the primate SNc identified neurons that showed an increased firing rate in response to an unexpected juice reward (a positive prediction error, PE) (Bayer and Glimcher, 2005; Fiorillo et al., 2008; Fiorillo et al., 2003; Schultz et al., 1997; Tobler et al., 2005). Once the juice reward had been repeatedly paired with a light stimulus, the monkeys learnt that the light predicted the future occurrence of the juice reward. Subsequently, the neurons showed no change in firing rate to a reward fully predicted by the light, and it was the onset of the light that elicited the neural response. However, if there was an unexpected omission of the expected juice reward (a negative PE), the dopaminergic neurons decreased their firing rate below background. It appears, therefore, that these neurons respond to the difference between the observed and expected reward value, coding for errors in prediction, rather than coding the absolute reward level.

This theory has been extended to characterise factors that are involved in the calculation of a PE. Tobler and colleagues (2005) found that the magnitude of the expected reward influenced the PE response, and Fiorillo and colleagues (2003) demonstrated that the probability of an expected reward occurring also influenced the PE response; the more unlikely a reward, the greater the increase in firing rate. Tobler and colleagues (2005) also demonstrated that if an observed reward is of an absolute positive value, but is less than expected, this is reflected by a reduction in firing rate – a less-than-expected reward is coded by a negative PE.

Although the initial PE model was founded on responses to rewarding events, it has since been extended to model the response to punishing, aversive events. There is some confusion in the literature when defining PEs due to the different terms that can be used to describe the same phenomenon. In this thesis I shall use a positive PE to refer to a response to an event that is better than expected, whilst a negative PE will refer to a response to an event that is

worse than expected. These terms do not indicate the valence of a stimulus (i.e., whether it is rewarding or punishing). Thus the following terms can explain all possible types of PE:

1. Positive reward PE: elicited by an event that is more rewarding than expected;
2. Positive punishment PE: elicited by an event that is less punishing than expected;
3. Negative reward PE: elicited by an event that is less rewarding then expected;
4. Negative punishment PE: elicited by an event that is more punishing than expected;

The temporal difference theory would predict that neural activity of PE neurons would reflect only the positive/negative dichotomy; the response should not be modulated by whether or not the stimulus is rewarding or punishing. However experiments don't usually interrogate all four conditions, so it is useful to have access to all four terms when describing existing results. Although the PE hypothesis offers a good explanation of how an increase in firing rate can efficiently code a positive PE, it is not clear if the decrease in firing rate in response to a negative PE is providing a neural response that is sufficiently sensitive to encode worse than expected events - the basal firing rate of midbrain dopamine neurons is only around 4Hz (Schultz et al., 1993). Consequently, a decrease in such a slow basal firing rate can only signal a limited amount of information, and is a relatively slow signal in comparison to the increase in firing rate that signals a positive PE (Daw et al., 2002). Psychological theories of motivation suggest that affective states are modulated by two opponent systems (Solomon and Corbit, 1974), and thus Daw and colleagues (2002) have suggested such an opponent system to dopamine codes for worse than expected events. They postulate that midbrain serotonin neurons in the dorsal raphe fulfil this role. However, electrophysiological evidence has not yet been found to support this hypothesis (Bromberg-Martin et al., 2010a; Ranade and Mainen, 2009).

An alternative concept that has been investigated is salience. Rather than coding for the PE, dopamine neurons are instead coding for an aspect of salience. According to Redgrave and colleagues (1999) the short-latency of the dopamine signal suggests that it cannot be encoding PE, which requires an assessment of expected value, but instead signals any salient stimuli that require attention. The PE hypothesis predicts that dopamine neurons will differentially respond to better than expected (a positive PE) or worse than expected (a negative PE) events. Redgrave and colleagues, on the other hand, suggest that neurons will respond similarly to oppositely signed stimuli as long as they are equally salient. Thus the decrease in firing rate of dopamine neurons is not required to signal negative punishment PEs, as all salient stimuli will lead to an increase in firing rate.

It has also been suggested that dopamine neurons are not coding PE, but incentive salience (Berridge and Robinson, 1998). According to this theory the firing rate of the dopamine neurons is modulated by the internal state of the animal. For example, when hungry, a food cue may elicit an increase in firing rate. However during a period of satiety, the same cue may no longer elicit a dopamine response. Thus the firing rate of dopamine neurons is modulated by the current motivational state of the animal. However this model does not describe if or how worse than expected events may be coded for in the dopaminergic midbrain.

There are two emerging threads of research that are beginning to provide a fuller picture of how negative PEs may be encoded by the brain, and may help determine whether there is an opponent process, or that neurons are actually coding for incentive salience. The first is the investigation of the possibility that there are different populations of dopaminergic neurons within the midbrain that respond in a different manner to the PE neurons observed by Shultz, Dayan, and Montague (1997). The second is the role of regions outside the dopaminergic midbrain that project to the VTA or SNc and inhibit the firing rate of the midbrain dopaminergic neurons that do reflect a traditional PE signal. The majority of experiments investigating negative PEs have used

punishing events, or cues predicting punishing events, rather than eliciting a negative reward PE.

1.1.2.1. Subpopulations of midbrain dopamine neurons

Early investigations into the dopaminergic midbrain did suggest that there was a subpopulation of neurons that increased their firing rate in response to punishing stimuli (Guarraci and Kapp, 1999; Mantz et al., 1989; Mirenowicz and Schultz, 1996). However, the neurons in these papers were identified using electrophysiological characteristics alone. Ungless et al. (2004) found that, in the anaesthetised rat, dopaminergic neurons were uniformly inhibited by punishing stimuli. A population of cells with electrophysiological profiles similar to dopamine neurons did increase their firing rate in response to punishing events, but labelling for tyrosine hydroxlase (TH), a dopamine precursor, revealed that they were non-dopaminergic.

The recent literature has once again opened up the possibility of a dopaminergic response to punishing stimulation, using either a strict electrophysiological definition to locate dopaminergic neurons, or labelling the cells for TH. There is a growing body of evidence that suggests dopamine neurons are not uniformly inhibited by punishing stimuli. Brischoux et al. (2009) identified and labelled dopaminergic neurons in the ventral VTA of the anaesthetised rat that were excited by foot shocks, clearly a punishing event. In support of this result, Valenti, Lodge and Grace (2011) exposed anaesthetised rats to repeated foot shocks. They found a large proportion of neurons in the lateral VTA were excited by this stimulus. Wang and Tsien (2011) recorded from putative dopamine neurons in freely moving mice as they were exposed to either a tone that had been paired with a food reward, or a punishing event (a free fall or shake). They identified three types of putative dopamine neurons defined by their response to the punishing events. Type-1 neurons were excited by the reward predicting tone, but were initially suppressed by the punishing event, but this suppression was quickly followed by a rebound excitation. Type-2 neurons were similar to traditional PE neurons; they were excited by the reward predicting tone, and suppressed by the punishing event with no rebound excitation. Type-3 neurons were excited

by both the reward predicting tone, and the punishing events. The proportions of these types from the whole population of putative dopaminergic neurons were 59%, 13% and 25%, respectively. Brischoux and colleagues (2009) also identified dopaminergic neurons that, although initially suppressed by punishing events, showed a rebound excitation at the time of stimulus offset, similar to the Type-1 neurons of Wang and Tsien (2011).

Other experiments have measured the dopaminergic response to cues predicting punishing events. Joshua et al. (2008) found that putative dopaminergic neurons in the SNc of the primate responded to cues that predicted punishing events, although the response of these neurons to punishing events was not as great as the response to rewarding events. Matsumoto and Hikosaka (2009) found two groups of putative dopaminergic neurons within SNc of the primate. Neurons within the dorsolateral SNc were excited by cues predicting both rewarding and punishing events, whilst neurons in the ventromedial SNc and VTA were inhibited by cues predicting punishing events and excited by cues predicting rewarding events. Mileykovsky and Morales (2011) trained rats to associate a tone with an electric shock and measured the neural response to the tone in VTA. Three types of VTA dopamine neurons were found; the first type of neurons was inhibited by the shock predicting cue, a second type were inhibited in a biphasic manner to the stimulus onset and offset, and a final type were first excited by the cue, then inhibited. In the majority of cells the inhibitory phase was followed by a transient increase in firing rate. Bromberg-Martin, Matsumoto and Hikosaka (2010b) recorded from the dopaminergic midbrain neurons of the awake primate. They used cues that predicted punishing airpuffs. They found two types of responses to the cues. The first type was excited by reward predicting cues, and inhibited by airpuff predicting cues. The second type was excited by both reward and punishment predicting cues.

This is an area of research where more work needs to be done to build a comprehensive model of the neural response to negative punishment PEs. A complex picture is emerging, with multiple sub-populations of dopamine neurons that differentially respond to punishing, or punishment predicting

stimuli. To establish whether or not negative punishment PEs are coded in the same way as negative reward PEs, experiments must be carried out that test the response of neurons to both types of worse than expected events. Only then will it be known if both types of stimuli can be classed as a single concept of negative PE.

What this literature demonstrates is that the dopaminergic midbrain is a heterogeneous population, and there are likely to be functional differences between sub-populations of cells within the VTA and SNc. The observed response to punishing events or punishment PEs includes inhibition, excitation, inhibition followed by rebound excitation, and biphasic excitation at stimulus onset and offset. The concept of a unitary population of cells that all express an increase in firing rate to a positive PE and a decrease in firing rate to a negative PE no longer seems a viable theory.

1.1.2.2. Other brain regions act as opponent systems

The second branch of research that has investigated the neural response to negative PE concerns the inputs of the dopaminergic midbrain, and the source of the inhibition that is seen in many PE dopamine neurons. The particular input nuclei of interest are the lateral habenula (LHb) and the tail of the VTA (tVTA), which is also known as the rostromedial mesopontine tegmental nucleus.

The LHb is a small nucleus within the epithalamus. Early evidence suggested it had a role in the inhibitory response of the dopaminergic midbrain to negative PE as electrical simulation of the LHb led to inhibition of the dopaminergic neurons within the VTA and SNc (Christoph et al., 1986). More recent evidence has supported this hypothesis. Matsumoto and Hikosaka (2007) recorded the activity of LHb and midbrain dopamine neurons in the awake primate during a reward task. A cue predicted a juice reward or no reward. LHb neurons were excited by the no reward cue, and inhibited by the reward cue. The dopaminergic neurons responded in the opposite manner. Additionally the excitatory response of the LHb occurred before the dopaminergic inhibition.

Although the LHb does provide inputs to the dopaminergic midbrain, these inputs are relatively sparse (Omelchenko et al., 2009). For the LHb to successfully inhibit midbrain dopaminergic neurons, it must do so through an intermediary. A recently defined area of the midbrain, the tVTA, receives inputs from the LHb and projects to the dopaminergic cells of the midbrain (Balcita-Pedicino et al., 2011; Brinschwitz et al., 2010). Recordings from the LHb, dopaminergic midbrain, and tVTA have shown that the tVTA responds in a similar manner to the LHb, showing an excitatory response to cues predicting no-reward and an inhibitory response to cues predicting reward. Thus it seems likely that the excitatory response in the LHb inhibits the dopaminergic neurons of the midbrain via the tVTA.

The dopaminergic midbrain is just one part of a complex network that has many excitatory and inhibitory components. It is a very active area of research with new findings constantly modifying and updating the existing animal models. Thus it is appropriate to investigate reward in the human, not just to test if the models apply to human behaviour, but also to see if further advances can be made in our understanding of the dopamine system. Investigating reward networks at a different scale with a different tool should provide new results that will enrich our understanding of the dopamine system.

1.1.3. The role of the dopaminergic midbrain in human reward and punishment

FMRI has been used as an indirect measure of neuronal activity to investigate the reward systems in the human brain, but several methodological challenges have hindered fMRI of the midbrain itself. The midbrain nuclei are very small, and thus a high spatial resolution is required to localise activity to individual nuclei. As spatial resolution increases, the signal-to-noise ratio (SNR) of the data decreases and it becomes more difficult to detect signal from the background noise. Also the proximity of the midbrain to large blood vessels leaves the area prone to magnetic field inhomogeneities, and cardiac and respiratory artefacts can interfere with the measurement of a genuine

signal. As a consequence, researchers of the human brain have usually investigated the projection targets of the midbrain dopaminergic neurons. It has been shown that there is a signal increase in the ventral striatum to a positive reward PE, (Abler et al., 2006; McClure et al., 2003; O'Doherty et al., 2003; Rutledge et al., 2010; Seymour et al., 2007). Increases in the ventral striatal signal have also been observed in response to a negative PE, both to a negative punishment PE (Seymour et al., 2007; Seymour et al., 2004) and a negative reward PE (Pagnoni et al., 2002). However a decrease in response to a negative reward PE has also been observed (McClure et al., 2003; O'Doherty et al., 2003).

It has been assumed that the blood oxygen dependent level (BOLD) signal, the indirect measure of neural activity utilised by fMRI, observed in the striatum reflects an increase in the firing rate of the dopaminergic inputs to the region. However the ventral striatum receives convergent inputs from multiple brain regions so, although it is likely that dopaminergic inputs can change the fMRI signal, these are not the only inputs. Therefore, the conclusions that can be drawn from studies of the ventral striatum are limited with regard to midbrain dopamine function.

D’Ardenne et al. (2008) made the first attempt to overcome the technical difficulties in imaging the dopaminergic midbrain, and investigate midbrain sources of PE signals in the human using fMRI. Scanning parameters were optimised to achieve a relatively high spatial resolution, and cardiac gating was used to suppress cardiac artefacts. They aimed to elicit positive reward PEs and negative reward PEs with a traditional Pavlovian conditioning experiment using juice rewards. They found a region of the VTA that correlated with a positive reward PE signal, but did not show a negative reward PE signal. They also aimed to elicit PEs with a number higher/lower guessing task. Correct guesses were rewarded with financial gains (eliciting a positive reward PE), and incorrect guesses were punished with financial losses (eliciting a negative punishment PE). An area within the VTA showed increased BOLD signal with increasing magnitude of positive reward PE.

However, no midbrain nuclei were found to correlate with negative punishment PE.

There have been other recent investigations into the human dopaminergic midbrain using fMRI, but with standard voxel sizes. Therefore localisation to a specific midbrain nucleus cannot be as reliable as it would with smaller voxels. Technical issues aside, these papers have reported that the human dopaminergic midbrain represents task load in the absence of reward (Boehler et al., 2011), that action representations dominate over valence representations (Guitart-Masip et al., 2011), and that novelty seeking correlates with midbrain dopaminergic activation (Krebs et al., 2011).

Although recording directly from human midbrain neurons can only be performed rarely, Zaghloul and colleagues (2009) recorded directly from the human SNc during surgery for deep brain stimulation. Participants were exposed to unexpected financial losses and gains. They found that there was a higher firing rate for unexpected gains than unexpected losses. This difference was driven by a higher firing rate for unexpected gains against the baseline-firing rate.

Although there is a growing fMRI literature concerning the dopaminergic midbrain, there is a scarcity of experiments that use high-resolution midbrain optimised fMRI. Due to the lack of experiments investigating negative PEs it is not known how well the recent literature concerning negative PEs translates to the human.

1.2. Anatomy of the midbrain

Most research on midbrain function has been carried out on experimental animals, so to apply these theories to the human depends on the unproven assumption that this brain region is anatomically and functionally similar across species. Therefore, the main reason to investigate the human midbrain is to investigate comparative functional anatomy across species.

There are several ways of describing locations within the brain, but the convention used throughout this document is displayed in Figure 1. The midbrain, relative to the body, is oriented differently across species. This is due to evolutionary changes as primates evolved to walk on two legs with an upright spine. Thus it is important to use the same convention across species, so that direct comparisons can be made. Throughout this document, the caudal midbrain, for example, will refer to the same location across species.

1.2.1. Comparative anatomy

Catecholamine containing neurons in the brain stem were first described by Dahlstroem and Fuxe (1964) in the rat brain, and separate nuclei were identified based on cell location and morphology. Three dopamine-containing nuclei were identified in the midbrain. The A8 region, which corresponds to the retrorubral field (RRF), lies dorsal to the SN. The A9 region co-localises with the SNc, dorsal to the cerebral peduncles. The final region, A10, lies medial to the SN and has been termed the VTA. The VTA consists of the paranigral nucleus (PN), the parabrachial pigmented nucleus (PBP), the rostral linear nucleus (Rli), caudal linear nucleus (CLi), the interfascicular nucleus (IFN) and the parainterfascicular nucleus (PIF).

As these regions were defined in the rat brain, it is important to investigate the cytoarchitecture and connectivity of these regions across species to highlight any anatomical variability that may suggest functional differences of these regions across species. As most animal experiments have been carried out on rodents and non-human primates, these are the species of most interest.

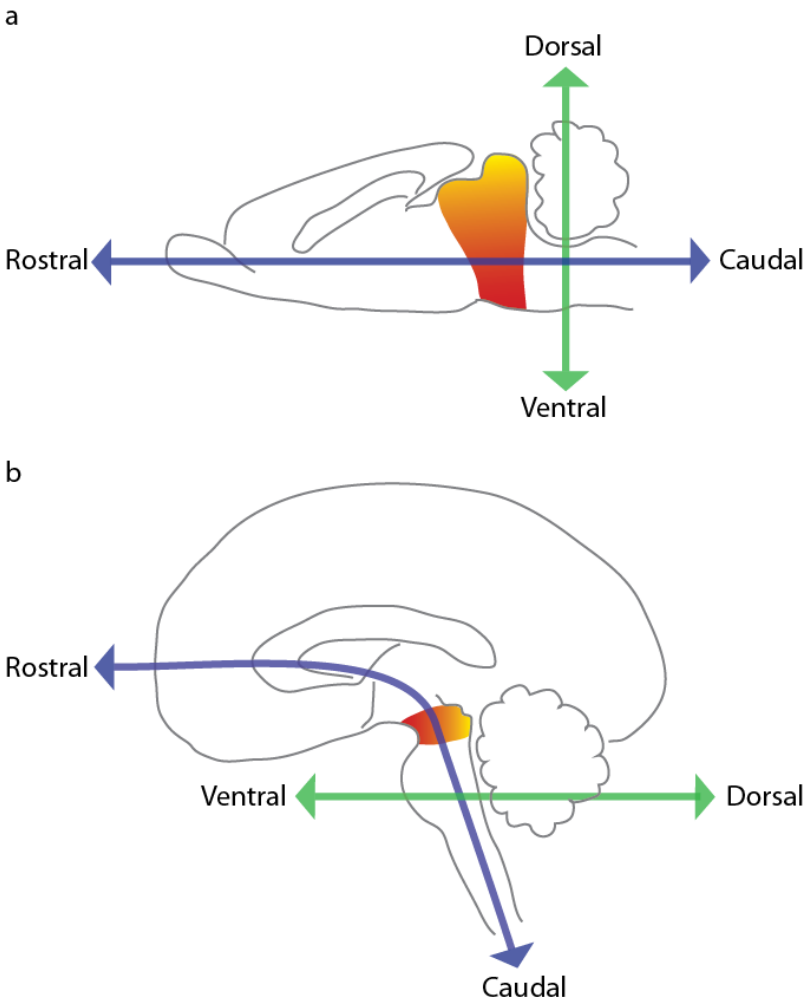

Figure 1: *Anatomical terms of location for the human and rodent. Cartoon representation of the (a) rodent brain (b) human brain. The red-yellow shaded area represents the midbrain. Red = ventral midbrain, yellow= dorsal midbrain. Notice the curvature of the rostral-caudal dimension in the human that is straight in the rodent. Not to scale.*

1.2.1.1. Morphology and cell counting

Although initially defined in the rat, the general morphology of the dopaminergic midbrain is similar in non-human primates (Halliday and Törk, 1986; McRitchie et al., 1996) and humans (McRitchie et al., 1996). However there are species differences.

The most striking difference across species is size of the regions. Figure 2 shows the relative size of the midbrain of the rat, the macaque, and human. The volume of the VTA in these species is 1.2mm^3, 6.5mm^3 and 183mm^3, respectively.

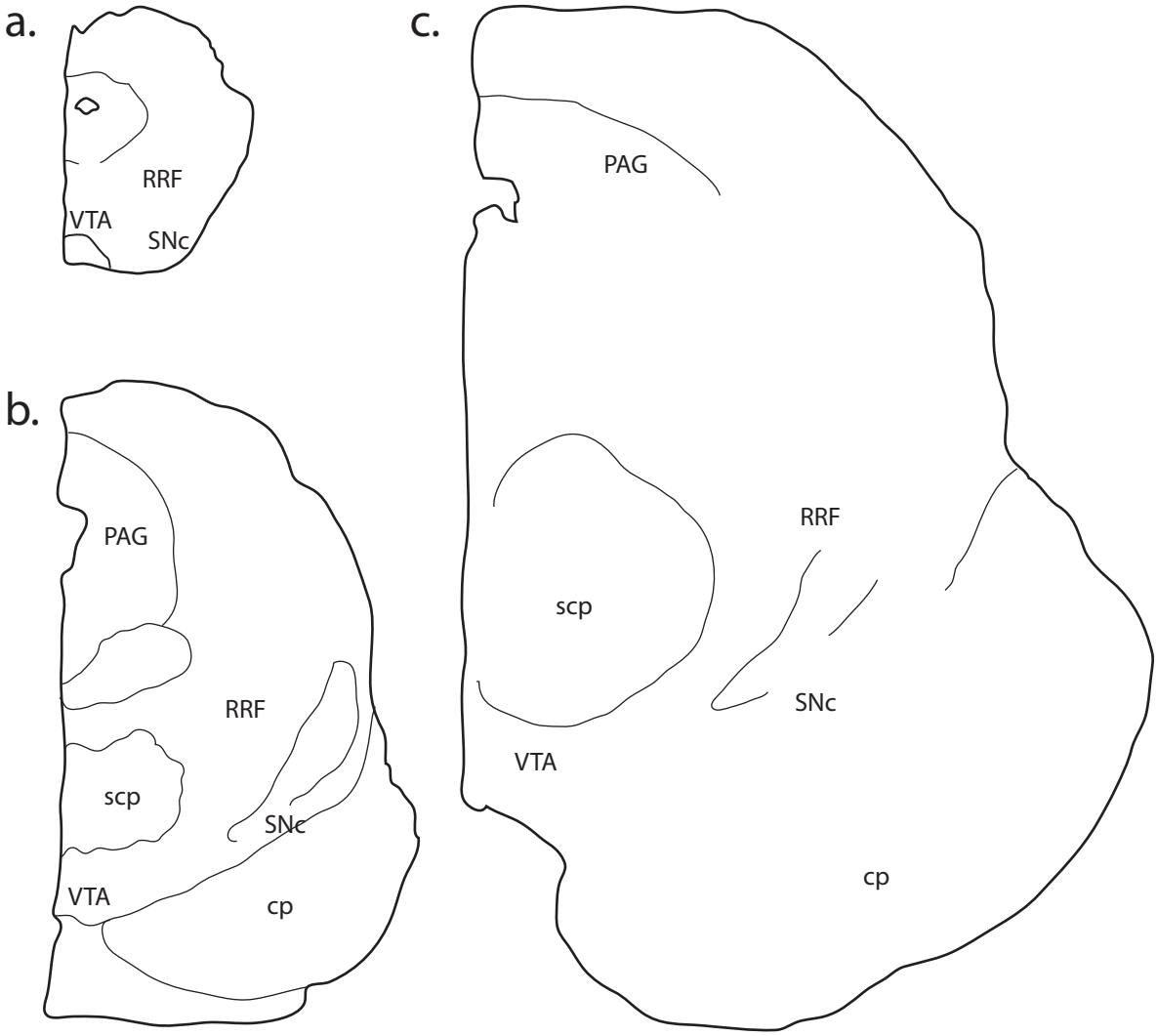

Figure 2: *The relative size of the midbrain of the a) rat b) macaca fuscata c) human. PAG = periaqueductal gray, cp = cerebral peduncle, scp = superior cerebeller peduncle. Adapted from Kitahama and colleagues (1994).*

However, size differences are not very informative when it comes to functional interpretations, as cell densities may differ across species. A more informative measurement than total volume is cell number. Table 1 shows the cell counts from several experiments. Early studies used computer algorithms to automatically count either total cells or dopaminergic cells, whilst Nair-Roberts and colleagues (2008) used an unbiased estimation technique and counted dopamine, gamma-aminobutyric acid (GABA) and glutamate neurons.

	Rat	Non-human primate	Human
(Swanson, 1982)	Counted: DA (TH+) neurons Results: VTA = 17,892		
(German et al., 1983)	*Counted:* DA (TH+) neurons *Results:* VTA/SNc = 40,000		*Counted:* DA (NM+) neurons *Results:* VTA/SNc = 450,000
(Poirier et al., 1983)	*Counted:* all neurons *Results:* SNc = 9,925	*Counted:* all neurons *Results:* SNc = 62,624	
(Halliday and Törk, 1986)	*Counted:* all neurons *Results:* SNc = 12,000 VTA = 27,000	*Counted:* all neurons *Results:* SNc = 72,000 VTA = 47,000	*Counted:* all neurons *Results:* SNc = 436,000 VTA = 690,000
(Hirsch et al., 1988)			*Counted:* DA (TH+) neurons *Results:* SNc = 213,186 VTA = 32,314
(German and Manaye, 1993)	*Counted:* DA (TH+) neurons *Results:* SNc = 19214 VTA= 20,418		
(François et al., 1999)		*Counted:* DA (TH+) neurons *Results:* SNc = 70,490 VTA = 12,800	
(Nair-Roberts et al., 2008)	*Counted:* DA (TH+) neurons *Results:* SNc = 15,772 VTA = 40,174		

Table 1: *The results of midbrain cell counting studies of the rat, non-human primate and human. DA=dopamine, TH=Tyrosine hydroxylase, NM=Neuromelanin, VTA= ventral tegmental area, SNc= substantia nigra pars compacta.*

Estimates vary but some trends across studies can be seen. The total number of neurons and estimation of dopamine cells increases from rat, to the non-human primate to the human. In the rat the number of DA neurons in the VTA is greater than in the SNc, although this estimate varies considerably, from a difference of about 1600 neurons (German and Manaye, 1993) to 35,000 neurons (Nair-Roberts et al., 2008).

In the non-human primate this ratio is reversed, with the number of dopamine neurons in the SNc outnumbering those of the VTA (François et al., 1999). Human cell counting studies are limited, but an early study found almost seven times as many dopamine neurons in the SNc compared to the VTA. Caution should be taken when interpreting the results in non-human primates and humans, as these dramatic differences to the non-human animal brain could be to do with the definition of the boundaries of the individual nuclei. It has been shown that the medial border of the SNc is not easily distinguished from the VTA in the human (Afshar et al., 1978). To further investigate the species differences in the anatomy of the VTA and SNc, particularly with respect to the increased relative cell number of the SNc in the human, it is important to look at the distribution of dopamine neurons within these regions, rather than simply splitting neurons into VTA and SNc. Figure 3 shows the distribution of TH+ neurons in the rat, non-human primate and human.

This figure shows that in the rat midbrain there is a clear area of the VTA with a high density of dopamine neurons that extends out to the SNc. In the non-human primate there is also an area of dopamine neurons in the VTA, but the high-density region of the SNc is pushed laterally in comparison to the rat. In the human there is a very dense and widespread population of dopamine neurons in the SNc. This population extends to the PN nucleus of the VTA and forms one continuous population, rather than discrete groups. This region may have been included in the SNc in human cell counting studies, explaining the relatively small number of VTA dopamine cells in the human. The neurons in the human PN are tightly packed (Pearson et al., 1983). Throughout the rest of the VTA there is a steady distribution of dopamine neurons, though the density is sparse in comparison with the SNc and PN. It should also be noted that the dopamine population in the human, unlike the non-human primate and rat, extends to the substantia nigra pars reticulata (SNr) (Deutch et al., 1986), and so it is possible that this

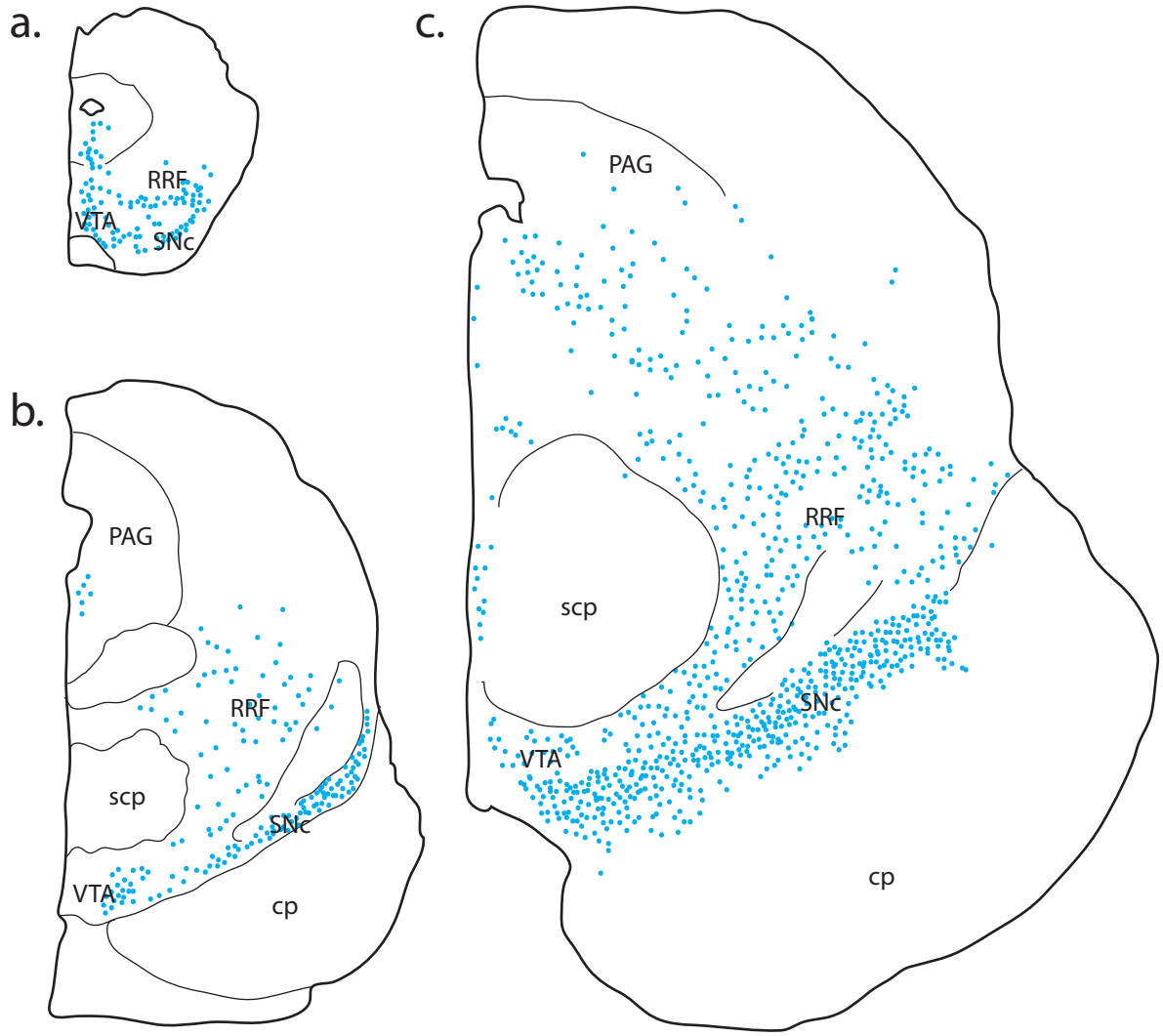

Figure 3: *A semi-schematic drawing of the distribution of dopamine neurons in the a) rat b) macaca fuscata c) human.Blue dots represent distribution of tyrosine hydroxylase immunoreactive cells. PAG = periaqueductal gray, cp = cerebral peduncle, scp = superior cerebeller peduncle. Adapted from Kitahama and colleagues (1994).*

region is involved in the coding of reward. Before we can be certain about the cell numbers, distribution, and density in the human, an unbiased method like that presented by Nair Roberts et al. (2008) needs to be applied to human. The original computer based counting methods may have been biased to count certain types of cells, and missed any dopamine neurons that did not meet these standard criteria. In addition, Nair Roberts and colleagues counted not only the dopamine neurons in the midbrain of the rat, but also the GABA and glutamate neurons. The relative number of non-dopamine neurons within the VTA and SNc could have major implications on the interpretation of an fMRI result in the region.

1.2.1.2. Connectivity

In addition to characterizing the morphology and cell numbers in the dopamine midbrain, it is useful to investigate the afferent and efferent connections of the dopamine neurons in the VTA and SNc. There are three reasons that this is informative. First, differences between VTA and SNc circuits within a species provide information about the possible functional roles of these regions. Second, species differences in connectivity indicate differences across species. Finally, it may be possible to segregate the dopamine midbrain based on connectivity profiles, instead of cell morphology alone. This may lead to a more informative segregation that is more applicable to the human.

The dopaminergic midbrain connects to, and receives inputs from, many cortical and subcortical regions, including the prefrontal cortex, the striatum, the amygdala, and the hippocampus. The most intensively studied region is the striatum. The striatum can be subdivided into three functional subdivisions, the motor, associative and limbic striatum (Parent, 1990), which corresponds to the putamen, the dorsal caudate nucleus, and the ventral striatum, respectively (Yelnik, 2002). It is the limbic, or ventral, striatum that processes motivational information.

The dopaminergic efferents that project to the ventral striatum are organised in a topographical manner. In the rat the main dopamine efferent to the ventral striatum is the VTA and medial SNc (Albanese and Minciacchi, 1983; Beckstead et al., 1979; Brog et al., 1993). In the non-human primate the cells projecting to the ventral striatum also originate from the VTA, but in addition there is a horizontal band of dopamine cells in the SNc that project to the ventral striatum (Lynd-Balta and Haber, 1994). This band follows the full lateral extent of the SNc. There are also afferents to the dopaminergic midbrain from the ventral striatum, and these also have a topographical organisation. In the rat the shell of the ventral striatum is the main striatal input to the dopamine midbrain, and the receiving neurons are mainly in the VTA (Berendse et al., 1992; Groenewegen et al., 1993). In the non-human primate, afferents to the dopaminergic midbrain from the ventral striatum cover the VTA and the full extent of the SNc (Haber et al., 1990; Lynd-Balta and Haber, 1994). Thus there are species differences in the ventral striatal connectivity profile of the

dopamine midbrain. In rats there seems to be a clear functional subdivision between the SNc and VTA, reflected by the different projection targets of these regions. In the non-human primate the segregation does not appear to lie just on the medial-lateral dimension, as neurons within the dorsal SNc also project to the ventral striatum (Joel and Weiner, 2000). This may indicate that the dopamine functional divisions of the rat may be different to that of the human. Investigation of the connectivity of the SN in the human, using DTI, provides evidence that the human organization of the dopamine projections may be similar to the primate (Menke et al., 2010). The substantia nigra (SN) was found to connect to the ventral striatum, and this region of the SN corresponded to the likely location of the SNc. Whether this represents inputs to the SNc or projections is unknown.

Due to the highlighted differences in dopamine midbrain morphology and connectivity, it seems appropriate to consider the VTA and SNc in the human as a continuous complex. Until the connectivity profile and the composition of the VTA and SNc has been extensively studied in the human, the full extent of species differences will not be known. At the present time, it is not possible to functionally subdivide the human dopamine midbrain, and care should be taken when applying non-human research to human brain function.

1.2.2. Localising the midbrain nuclei in the human with MRI

In conventional fMRI studies, activity maps are overlaid on a standard brain template. Areas of activity can then be labelled using anatomical landmarks, such as the sulci and gyri of the cortex. Probabilistic atlases of brain regions can also be referred to, such as the Harvard-Oxford cortical structural atlas. No such probabilistic atlas exists for the human midbrain, due to the relative scarcity of midbrain neuroimaging studies.

Instead, detailed structural MRI scans need to be collected from each individual, and a group template created that reflects the midbrain anatomy of the group being studied. The choice of the sequence used to collect this structural data is important. T1-weighted scans, those traditionally used as reference anatomical images in fMRI studies, have relatively homogenous signal intensity within the midbrain, as all tissues within the midbrain have a similar T1 (longitudinal) relaxation constant. However, tissues within the midbrain have variable T2 (transverse) relaxation times

and density of protons, so it is these properties that must be manipulated to acquire informative structural scans on which activity can be overlaid.

The two sets of nuclei that are visible in such images are the red nuclei (RN) and the SN. The SN is visible on proton density (PD) and T2-weighted scans. These landmarks can then be used to localise activity in structures that are positioned relative to these nuclei. Much work has been carried out to investigate the property of the SN that leads to its visibility on PD and T2-weighted scans.

Initial attempts to image the midbrain nuclei in the human using MRI focused on the increased iron content in the SN and RN. Iron is an essential element required for the synthesis of TH. As the human brain matures, iron deposits build up in this region. Iron is paramagnetic, so induces magnetic susceptibility in the local region, which reduces the T2-relaxation time of the surrounding tissue of the iron containing tissue (see section 2.1.2 for an explanation of T2-relaxation). Drayer and colleagues (1986) imaged the iron containing regions of the brain using T2-weighted scans. Comparison with iron deposits in the post-mortem human brain confirmed that the regions of hypointensity were likely caused by increased concentration of iron. The benefit of collecting a T2-weighted scan is that it is possible to delineate the SNc from the SNr (Oikawa et al., 2002). With high magnetic fields this delineation becomes easier to detect (Eapen et al., 2011). However, the SN is not fully represented on a T2 scan, with lateral and ventral regions appearing at a uniform intensity to the surrounding non-SN tissue, and the dorsal regions including fibres of the cerebral peduncles (Oikawa et al., 2002). Also, the delineation of the two structures is currently done by sight, and is prone to human error and bias.

An alternative option is to measure the midbrain nuclei with a PD-weighted scan. With this image contrast the full extent of the SN is hyperintense, but it is not possible to differentiate the SNc from the SNr (Oikawa et al., 2002). However the location of the SNc can be inferred, using anatomical knowledge, as the posterior portion of the SN. A solution to the problem is to collect a dual-echo scan that has a T2-weighted contrast and a PD contrast, and use both to form a fuller picture of the location of the SNc.

Although there is not a standard brainstem atlas available for use with fMRI studies, there are two sources of information that can help to localise the SNc and VTA once the structural scans have been collected. Naidich et al. (2009) have localised midbrain nuclei, including the SNc and VTA, using MR 'microscopy' at 9.4T and post-mortem brains. However, there are no direct measurements in this atlas, and the images are based on single specimen. An earlier atlas (Afshar et al., 1978) created an average map of the SN from a group of nineteen brains. Each slice was 1mm thick, and the atlas images are drawn to scale using boundaries derived from areas where 70% of the specimens had the nucleus. They found a large amount of variability across participants in the location of the midbrain nuclei, which demonstrates that a standard atlas from a group of people is required to get the best estimate of the anatomical location of midbrain nuclei. This atlas is useful in localising the SN as a whole, and the anatomical location of the SNc and VTA can be inferred relative to the SN using the atlas of Naidich and colleagues (2009).

In conclusion, although there is no standard atlas designed for use in fMRI to localise midbrain structures, the combination of the information we have gained from post-mortem studies and our ability to image properties of the human midbrain, such as proton density, allow us to make informed decisions about the location of these midbrain structures on a standard brain atlas.

1.3. The challenges of midbrain fMRI

In this section I will outline the technical challenges that face any attempt to accurately and reliably carry out and analyse a midbrain fMRI study.

1.3.1. High resolution scanning

The human midbrain nuclei are small in comparison to the cortical and subcortical regions that are usually investigated with fMRI. The voxel size of standard fMRI experiments tends to be around 3x3x3mm, as this has proved to be a useful resolution for localising activity in the human cortex. Changing the voxel size has impacts on many factors, including the contribution of noise in the data, the influence of partial volume effects, and the amount of task-related signal that can be

measured. All these factors impact on the final SNR, which decreases as the voxel size gets smaller (Edelstein et al., 1986; Triantafyllou et al., 2011). A decrease in SNR means that it the protocol is less sensitive to BOLD changes.

Despite this general decrease in SNR, there are two reasons why it is advantageous to use high resolution scanning for midbrain fMRI. First, as the nuclei are small and tightly packed, small voxels allow activity to be localised to a specific nucleus. Larger voxels would likely overlap across nuclei, and there would be an increase in partial volume effects. Voxels that are covering the region of interest may also be measuring a BOLD signal generated by adjacent voxels. This is also true of nuclei that border tissue-CSF boundaries, or tissue-large blood vessel boundaries. As voxel size increases, there is an increased contribution of physiological noise on the data (Yoo et al., 1999). Second, the use of small voxels allows the investigation of possible functional subdivisions within nuclei.

1.3.2. Image co-registration and normalisation

In cognitive neuroimaging the process of 'co-registration' typically involves transforming functional data to a high-resolution structural image of the participant. Normalisation refers to transforming the high-resolution image to a standard space template to facilitate between-subject group analysis. These two steps are then concatenated and applied to the fMRI data. The high-resolution structural image acts as an intermediate between the functional data, which contains low-resolution information, and the standard template.

Midbrain fMRI studies have employed this conventional approach, using either a T1-weighted structural image (Krebs et al., 2010; Sigalovsky and Melcher, 2006; Zhang et al., 2006) or a PD structural image (Dunckley et al., 2005). However, there are two reasons to suggest that such methodology does not lead to robust midbrain registration. First, fMRI optimised for the midbrain typically has a limited field-of-view (FOV). This is because high-resolution functional scans are required to localise activity accurately to a specific midbrain nucleus, so a long repetition time (TR) would be required to collect data from the whole brain. In order to fit an experiment within a reasonable scan time and maintain temporal resolution, data are collected from slices over the midbrain only. Within this limited FOV there is less structural

information than would be available in a whole-brain FOV, so the transformation of the functional data onto the high-resolution structural image is not as reliable or as accurate as the whole-brain equivalent. Second, registration accuracy in midbrain fMRI needs to exceed the accuracy that would normally be expected with whole-brain fMRI. This is due to the smaller size of the midbrain nuclei, and the close proximity of the nuclei to each other.

In recognition of the challenges facing midbrain registration, many fMRI studies have circumvented the need for registration completely, and used a region-of-interest (ROI) approach. Voxels within individually defined ROIs are averaged and these averages are compared at a group level (DuBois and Cohen, 2000; Guimaraes et al., 1998; Hawley et al., 2005; Schneider and Kastner, 2005; Topolovec et al., 2004; Tracey et al., 2002; Wall et al., 2009). However, ROI analyses rely strongly on *a priori* predictions, so may miss unexpected results. Furthermore, the inclusion of non-active voxels in the ROI average can remove genuine effects, and increase the likelihood of accepting false negatives. Alternatively, manual registration has been used for midbrain fMRI (Sylvester et al., 2007), but this is a time consuming method and may be vulnerable to investigator bias. Automated linear registration of structural images into standard space has been optimised for the midbrain (Napadow et al., 2006; Pattinson et al., 2009b). However, the use of non-linear registration methods may circumvent the need for this optimisation, as these methods apply transformation to standard space at a local level, rather than applying the same transformation to the whole brain, as is the case with linear registration (Klein et al., 2009). Non-linear registration has previously been used in a brainstem fMRI study (Pattinson et al., 2009a).

1.3.3. Physiological noise

A major challenge facing midbrain fMRI is that, due to its anatomical location, it is prone to physiological artefacts. During the cardiac cycle the midbrain undergoes a bulk motion in the direction of the foramen magnum, due to the increased intracranial pressure as blood enters the brain (Poncelet et al., 1992). Such bulk motion causes spatio-temporal blurring of the BOLD signal across voxels. Also the large blood vessels adjacent to the midbrain are subject to cardiac pulsations (Dagli et al., 1999; Greitz et al., 1992) causing BOLD signal intensity changes in nearby tissue.

Furthermore, intracranial pressure changes and pulsatile movement of blood vessels produce oscillatory motion in the cerebrospinal fluid (CSF) surrounding the brain and brainstem (Friese et al., 2004; Klose et al., 2000), which gives rise to in-flow signal artefact on the echo-planar image (EPI) typically used to record functional information (Piché et al., 2009). In addition to cardiac related artefacts, the respiratory cycle also causes bulk magnetic susceptibility changes within the brain tissue during the respiratory cycle (Raj et al., 2001). There is also a significant interaction between these two sources of noise (Brooks et al., 2008; Harvey et al., 2008).

Due to the increased sources of physiological noise in the midbrain, the SNR ratio may be less than that of cortical regions that are not so prone to physiological artefacts. Therefore, a method to reduce this noise should be utilised to optimise midbrain fMRI. There are two main approaches to do this. The first option is to use cardiac gating to acquire the data. Using this method, data is collected only between the heartbeats, avoiding the peak cardiac noise. A second option is to collect the data continuously then remove the noise during the analysis stage. RETROICOR (retrospective image correction) is the most common correction method (Glover et al., 2000), as will be discussed in succeeding chapters.

1.4. Aim of this PhD

The aim of this PhD was to accurately and reliably measure an fMRI signal in the human midbrain, to elucidate the role of the human dopaminergic midbrain in reward and punishment. To this end, the thesis is organised into the following chapters:

Chapter 3: **Midbrain optimised fMRI: registration.**
Different registration pathways for transforming functional data onto a standard template are outlined and tested at the level of the midbrain.

Chapter 4: **Midbrain optimised fMRI: physiological noise modelling.**
A simple visual experiment that elicits activity in the superior colliculi is presented to test the effect of modelling physiological noise. The data were analysed using a conventional general linear model, and a model

that included physiological noise regressors. The effect of the modelling this noise on the observed response is investigated.

Chapter 5: **Reward and punishment prediction errors in the dopaminergic midbrain**

Using the optimised midbrain methods the role of the dopaminergic midbrain in positive and negative PEs is investigated. Here the results of a learning experiment that elicits PEs are presented. In addition, the optimised methods that proved effective in the superior colliculi are tested to ascertain if these methods are effective at reducing physiological noise in the dopaminergic midbrain.

2. Methods

2.1. Magnetic resonance imaging

FMRI allows the safe and non-invasive investigation of the location of neural activity and the strength of distributed functional connection between brain regions while subjects perform mental tasks. In order to successfully design and interpret the results of fMRI studies, it is necessary to have a thorough understanding of how magnetic resonance imaging (MRI) works, and what is being measured. This section will outline the principles of MRI, and explain how it can be utilised to obtain both structural and functional information from the human brain.

2.1.1. Scanner hardware

MRI scanning depends on the static magnetic field (the B0 field) that is created by a superconducting electromagnet. As current passes through coils of wire, a magnetic field is created. The current that flows through the wire controls the strength of the magnet. In an MRI scanner these coils are arranged in the body of the scanner, and within the coils of the electromagnets lies the scanner bore. The wire loops are arranged in a way that creates a relatively homogenous field through the bore of the scanner. These wires are housed within a liquid helium bath to reduce the temperature to such an extent that the wires have no resistance and current can flow with little power required.

In order to measure a signal of a sample within the scanner bore, radiofrequency (RF) coils are required. In the case of brain imaging this is a phased-array volume coil within which the participants' head can fit. The volume coil contains two types of electromagnets: transmitter coils generate electromagnetic fields to excite the nuclei within the volume coil; receiver coils measure electromagnetic fields that are generated by the nuclei within the volume coil when they fall from their excited state. The energy of these coils is within the RF range of the electromagnetic spectrum, hence the name.

To localise a signal as being emitted from a particular location within the volume coil, and to allow the generation of an image that contains spatial information, gradient

coils are required. There are three gradient coils; each modifies the magnetic filed within the bore in one of three directions, so that the magnetic field can be manipulated in an x, y and z direction. This allows locations within the bore to contribute to the measured signal differentially over time.

The final piece of hardware to discuss is the shimming coils. To obtain undistorted images from the scanner, the B0 magnetic field must be homogenous. To ensure that this is the case shimming coils are required to apply additional electromagnetic fields to correct for any inhomogeneities in the magnetic field within the bore of the scanner.

2.1.2. Magnetic resonance

I have alluded to the mechanism by which a magnetic resonance (MR) signal is measured in the above section, in that I mentioned the RF coil emits electromagnetic fields that excite nuclei within the coil, and receives electromagnetic fields emitted by the nuclei when they relax. It is this process of excitation and relaxation that I will now describe.

Due to the abundance of water molecules in the brain, it is the hydrogen nuclei that are most commonly imaged with MRI. Hydrogen nuclei contain a single proton. Each proton spins around itself, due to thermal energy. Under normal conditions the orientations of the spins are random and cancel each other out. The net magnetisation of the hydrogen protons would be zero. When a sample of hydrogen protons is placed inside a magnetic field, the protons precess around the main axis of the B0 magnetic field, analogous to a spinning top. There are two energy states within which protons can precess: parallel and anti-parallel to the magnetic field. A higher proportion of protons will lie in the parallel state, as this is a marginally more stable state. As magnetic field strength increases, the proportion of protons in the parallel state will increase, as the energy difference between the parallel and anti-parallel states increases. The proportion of protons in each state determines the net magnetisation of a sample.

The energy state of a proton is not static, and a proton in the parallel state can change to the anti-parallel state if it absorbs energy that matches the difference

between the two energy states. This energy is emitted by the RF coil in the form of electromagnetic fields that oscillate at the resonant frequency required to flip the proton from parallel to anti-parallel state. The resonant frequency of a sample is the Larmor frequency. This frequency is modulated by the atomic nucleus of interest and the field strength of the scanner. There will be a change in the net magnetisation of a sample when the proportion of anti-parallel protons increases. Once a proton has absorbed energy and moved into the anti-parallel state, equilibrium must be restored and the proton falls back to the parallel state, emitting an electromagnetic field that is detected by the RF coil. Again, the frequency of this emitted energy will be equal to the Larmor frequency. It is the properties of this emitted energy that can tell us about the properties of a sample contained within the RF coil.

The emission of energy by the protons as they fall back into the parallel state is termed relaxation. There are two types of relaxation that occur and lead to the decay of the MR signal that immediately follows an excitation pulse. Longitudinal relaxation is the recovery of the net magnetisation as protons move from the anti-parallel to parallel state. This relaxation, also called T1 recovery, occurs over a time period of seconds. When the MR signal is fully recovered the equilibrium of the two energy states has been restored, and the net magnetisation in the longitudinal plane is recovered to its initial state. Transverse relaxation is the decay in magnetisation that occurs within the transverse plane. Immediately after the RF pulse the transverse MR signal is at its strongest, and the excited protons are aligned in phase. These spins dephase due to spin-spin interactions and the MR signal lessens. This relaxation, also called T2 decay, occurs at a faster timescale than T1 recovery. Both types of relaxation have time constants that depend upon the substance that the proton is contained within. Different tissue types within the human body have different relaxation constants.

T2* decay, the basis of fMRI, is also sensitive to local magnetic field inhomogeneities. Deoxyhaemoglobin (dHb) is paramagnetic and increases the spin dephasing rate, decreasing the T2* constant. T2* weighted images show decreased MR signal in regions of higher dHb concentration. This is referred to as the BOLD contrast.

2.1.3. Spatial localization of a signal

If the magnetic field was uniform across a sample when the RF coil emitted an excitation pulse the entire sample would be excited, and there would be no information about the source of the signal. The application of magnetic gradients allows the excitation of a single slice of a sample. A magnetic field gradient in the z direction can be applied so that the excitation pulse will excite a single slice. The Larmor frequency of a proton depends upon the magnetic field strength, so by modulating the strength we can ensure that the pulse excites only a slice of the sample. This is not an entirely accurate process, and there is bleeding of excitation into adjacent tissue. By collecting slices in an interleaved order, or leaving a gap between slices, this problem can be minimised.

Now that an entire slice has been excited, the location of the excited protons within the slice must be calculated. To encode two-dimensional spatial information within a slice, a second gradient coil (y) is briefly switched on after the excitation pulse from the RF coil. The brief application of a gradient in the y directions causes the relative phase of the protons in the transverse plane to change. In the centre of the gradient the magnetic field strength will remain constant and there will be no change in phase. To either side of the centre the phase of the protons will be modulated, as the temporary application of the gradient causes spins to speed up or slow down. This gradient is termed the phase encoding gradient. Information on proton phase is encoded by the scanner hardware to localise signal in the y direction. During data acquisition a gradient coil is switched on in the x direction, which modulates the frequency of the precession of the protons in the x direction. This frequency-encoding gradient is utilised by the scanner hardware, as the frequency of the precessions during acquisition will indicate from which location in the x direction the signal is being measured.

2.1.4. Gradient-echo and spin-echo imaging

The sequence described above is typical of gradient-echo images. These sequences allow images to be acquired quickly. However, the disadvantage of this type of sequence is that the signal is affected by local magnetic field inhomogeneities and so the images are prone to susceptibility artefacts. Spin-echo sequences use a second

RF pulse after the initial excitation pulse that flips the protons 180°. This refocuses the proton phases in the transverse plane and removes any phase changes due to local field inhomogeneities.

2.1.5. Sensitivity Encoding

It is often necessary to collect images as quickly as possible. To speed up acquisition parallel imaging can be utilised. Parallel imaging reduces the amount of data collected in the phase-encoding direction. The spatial arrangement of the overlapping coils in the head coil (a phased array coil) is used to reduce the amount of data encoded. For data acquisition in the studies described in this thesis, sensitivity encoding (SENSE) was used. The disadvantage of parallel imaging is that the SNR of the image is decreased.

2.1.6. Contrasts/Image types

By utilising the differential T1 and T2 constants of protons within different tissue types, images of the brain can be obtained that give different contrasts. In addition, either spin-echo or gradient-echo sequences can be acquired, depending upon the properties of tissue that we want to measure. There are two main parameters of a sequence that can be manipulated in order to achieve different contrasts. The first, TR, is the time between successive excitation pulses. The second, echo time (TE), is the time between the pulse from the RF coil and the time the data is acquired.

2.1.6.1. Proton density-weighted images

Images using this contrast reduce the effects of differential T1 and T2 constants in different tissue types, and instead measure the density of protons in the tissue. Long TRs are used to reduce the differential T1 recovery times, and short TEs to minimize differential T2 decay times. Instead the signal is based purely on different concentrations of hydrogen protons: the higher the concentration of protons, the brighter the image. White matter appears darkest on PD images, grey matter is medium intensity, and cerebrospinal fluid (CSF) is brightest. The proton density images presented in this paper have been acquired using a dual echo turbo spin-echo (TSE) sequence with a SENSE factor of 1.5. This dual echo allowed the collection of a PD weighted image at the first echo. TSE imaging is a fast method

which contains several refocusing pulses after each initial excitation pulse, each one followed by a data acquisition phase.

2.1.6.2. T1-weighted images

T1-weighted images rely on the differential T1 constants within different tissue types. A short TE is used to minimise T2 decay differences between tissue types. An intermediate TR is used that maximises the different T1 recovery times of different tissues. On these images, white matter is brightest as it has the shortest T1 constant, grey matter is intermediate, and CSF darkest as it has a relatively long T1 constant. A long T1 constant means that fewer protons will have returned to a relaxed state, so there will be fewer protons to excite with the next RF excitation pulse, so the MR signal will be less. The T1-weighted images in this thesis have been acquired using a magnetisation prepared rapid gradient echo (MPRAGE) sequence. In this sequence the excitation pulse is preceded by a 180° inversion pulse. This increases the T1 contrast between tissues of interest.

2.1.6.3. T2-weighted images

T2-weighted images use an intermediate TE to measure the differential T2 decay times of different tissues. A long TR must be used so that T1 recovery is complete for all protons. In T2 images, CSF is brightest as it has long T2 constants, grey matter is intermediate, and white matter darkest as it has short T2 constants. A short T2 constant will mean that a greater proportion of transverse magnetisation will have been lost by the acquisition time, so the MR signal will be less. Some T2 images in this thesis were acquired using the same dual-echo sequence as was used for the PD images. Other T2-weighted images were collected using a TSE sequence with a SENSE factor of 2. Spin-echo sequences must be used when measuring a T2 contrast, to reduce the effects of local field inhomogeneities caused by dHb.

2.1.6.4. Echo-Planar Imaging

EPI is a fast imaging technique that is used in fMRI. As whole volume images need to be collected over a matter of seconds, traditional techniques designed for measuring the structure of the brain cannot be used. Instead a fast method is required that will give a low resolution T2*-weighted image in less than three

seconds. A single excitation followed by rapid gradient switching allows for data to be collected over the whole volume of interest at a relatively low resolution. This method is prone to artefacts and distortions, such as signal dropout near air containing regions such as the sinuses, and distortion in the phase-encoding direction.

2.1.7. Signal-to-noise ratio in fMRI

Functional imaging is usually carried out with a voxel size of around 3x3x3mm. This means each voxel contains 27mm^3 of tissue. As the structures of interest in this thesis are relatively small, high-resolution imaging was used to try to differentiate activity of adjacent structures, and accurately localize a functional signal. The smallest voxel size used in this thesis was 1.7x1.7x1.7mm, so the volume of a voxel was just 4.9mm^3. This had important implications for the SNR of the functional images.

The ability to detect a signal depends on the relative proportion of noise that confounds the measurement. Noise sources include thermal, system, physiological, and global head motion. Whilst the influence of such noise sources can be reduced with temporal filtering and averaging of a functional signal across many trials, it is impossible to remove all the noise. This problem is exacerbated by the use of small voxels. With smaller voxels the SNR is decreased, and it is more difficult to detect a signal. Methods in this thesis designed to reduce the effect of noise include modelling the sources of physiological noise (see Chapter 4) and using a strict head motion threshold, above which data were excluded from analysis. Whilst it is desirable to use small voxels for midbrain imaging, it comes with a steep cost in terms of the SNR.

2.2. What are we measuring with fMRI?

To be able to interpret an fMRI experiment, it is important to understand whether a change in BOLD signal accurately reflects a change in regional net synaptic function. This includes understanding the properties of the hemodynamic response and the neural events that lead to a change in BOLD signal.

2.2.1. The neural basis of the BOLD signal

The ultimate outcome of neural activity is the proliferation of action potentials from one neuron to another, to transmit encoded information around a local or widely distributed neural network. An action potential occurs when the sum of excitatory post-synaptic potentials (EPSPs) generated within the dendrites of a neuron reach a certain threshold. It is then propagated along the length of the neuron's axon as an electrical impulse. When this impulse reaches the synaptic button, either an excitatory or inhibitory neurotransmitter is released into the synapse, depending on the property of the pre-synaptic neuron, which diffuses to the post-synaptic membrane of the next neuron. This results in an EPSP or an inhibitory post-synaptic potential (IPSP) within the post-synaptic membrane. Each neuron has many dendrites receiving inputs from many different neurons. If enough EPSPs are generated relative to IPSPs, an action potential will be generated in the post-synaptic neuron. As the generation of an action potential depends on this balance of excitatory and inhibitory synaptic influences, metabolic activity within a neuron's dendritic tree does not necessarily relate in a simple way to the rate of firing of that neuron. So, an increase in local energy metabolism, indexed by an increase in local blood flow, does not necessarily correlate linearly with in the rate of generation of propagated action potentials.

These neurophysiological considerations are a major issue for fMRI, which is an indirect measure of neural activity that relies on changes in cerebral blood flow (CBF). The increase in CBF reflects the increase in glucose metabolism that occurs when there is more neural activity. It is important to know exactly what aspects of neural activity correlate with this change in CBF, to understand what the BOLD signal means in terms of neural processing. To this end, investigators have compared BOLD signals in non-humans to extracellular field potentials (EFPs). EFPs are measurements of local neural activity that sum action potentials, EPSPs and IPSPs. If the microelectrode tip is close to a source of action potentials (a soma or axon) then this signal will dominate the EFP. However if the tip is further away from a single source, the EFP will include neural activity from a local region of cells. The high-frequency range of this EFP will contain information about action potentials of multiple units. The lower-frequency range of the EFP is called the local field potential (LFP). The LFP contains information about the dendrosomatic processes, and

reflects dendritic inputs to the region and the activity of local interneurons (Logothetis, 2003). Logothetis et al. (2001) simultaneously measured the BOLD response and extracellular field potentials in the monkey visual cortex. LFPs better predicted the BOLD response. The high-frequency signal associated with action potentials adapted soon after stimulus onset, whereas the LFP response correlated with the time course and magnitude of the BOLD response. Thus, the BOLD response tends to be dominated by the neural input to a region and the activity this generates within local interneurons, rather than the net output to other brain regions.

2.2.2. Properties of the haemodynamic response

In order to accurately model the underlying neural activity of the BOLD response, it is important to properties of the hemodynamic response. Increases in CBF occur as a result of neural activity, but timing, spatial specificity, and scaling of the CBF response must be investigated.

The haemodynamic response function (HRF) describes the onset and shape of the expected haemodynamic response, and is used to model the expected BOLD signal changes that will be elicited by the presentation of a stimulus. This function is based on the temporal properties of the CBF response to an increase in neural activity. It is delayed by approximately 2s (Kwong et al., 1992), reaches a plateau after 6-12s (Logothetis et al., 1999), and returns to baseline by 18s. The temporal resolution of fMRI is ultimately constrained by these blood flow properties. The canonical HRF used in most fMRI analyses is a generalisation based on cortical studies, and it may not accurately describe the CBF response in all brain regions. In the midbrain it has been shown that the delay in the HRF is better modelled as a shorter time period (Wall et al., 2009). As a result, a shorter HRF has been used for the analyses presented in this thesis.

The ultimate spatial resolution available with fMRI is constrained not by scanner hardware, but by the spatial resolution afforded by the HRF. The signal originates from draining venules (when using a magnet strength of 3 Tesla), which means that the signal is obtained from tissue a little remote from the neural tissue of interest. Comparing fMRI data to electrophysiological recordings has given a measure of this spread. Disbrow and colleagues (2000) constructed cortical maps of the

somatosensory area of the anaesthetized macaque using fMRI and microelectrode recordings, finding only a 55% concordance between the maps. The fMRI areas of activation were larger than the electrophysiological areas, consistent with the assumption that fMRI results in a spread of activation larger than the initial neuronal activity. No investigation of the spatial resolution of the midbrain BOLD response has been carried out, so the assumption I have adopted is that the spatial resolution of the BOLD signal in the midbrain is similar to that of the cortex.

The final property of importance is the linearity of the BOLD response. This is of particular importance when investigating reward, as it has been shown that a PE response, in terms of action potentials, scales linearly with the level of PE. There is then a question as to whether the BOLD response relates linearly to the level of neural activity? The Linear Transform Model states that the fMRI response should be proportional to neuronal activity (Boynton et al., 1996). If the scaling of a system is linear then the output of the system is proportional to the input. Boynton and colleagues found evidence for linearity of the fMRI response in human primary visual cortex. Luminance of the stimuli were linearly related to the amplitude of the BOLD signal. A linear response has also been observed in visual association cortex (area V5) (Rees et al., 2000).

Whilst linearity has been observed in early sensory areas of the human cortex, the linearity if the BOLD response in the midbrain has not been investigated. Furthermore, Caplin and Dean (2008) highlight the weakness of assuming a linearity of the BOLD response in reward studies that used the temporal difference model to precisely predict the expected level of neural activity. Using such a model may lead to an increase in false negatives, as the BOLD response may not follow the linear scaling properties that are expected if the response is to conform to the temporal difference model. To overcome these problems it is possible to model the response in a non-linear fashion using a first-order Taylor expansion that assumes there is an initial non-linear increase that is elicited by all stimuli, followed by linear changes with increasing strength of the response to a stimulus. A second option is to place stimuli of similar strength into groups, and then model the difference to investigate both linear and non-linear responses.

2.3. fMRI data analysis

2.3.1. Experimental design

To maximize the likelihood of observing a genuine BOLD signal, the experimental design must be optimised before any data are collected. The experiments presented in this thesis used event-related designs. Many fMRI studies use blocked-designs, whereby several examples of the same stimuli are presented in a row, and explanatory variables (EVs) are manipulated on a block-by-block basis. The repetition within a block gives the HRF time to reach its peak, and there is a cumulative effect of repetition. Event-related designs, on the other hand, present single events in a pseudo-random order, and the HRF is modelled separately for each event. This allows unexpected events to be presented, and also allows different components of a trial to be separated. In order to optimise event-related designs the trial order must be carefully manipulated so that each trial follows itself and every other trial type equally. Trials far apart in time should also not be compared, due to changing noise properties over time such as scanner drift. In addition the inter-trial intervals should be jittered, so that there are longer gaps between some trials, so the HRF can reach its peak. Using this type of design, the HRF to each trial type can be fully modelled. Optseq2 (http://www.nitrc.org/projects/optseq/) was used to optimise stimulus order and timings for the experiments in this thesis. In addition the trial lengths should not be a multiple of the TR, so that the same slice is not always collected at the same point in the trial. Whilst event-related designs are more flexible, they are less powerful as, due to the reduced time between single events, the baseline to peak range of the BOLD response will be smaller than with a blocked-design.

2.3.2. Preprocessing

Prior to statistical testing, the raw data must be manipulated and prepared. The data presented in this thesis were preprocessed using the FMRIB software library (FSL) tools. This section will describe these preprocessing steps.

2.3.2.1. Motion Correction

Whilst in the scanner a participant will move their head. Whilst making participants comfortable can minimize the amount of movement, it cannot be completely abolished. Runs of functional data were excluded from analysis throughout this thesis if they moved >2mm in any plane. Head motion is a concern when analysing functional data, as we want to be sure that a voxel refers to the same structural location over time. Otherwise signal can be spatially blurred and the SNR reduced. In addition, spin-history artefacts occur with head motion. The signal depends on the spin-history of the tissue, and tissue displacement means that the data acquired over the next few volumes will have a modified spin-history affecting the measured signal (Muresan et al., 2005). To attempt to reduce the effects of head motion I applied McFLIRT (Motion Correction FMRIB's Linear Registration Tool) (Jenkinson et al., 2002; Jenkinson and Smith, 2001) to the data. Successive volumes of the image were co-registered to a mean image calculated from the entire time-series. A rigid body transform was applied using a normalised correlation cost function. A rigid body transform is optimal for co-registering images from the same participant in the same scan mode (intramodal) as the same brain is being matched across time, so all movement can be described with three rotations (pitch, yaw, and roll) and three translations (x, y and z).

2.3.2.2. Temporal filtering

Over time, the data time-series will be influenced by low frequency noise or scanner-drift that may interfere with the detection of any signals of interest. By applying a high-pass filter to the data these low-frequency noise components can be removed from the data. The data in this thesis have been high-pass filtered using a 50s cut off.

2.3.2.3. Pre-whitening

Due to the nature of fMRI time-series there will be temporal autocorrelation within a voxel over time. This means that the intensity of a voxel will not be independent from the intensity of the same voxel at time points before and after. This will not be removed by high-pass filtering, as it exists in the same frequency band as a BOLD signal of interest. Instead the data must be pre-whitened. To do this an estimate is made of the auto-correlation in the data, and a filter created to remove it. Once data

that can be predicted from adjacent time-points has been removed, a signal is created in which adjacent time points are statistically independent from each other.

2.3.2.4. Spatial Smoothing

In order to increase the SNR, fMRI data are usually smoothed in space. Spatial smoothing takes advantage of the spatial correlation in the data. This spatial correlation is due to the similarity of function in adjacent voxels, and the spatial smoothing that exists in the data due to the underlying vasculature. In this thesis, a Gaussian blur with a full width half maximum (FWHM) of 2mm or 3mm was applied to the raw data. In order to optimize the increase in SNR that can be achieved, smoothing must be applied that is of similar extent to the spatial extent of the underlying neural activity. The smoothing I used was less than that routinely applied to fMRI data because the signal of interest within the midbrain was smaller than that of the brain regions usually studied with fMRI.

2.3.2.5. Brain extraction

Prior to analysis, the images were stripped of extracerebral tissue using the FSL brain extraction tool (BET) (Smith, 2002). This algorithm delineates brain tissue from surrounding non-brain tissue. The removal of non-brain tissue from the images confines analyses solely to brain tissue.

2.3.3. Statistical maps

In order to calculate the effects of each EV on intensity values of voxels across the brain, statistical maps must be created. A general linear model (GLM) was used, and regressors were entered into this model that represented stimulus onset. At the first level analysis, each voxel in each individual was assessed to investigate how well it correlated with these experimental regressors. At the higher-level analysis, the maps generated for each individual were compared, so the signal across participants were averaged and general population-level inferences made.

2.3.3.1. The general linear model

Data in this thesis were analysed using the GLM approach. The first stage of the creation of the GLM involved defining the stimulus timings for each EV. EVs must be

defined to allow the effect of interest to be interrogated. EVs must also be created for parameters of no interest such as head motion, instructions screens, and physiological noise. Explaining structured noise in the data this way reduces the amount of noise left in the data, and makes the statistics stronger. Each EV was convolved with an HRF, as this better reflected the actual response that was measured. To allow for deviations from the expected HRF temporal derivatives were included in the model. The inclusion of a temporal derivative for each of the EVs explains variance in the data that may be due to the HRF being slightly slower or faster than expected. Thus temporal derivatives explain this source of 'noise' and improve detection of signal.

Statistical maps were then created that reflected the amount of variance in the data that had been explained by each EV. This was done on a voxel-wise basis, and a map (a parameter estimate) was created that showed this measure for each voxel. Thus, the GLM attempts to 'fit' the model to the data in the best way, with the minimum variance remaining. The simplified equation for the linear model is:

$$Y = \mathrm{X}\beta + \varepsilon$$

where Y is the observed data, ε is the error, or variance remaining as noise, X is the EV, and β is the beta value, the weight that is applied to the EV (X) to explain the data. The parameter estimate for each EV consisted of a voxel-wise map of the beta values. Once the parameter estimates for each EV had been calculated, parameter estimates of EVs of interest were compared, leading to COPE images (contrast of parameter estimates). When two EVs were directly compared, a *t* -statistic was calculated for each voxel to assess whether the difference between the two parameter estimates was significantly different from zero. When an implicit rest baseline is used, the parameter estimates are identical to the COPEs. As the denominator in a *t*-test is a measure of the noise, reducing noise in the data increases the *t* value and hence increases the sensitivity of the analysis.

2.3.3.2. Individual Level analysis

Fixed-effects analyses assume that the EVs have the same effect on every dataset. If the same subject has undergone several runs of data acquisition, the results of these are combined using a fixed effects analysis.

2.3.3.3. Group level analysis

Random-effects analysis allows inferences to generalise from the small population studied to encompass the population in general, by accounting for between-subject variance. FMRIB's local analysis of mixed effects (FLAME) (Beckmann et al., 2003; Woolrich et al., 2004) was used for the results presented in this thesis for analysing data across groups.

2.3.4. Post-stats

Once variance had been assigned to each condition, and statistical maps calculated, these statistics were assessed for significance. This stage is termed post-stats.

2.3.4.1. Multiple comparison problem

FMRI data must be corrected for multiple comparisons. During voxel-wise statistical modelling, a statistical test was carried out on each voxel. At a standard significance threshold of $p < 0.05$, one in twenty of the voxels would appear significant when there was no underlying effect to observe (a Type I error). However, if traditional multiple comparison corrections are applied, such as the Bonferonni correction, Type II errors will occur due to the threshold being too conservative. Thus, alternative thresholding methods have been developed for neuroimaging data. Cluster-based thresholding methods were used on the data in this thesis (Worsley et al., 1992), whereby for a voxel to be classed as significant it had to be surrounded by a thresholded number of adjacent voxels, the cluster-level threshold in turn being dependent upon the level set for the peak-level threshold.

2.3.4.2. Pre-Threshold masking

The voxel-wise statistics in this thesis were masked to include just the area of interest. Thus regions that were included in the FOV of the acquisition were excluded if there was no *a priori* hypothesis about activity in those regions. In addition, areas

outside of the midbrain were likely to be very noisy due to poor registration (in the case of the cortex) and large physiological noise influence (in the case of the lower brainstem), so they were removed from the analysis prior to thresholding. To do this a mask was drawn in standard space, and only voxels within this mask were included in the post-stats.

2.3.4.3. Non-parametric statistics

The statistical maps that were tested for significance were within pre-defined anatomical masks. As these restricted volumes were relatively small, I could not assume that data within this volume followed a normal distribution. As a result, traditional parametric tests could not be used. Nichols and Holmes (2002) devised an alternative non-parametric test for functional neuroimaging data based on permutation test theory. The statistical map was given a peak-level threshold, and then the pattern of suprathreshold activity clusters was assessed. The data was permuted and thresholded to create a permutation distribution of cluster sizes. The clusters that localised with the actual data were compared to the permuted data, to see if the size of the clusters exceeded the size that would be expected if there was no significant clusters in the data. Using this method, the initial threshold must be chosen carefully, as low peak-level thresholds will return large clusters, but smaller clusters of biological significance may be overlooked. Conversely, higher thresholds will lead to the detection of small clusters with higher *t*-scores, but may miss larger activated clusters with lower *t*-scores.

2.3.4.4. Region of interest analysis

ROI analyses are used in this thesis to further interrogate the changes in BOLD signal that are revealed in the voxel-based statistics just discussed. Whilst voxel based statistics are used to reveal patterns of activity across all voxels of interest, and show local heterogeneity of activity, ROI analyses can be used to investigate signal change in a specific region to test a specific hypothesis. First, a region was defined using an inclusive mask based on previous analyses. Statistics were then averaged within these masks and a signal change extracted from the region as a whole. The ROI analyses presented in this thesis were calculated using Featquery.

2.3.5. Coregistration and Normalisation

To allow the testing of group data, individual statistical maps must be transformed into a standard space. In standard functional neuroimaging this consists of the concatenation of two steps: the functional data is first transformed onto a high-resolution structural image, then the structural image is transformed onto a standard brain. Chapter 3 of this thesis discusses the optimisation of this pathway for the midbrain, but here I present the standard methodology. Two tools are available in the FSL toolbox for coregistration and normalization. FLIRT (Jenkinson et al., 2002; Jenkinson and Smith, 2001) applies linear transforms to images, in up to 12 dimensions. Using linear methods the same transform is applied globally, such as scaling, skew, translation, and rotation. FNIRT (FMRIBs non-linear registration tool) can be used to apply non-linear local transformations. This means that each area of the brain is separately matched to the destination image.

2.3.5.1. Functional to structural (Coregistration)

Functional MRI data is low resolution and low contrast. The final goal of coregistration and normalization is to get the functional data into a standard coordinate space. The use of an intermediate high-resolution structural image (usually T1-weighted) is because these images contain more structural information; for example, the sulci and gyri of the cortex are much more clearly visualised on a T1- weighted rather than an EP image. This assists the mapping of the low-resolution image. As the functional and structural images are from the same individual they should, in theory, be easy to map one on to the other. However, there will be differences in shape and size, due to distortions, which must be corrected. Further, a cost function algorithm must be used that does not rely on absolute intensity differences, as the images have different contrasts. A rigid body transform can be used for this step, but there may be more differences that are not accounted for with translations and rotations, so skews and scaling can also be applied to the functional data until it maps well onto the structural image.

2.3.5.2. Structural to standard (Normalization)

The demands of normalisation are different from those of coregistration. There is significant variability in brain size, shape and structures between people. Simply

applying a linear transform would not account for these individual differences. For example, the relative size of lobes may differ, or the angle with which the brainstem lies relative to the cortex. To correct such differences, and accurately map all structural brains into the same space, non-linear registration (FNIRT) can be used. In this process the structural image is first mapped into a standard space with FLIRT. Then FNIRT calculates local deformations in the transform to correct local differences, and creates a warp file that is applied to the structural data to transform it into standard space. The standard space is the MNI-152 template, created by the Montreal Neurological Institute, which consists of the average of 152 T1-weighted brain images.

2.3.5.3. Weighting masks

In order to optimise a linear registration step for a particular region, weighting masks can be used. In this situation a mask is drawn around the region of interest. When the cost function is then calculated, values in the mask indicate how important a region is, so the algorithms can give different regions different relative importance.

3. Midbrain optimised fMRI: registration

3.1. Summary

Localising activity in the human midbrain with conventional fMRI is challenging. One reason for this is that functional data must be transformed into a standard space, and methods that have been developed to do this have been optimised for the cortex. Here I present a replicable and automated method to improve the localisation of midbrain fMRI signals by improving midbrain registration. Two additional structural scans were used to improve registration between functional and structural T1-weighted images: an echo-planar image (EPI) that matched the functional data but had whole-brain coverage, and a whole-brain T2-weighted image. This pathway was compared to conventional registration pathways, and was shown to significantly improve midbrain registration.

3.2. Introduction

Due to the relatively low SNR of fMRI, the results from several participants must be grouped, and analysed for statistical significance. In order to achieve this, functional data is usually registered onto a standard space template. The registration pathway consists of two steps: coregistration and normalisation. The first step, coregistration, refers to transforming the low-resolution functional data onto a high-resolution structural scan, most often a T1-weighted image. The second step, normalisation, refers to transforming the structural image into standard space. Once data are in standard space, results can be compared across participants, and across studies. This pathway has been utilised by many researchers investigating midbrain function (Dunckley et al., 2005; Krebs et al., 2011; Krebs et al., 2010; Sigalovsky and Melcher, 2006; Zhang et al., 2006).

However, there are three reasons why it may be desirable to optimise the registration pathways for the midbrain, rather than use this default two-step pathway. First, the nuclei in the midbrain are small. A small error in registration reduces the chance of finding a significant effect as the functional signal becomes blurred in standard space. Second, in order to achieve high-resolution functional scans within a reasonable TR, data are collected over a limited FOV. Therefore the functional scans contain less structural information than would a whole-brain equivalent, thereby increasing the chances of inaccurate registration. Finally, the midbrain nuclei are not visible on T1-weighted scans. I hypothesised that if structural scans that do show contrast within the midbrain are utilised as intermediate steps in the registration pathway, then this would be likely to improve the co-localisation of nuclei within the midbrain.

Here, I present an unbiased, user independent, and novel registration pathway that improves on conventional registration to increase the accuracy with which functional data are transformed onto the standard brain template at the level of the midbrain. This was achieved with the modification of the coregistration step. Two intermediate whole-brain structural scans were used prior to transformation of the data to a T1-weighted high-resolution structural image. Functional data were first transformed onto a whole-brain EPI that matched the functional data, but with full FOV. This

overcame the problem created by having only a limited number of slices to drive registration. The resulting data was then transformed onto a high-resolution T2-weighted image. Both the functional images and T2-weighted images contain areas of low image intensity that correspond to the RN and SN, due to their high iron content (Drayer et al., 1986). The intensity boundaries surrounding these areas in the midbrain can then be utilised to drive registration algorithms. If a T1-weighted image were used as the initial high-resolution structural image, only the edges of the midbrain could be used for registration, as there is uniform signal throughout the midbrain structures with such a T1-weighted sequence. Thus, accuracy within the midbrain would be compromised. Further, weighting the cost function evaluation within the registration algorithm towards accurate sub-cortical registration (at the expense of accuracy with respect to registration of cortex) leads to more accurate midbrain registration. This evaluation study was designed to demonstrate the accuracy of this method at the level of the midbrain, compared with the accuracy of conventional registration methods.

3.3. Methods

3.3.1. Subjects

Sixteen healthy subjects (seven female) aged between 22 and 60 years, with normal or corrected to normal vision, participated in this study. Two subjects were excluded due to poor shimming during acquisition of the functional data. Two subjects were excluded due to an inability to detect their cardiac signal above background noise (which was required for the analysis reported in Chapter 4). Two subjects were excluded because I failed to secure revisits for structural scans.

3.3.2. Data acquisition

MR scanning was performed on a 3T Philips Intera scanner with an eight-channel phased array head coil. Subjects lay supine on the scanner, with padding underneath and surrounding the head. Functional MR images were obtained using a T2*-weighted, EPI sequence with a FOV that covered the long axis of the brainstem (TE, 44ms; TR,1600ms; flip angle, 90˚; resolution, 1.5 x 1.5 mm; matrix size, 144 x 144; slice thickness, 1.5 mm; 16 coronal slices; no slice gap; interleaved slice order; 322

dynamic scans; scan duration, 530s). A SENSE factor of two in the left-right direction was used to reduce susceptibility related artefacts in the data. Slices were aligned parallel to the ventral wall of the fourth ventricle. The slice orientation and placement was selected to minimise inhomogeneity in the main magnetic field (Dunckley et al., 2005). Care was taken to ensure the accurate placement of the functional slices. This was achieved with the use of two planning scans; the first scan was used to align the slices of the second scan perpendicular to the angle of the participant's head. This allowed the same brain region to be collected from each participant. A mean functional image was created from this functional scan, and was used as representative functional data in the testing of the registration pathways.

For midbrain registration optimisation, a whole-brain EPI scan was collected, using the same shim settings and voxel size as the functional run, but with more slices (147 slices; TE, 44ms; TR,14.3s; resolution, 1.5 x 1.5mm; slice thickness, 1.5mm; matrix size, 144 x 144). A T2-weighted structural scan (TE, 80ms; TR, 2000ms; resolution, 1.8 x 1.8 mm; slice thickness, 2.19 mm; 80 slices) and an MPRAGE T1-weighted structural scan (resolution, 1.15 x 1.15 mm; slice thickness, 1.2 mm; 150 slices) were also obtained.

3.3.3. Analysis

For the normalisation step, the use of nonlinear algorithms achieves accurate registration over the whole-brain (Klein et al., 2009). Nonlinear methods apply warps to local brain regions, rather than applying a transform globally. This means individual differences in brain region shape, size and alignment can be minimised as the brain is fitted to the standard template. The non-linear algorithm used here was FNIRT. For the coregistration step linear transforms were applied using FLIRT. Linear transforms are used for within subject coregistration, as there should be no local differences across brain scans from the same participant. Registration pathways were applied to the data using custom scripts that used command line functions from the FSL toolbox.

Three alternative registration pathways were tested for each participant (see Figure 4). For the two-step registration pathway the mean functional image was registered to the T1-weighted structural with a linear transform with three degrees of freedom,

this was then registered to the MNI standard brain template. A larger number of degrees of freedom were not used as this led to large registration errors. For the three-step registration pathway the mean functional image was first registered to the whole-brain EPI that matched the functional data in terms of contrast and resolution. This transform had seven degrees of freedom. This pathway is recommended by FSL (http://www.fmrib.ox.ac.uk/fsl/flirt/ztrans.html) as a way to improve the registration of data with a limited FOV. The whole-brain EPI was then registered to the T1-weighted image (with seven degrees of freedom), and then the T1-weighted image was registered to the MNI template.

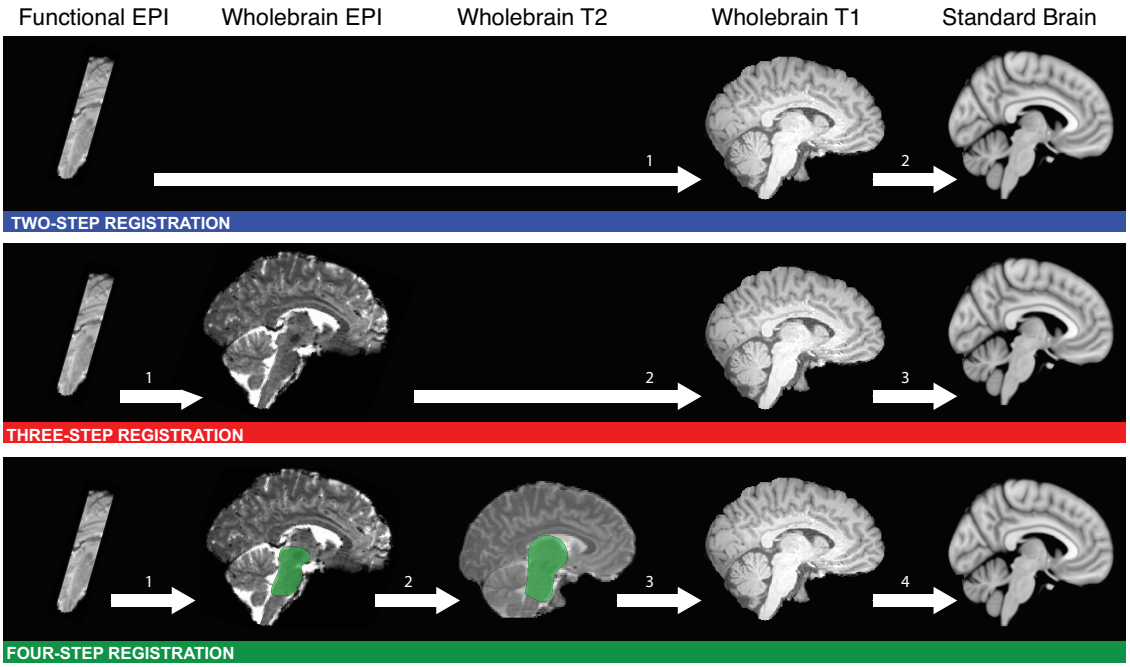

Figure 4: *Three alternative registration pathways. Functional data was co-registered into MNI standard space using three alternative registration pathways. The presence of the green shaded areas in the four-step registration pathway indicates that a binary mask was used to weight the transform to the shaded area.*

Four-step registration started with the same transform of functional data to the whole-brain EPI. This step was then optimised for the midbrain: a hand drawn binary mask that covered the midbrain and pons of the EPI image was used to weight the transform for accuracy within these masked areas. Optimising a registration step in this way has previously been reported (Napadow et al., 2006; Pattinson et al., 2009b). This transform was carried out with seven degrees of freedom. This

corrected for any differences between the mean functional image and the whole-brain EPI image due to head movement between the two scans. The second step was transforming the whole-brain EPI onto a T2-weighted structural scan. As with the first step of this pathway, the transform was optimised using a weighting mask. This binary mask was in the T2-weighted space and covered the thalamus, midbrain and pons. It was drawn once in standard space and transformed onto the individual T2-weighted structural images. EPI images contain distortion in the phase-encode direction, so this adjustment to the transform allowed optimisation of the midbrain by ignoring areas of the brain subject to distortion. This second step was carried out in two stages. The EPI was first transformed to T2 space with seven degrees of freedom. This transformed EPI was the transformed again into T2 space, this time with the binary weighting mask, and again with seven degrees of freedom. The third step was transforming the T2-weighted image onto the T1-weighted structural, a transform that needed no optimisation. This transform was carried out with seven degrees of freedom. The fourth step was transforming the T1-weighted structural into the MNI template. In all three pathways FNIRT was used for this final step, with a warp of 10mm. In all cases, the initial steps (up to the T1-weighted structural) were concatenated into a single transform before being applied to the functional data to avoid image degradation through multiple transforms.

To test the three registration pathways the RN was defined in each participant and transformed into standard MNI space using the transforms derived from the three registration pathways. This structure was selected as it was fully within the FOV of the functional scans, and was clearly identifiable using an automated method free from experimenter bias. No other areas of high contrast were suitable as they were not completely covered by the FOV (e.g. the SN), or could not be defined using the automated method in a way that would ensure exactly the same structures has been selected for each participant (e.g., the tissue-CSF boundaries). In addition, activity was not predicted within the RN during the fMRI task, so the assessment of the registration pathways was independent of the activation results of Chapter 4. The RN was defined in the mean functional images using an automated tool that filled an area with a 3D mask, until a signal intensity change was detected (MRIcro 1.4, Chris Rorden, Georgia Institute of Technology, Atlanta, Georgia, http://www.cabiatl.com/mricro/). The standard location of the RN was identified using

the same tool on a standard MNI T2-weighted template (see Figure 5a). Thus, the location of the participant's RN in standard space, using three registration pathways, could be compared to the 'gold standard' of locating the RN on the T2-weighted standard template.

3.4. Results

For each of the registration pathways a group RN mask was created by adding together all ten individual RN masks that had been transformed into standard MNI space. Figure 5b shows the group RN mask for each of the registration pathways. Upon visual inspection, it is clear that the RN is poorly co-localised when the two-step registration pathway is used, with a maximal overlap of 4 individual RN masks. There is a marked improvement with the three-step registration with a greater maximal overlap of 7. However the four-step registration shows the greatest maximal overlap of 8, with a more symmetrical and tightly packed distribution of voxels. Comparing the location of these group RN masks (Figure 5c) shows that the four-step registration results in the best co-localisation with the standard RN mask.

The registration pathways were assessed statistically using a repeated measure analysis of variance (ANOVA). The number of voxels of the standard RN mask that were covered by the individual RN masks was significantly affected by the registration pathway used ($F_{(2, 18)} = 6.52$, $p < 0.05$). Planned contrasts showed that the four-step registration pathway led to more overlap between the group RN mask and the standard RN mask than the two-step registration ($F_{(1, 9)} = 8.89$, $p < 0.05$) and the three-step registration ($F_{(1, 9)} = 6.86$, $p < 0.05$). Accuracy of the different registration pathways was also made on the basis of the number of voxels from the individual masks that fell outside the standard RN mask after normalisation to the template. There was a significant main effect of chosen registration pathway ($F_{(2,18)} = 6.33$, $p < 0.05$). Planned contrasts showed the four-step registration pathway led to fewer voxels outside the standard RN mask than the two-step registration ($F_{(1, 9)} = 8.89$, $p < 0.05$) and the three-step registration ($F_{(1, 9)} = 6.86$, $p < 0.05$), indicating that the four-step registration protocol was more effective. Accordingly it was used to for all subsequent fMRI analyses in this thesis.

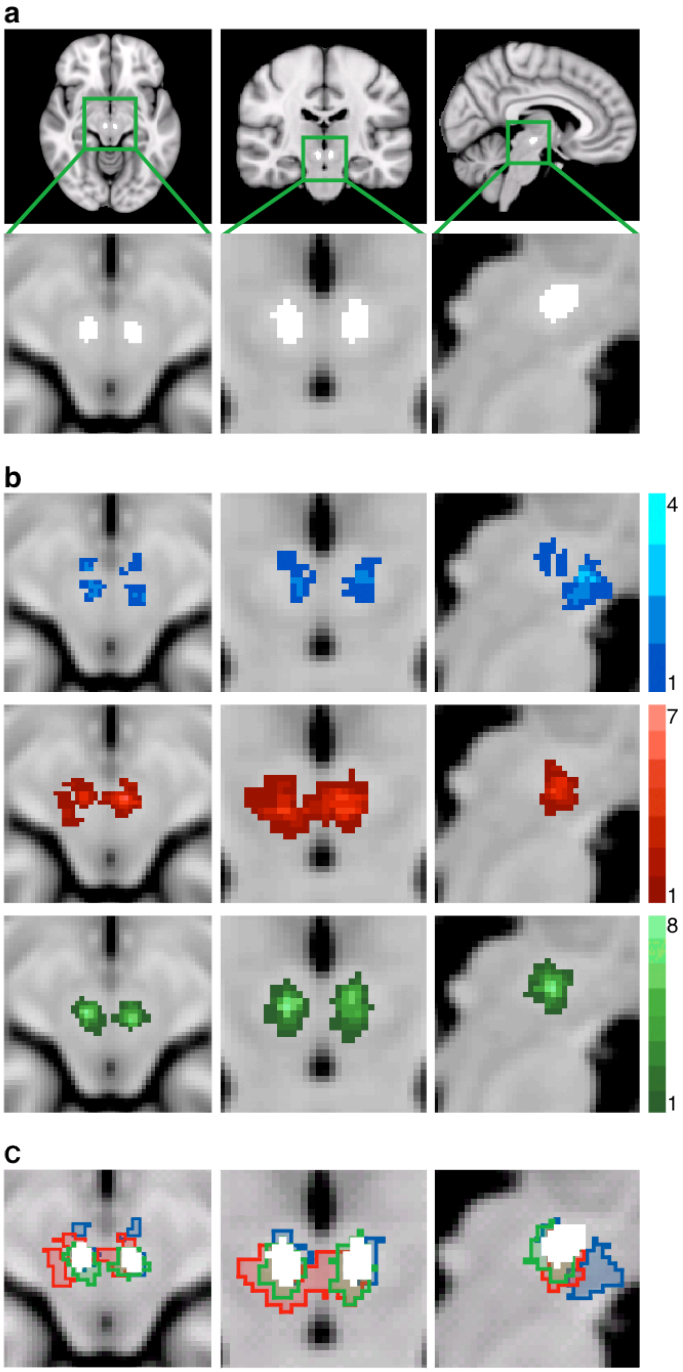

***Figure 5**: Assessing the accuracy of the registration pathways. All images are overlaid on an MNI T1 standard brain. (a) The standard location of the RN, derived from an MNI T2 template. The nuclei are shown in white in transverse, coronal and sagittal planes. (b) For each participant the RN were defined in functional space and then transformed into standard space using the three registration pathways. The group RN maps show the summation of all participants' RN in standard space for each registration pathway (blue = two-step registration, red = three-step registration, green = four-step registration). The legends indicate how many participants' nuclei overlap at each voxel. (c) The standard location of the RN is overlaid on the group RN maps as defined by the three registration methods. All images are shown in radiological convention.*

3.5. Discussion

The four-step registration pathway showed a significant improvement over both the conventional two-step registration used previously in midbrain studies (Krebs et al., 2010; Sigalovsky and Melcher, 2006; Zhang et al., 2006), and the three-step registration pathway recommended by and typically used within the FSL analysis pipeline. The optimised pathway improved the co-localisation of the RN across participants on the standard brain template. There was a greater overlap of the RN between participants and a significantly greater overlap of the group RN mask with the location of the RN on the standard brain template. There were also fewer voxels falsely identified as belonging to the RN when the optimised four-step registration pathway was used. The reasons for the improvement of this method were twofold. First, intermediate scans maintained the contrast of nuclei within the midbrain until the data had been transferred onto a high-resolution structural scan. Thus, the registration algorithms could utilise both the midbrain edges and the borders of the internal midbrain nuclei and maintain registration accuracy throughout this region. Second, the use of weighting volumes prioritised midbrain registration and ignored areas of the brain that suffered from EPI distortion or were of no interest. Although only one nucleus within the midbrain was used in the assessment of the midbrain registration accuracy, it is reasonable to assume that increased accuracy would persist throughout the entire midbrain, as no special efforts were made during the registration optimisation to co-localise the RN over and above any other midbrain area. The use of nonlinear algorithms (FNIRT) ensured accurate registration throughout the whole-brain for the transformation of high-resolution T1-weighted structural images to the standard T1 template, so this step did not require optimisation for the midbrain.

Optimising the registration in this way improved the accuracy with which the midbrain nuclei of individual participants' co-localised on the standard brain template. This reduced any blurring of a genuine signal that would occur with poor co-localisation, and afforded greater confidence when assigning activity to a specific structure.

The optimised registration pathway overcame many of the challenges of midbrain registration, and permits group level analyses across participants on a standard

template, rather than relying on ROI analyses. The use of this type of group level analysis permits voxel-wise comparisons that may reveal regions of activity that are not within pre-determined ROIs, and are not predicted by a prior hypothesis. It also provides the opportunity to detect patterns of activity within an area that have previously been regarded as a single ROI, as functional units of the midbrain may not match the anatomical subdivisions used to define ROIs.

The benefits of optimising fMRI for the midbrain, using the methods described here, also brings with it practical costs. In terms of data acquisition, the added T2-weighted scan requires an additional six minutes of scan time. It would also be difficult to achieve optimum registration at both the level of the cortex and the midbrain simultaneously. Thus the this method should be used in focused and high-resolution midbrain fMRI to identify regions of activity that are induced in certain tasks with greater reliability, which can then be combined with whole-brain studies to look for network interactions. In the following chapter of this thesis I will utilise this optimised four-step registration pathway in the analysis of visual fMRI data.

4. Midbrain optimised fMRI: physiological noise modelling

4.1. Summary

FMRI is relatively insensitive to midbrain changes in BOLD due to the interference of physiological noise. To optimise fMRI for the midbrain I designed a visual fMRI task that was predicted would activate the superior colliculi bilaterally. To reduce the physiological artefacts in the functional data, I estimated and removed structured noise using a modified version of a previously described physiological noise model (PNM). Whereas a conventional analysis revealed only unilateral superior colliculi activity, the PNM analysis revealed the predicted bilateral activity. These methods, when used in conjunction with the optimised registration pathway presented in Chapter 3, improve the measurement of a biologically plausible fMRI signal. Moreover they could be used to investigate the function of other midbrain nuclei.

4.2. Introduction

The midbrain, with the adjacent large basilar artery and its branches, moves in time with the cardiac cycle. Movement in response to the respiratory cycle and pulsatile flow of the cerebrospinal flow also contributes to midbrain movement. See section 1.3.3 for a full description of these sources of physiological noise. In order to reduce the interference from some of these sources of physiological noise, many midbrain fMRI studies use cardiac gating (D'Ardenne et al., 2008; DuBois and Cohen, 2000; Guimaraes et al., 1998; Hawley et al., 2005; Napadow et al., 2009; Sigalovsky and Melcher, 2006; Zhang et al., 2006). In this approach, imaging data is collected in between heartbeats. This assumes that the brain is relatively stable during this time, which will be partially true. Cardiac gating necessarily limits the number of slices that can be collected per volume. In addition, the TR that results from the variable heart rate causes differences in the T1 relaxation (Guimaraes et al., 1998) that requires correction. Most importantly, this approach does not correct for respiratory artefacts or the noise resulting from an interaction between the cardiac and respiratory cycles, or for low frequency fluctuations in heart rate.

Alternative methods have been developed that use physiological measures to model and remove structured noise from fMRI data (Glover et al., 2000; Hu et al., 1995; Liston et al., 2006). Retrospective Image Correction (RETROICOR; (Glover et al., 2000) was originally developed for whole-brain fMRI. Physiological noise is removed by first assigning a cardiac and respiratory phase to each slice of data based on its acquisition time relative to the physiological cycles, then modelling their likely effect on imaging data using a basis set including four Fourier terms. For my data, I used a modified version of RETRICOR, the PNM, which is implemented via the GLM and therefore avoids problems relating to adjusting variance estimates for the loss of degrees of freedom when pre-filtering. The PNM was developed for spinal (Brooks et al., 2008) and brainstem (Harvey et al., 2008) studies. In the brainstem, a significant amount of noise is generated by an interaction between the cardiac and respiratory cycles, which can be successfully modelled with the PNM (Harvey et al., 2008; Pattinson et al., 2009b). In addition, low frequency fluctuations in the heart rate may produce low-frequency noise in fMRI data (Chang et al., 2009), and this is also accounted for within the PNM.

In this study, I applied the PNM to an fMRI experiment using visual stimulation, and compared the resulting activation with those from a conventional analysis without any correction for physiological noise. The visual stimulus was a moving black and white checkerboard, that has been shown with fMRI and an ROI analysis to activate the superior colliculi (DuBois and Cohen, 2000; Schneider and Kastner, 2005) or manual registration (Sylvester et al., 2007). Therefore, any failure to detect a task-related BOLD signal change in the midbrain with this stimulus could primarily be attributed to sub-optimal processing.

4.3. Methods

4.3.1. Data Acquisition

The data collection has been described in Chapter 3, as the same dataset was used for both analyses. See section 3.3.2 for scan parameters used. The ten participants included in the analysis showed minimal movement during the functional scans (less than 1 mm), which improved the chances of good SNR within the midbrain.

Physiological data were recorded using the scanner's in-built system. This included a vector-cardiogram trace via electrocardiogram (ECG) pads on the chest, and a respiratory trace via a pneumatic belt. In order to synchronise the physiological data with the functional scans, the scanner's physiological recording software was modified to simultaneously record a trigger at the beginning of each slice acquisition.

4.3.2. fMRI Paradigm

During the functional scan a visual stimulus was repeatedly presented on a screen visible to subjects lying supine in the scanner. The stimulus was a smoothly rotating semi-circle made of alternating black and white checks that scaled linearly with eccentricity. The checks reversed contrast at 8Hz and the semi-circle rotated at 1Hz. Each presentation lasted for two seconds, with a variable inter-stimulus interval of between 1.4s and 11s. The trials were jittered. Stimuli were presented using the Psychophysics Toolbox extension (Brainard, 1997; Pelli, 1997) for MATLAB (2008b, The Mathworks Inc., Natick, Massachusetts, USA). The task lasted 530s.

4.3.3. Analysis

Data were analysed using FSL. Pre-processing of the functional data included motion correction to the mean volume using McFLIRT, spatial smoothing (FWHM = 2mm), and high pass temporal filtering, applied to all brain images. Prior to model estimation using FEAT (FSL Expert Analysis Tool) v5.98, cardiac peaks (the R-wave) were extracted from the ECG trace, and high frequency scanner noise was removed from the respiratory trace. The regressors of the PNM were estimated from physiological data using a custom MATLAB routine (Brooks et al., 2008).

Two sets of statistical analyses were carried out on the functional data, one with the PNM to remove physiological noise from the data, and one without. The analyses were identical, with the exception of the design matrix used in the GLM.

To estimate and remove the influence of physiological noise from the time series data in the PNM analysis, we applied a modified version of RETROICOR (Glover et al. 2000), which models the cardiac and respiratory cycles using sine, cosine and interaction terms (Brooks et al, 2008). For each slice in the volume, a phase was assigned independently according to its acquisition relative to the cardiac and respiratory cycles. In total, eight cardiac terms, eight respiratory terms, and sixteen interactions terms were used to model the structured physiological noise in the data. A heart rate regressor was also included (Chang et al., 2009). To remove the modelled noise from the data, these variables were included in the GLM. Removing structured noise from the data set in this way makes the detection of genuine effects more likely, and reduces the likelihood of accepting false positives (Harvey et al., 2008).

The PNM regressors were created using custom MATLAB scripts. They were based on the participants cardiac and respiratory traces acquired at the same time as the functional data. Prior to formation of the regressors the respiratory data were smoothed to remove scanner artefacts, and the peaks of the cardiac data were extracted. A cardiac phase was then assigned to each slice of acquired data, indicating during which phase of the cardiac cycle the data were acquired. For the respiratory trace a phase was calculated for each slice that also accounted for the depth of each breath (Glover et al., 2000). There were eight regressors for the

cardiac effects, and eight for the respiratory effects. The eight regressors consisted of the sine and cosine values of the fundamental frequency of the traces (θ_C and θ_R), and the next three harmonics of these sine and cosine terms (the sine and cosine of $2\theta_C$, $3\theta_C$, and $4\theta_C$ for the cardiac terms, and the sine and cosine of $2\theta_C$, $3\theta_C$, and $4\theta_C$ for the respiratory terms). The 16 interaction terms consisted of 8 additive terms, and eight subtractive terms. These were calculated using the following formula:

$$\sin \text{or} \cos\left(A \cdot \theta_C \pm A \cdot \theta_R\right), \text{ where } A = 1,2,3,4.$$

Each regressor was outputted as 4D nifti file. The 4D file had the dimensions:

$$1 \times 1 \times (number\ of\ slices) \times (number\ of\ volumes)$$

This allowed the PNM to apply the 33 terms on a slice by slice, volume by volume basis. A text file that listed the 33 regressors was created, and this text file was entered into the 'confound file list' beta option of FSL v5.98. Prior to analysis these regressors were filtered using a temporal filter identical to the temporal filter applied to the data.

The combination of regressors included in the PNM was not optimised as has previously been done for the brainstem (Brooks et al., 2008). However the inclusion of extra regressors would not impact significantly on the degrees of freedom used in the statistics, as the time-series used in the experiment was long. I therefore decided to include more regressors than had been previously used, to more completely model the physiological noise.

For both analyses, the first level of statistical analysis of the functional data (at the individual subject level) was carried out using a GLM approach. A model of the BOLD response to visual stimulation was constructed by convolving the stimulus input function with a gamma HRF with time-to-peak of four seconds. A temporal derivative of the visual stimulation and a single regressor that described global head motion were also included. For the PNM analysis, the 33 physiological regressors were also included in the GLM. Group statistics were carried out using FLAME (a mixed effects

analysis to account for between subject variance). Variance that was explained by, and was unique to the visual regressor, was represented as a statistical map, which was subsequently tested using RANDOMISE to correct for multiple comparisons. All statistical images were cluster-corrected to a significance level of $p < 0.05$, with a nominal *t*-value of 2.3, using standard cluster correction within RANDOMISE. Task activation was tested against an implicit 'rest' baseline. Prior to thresholding, a hand drawn mask was applied to the functional data to include only voxels from the superior and inferior colliculi. Voxels within the inferior colliculi were included to ensure that the visual response was correctly localised to the superior colliculi. The colliculi were defined on the MNI template using an anatomical atlas (Naidich et al., 2009). Figure 6a shows the location of the superior colliculi on the MNI template.

4.4. **Results**

The resulting statistical maps are shown in Figure 6b. Conventional analysis revealed a significant response in voxels within the right superior colliculus alone. When the PNM was included in the GLM, visual activity was localised to both superior colliculi. To check that possible left superior colliculi activity in the conventional analysis was not hidden due to conservative cluster thresholding, the analysis was repeated with a less conservative threshold ($T > 1.83$). Even with this low threshold (corresponding to uncorrected $p < 0.05$), no activity was revealed in the left superior colliculus without the PNM.

The distribution of the *Z*-scores of all voxels within the right and left superior colliculus in both the conventional and PNM analysis is shown in Figure 7. There is an increase in the number of significant voxels in the right superior colliculus when the PNM is included in the GLM (from 103 voxels to 148). However the main effect of the PNM is the recovery of significant voxels in the left superior colliculus (83 voxels with PNM). However, this cluster extends by 28 voxels into the left inferior colliculus, suggesting that it is not as well localised as the right superior colliculus activity.

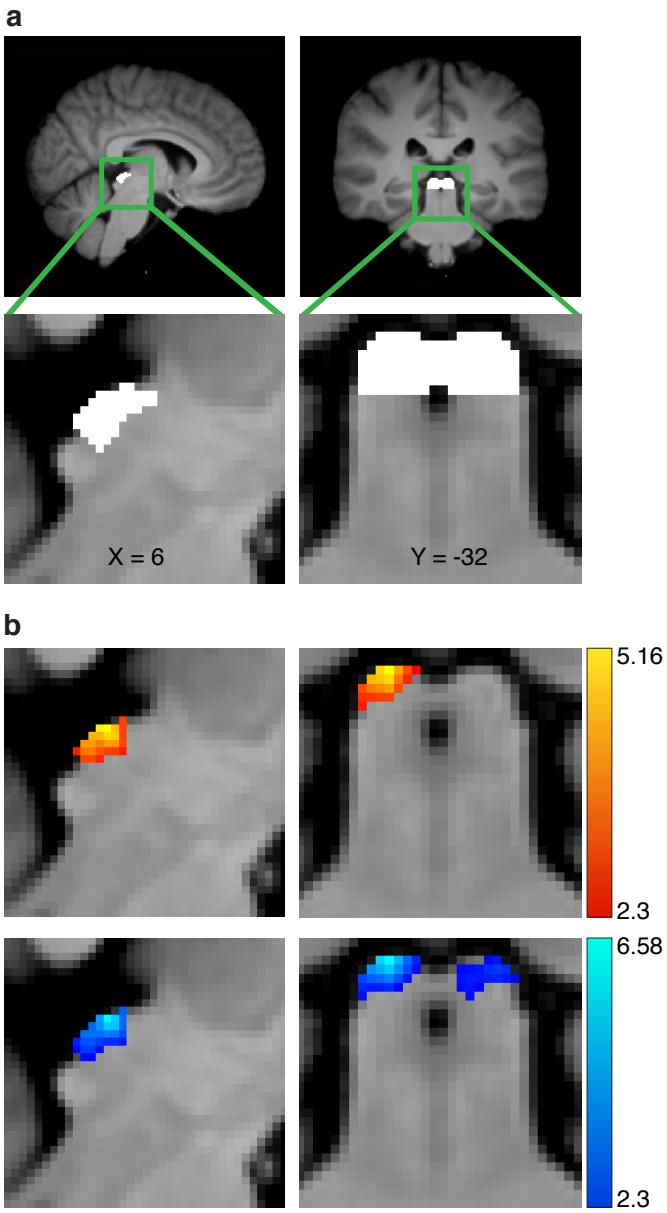

Figure 6: *Visual fMRI experiment results. (a) The location of the superior colliculi, defined using anatomical boundaries on the group T1 standard brain, are shown in coronal and sagittal planes. (b) The superior colliculi responded to visual stimulation. Statistical maps computed from data without PNM revealed activity in the right superior colliculus only. The pattern of activation was modified when including a PNM, to include activity in the superior colliculi bilaterally. The statistical maps show significant clusters of voxels within a colliculi mask (determined using non-parametric permutation testing with a corrected threshold of p b 0.05 and a nominal t-value of 2.3) The t-values of the voxels within significant clusters are indicated by the legends. The top panel (red-yellow) shows unilateral superior colliculus activity revealed using a traditional analysis. The lower panel (blue-light blue) shows bilateral superior colliculi activity revealed using the PNM analysis. All images are shown in radiological convention.*

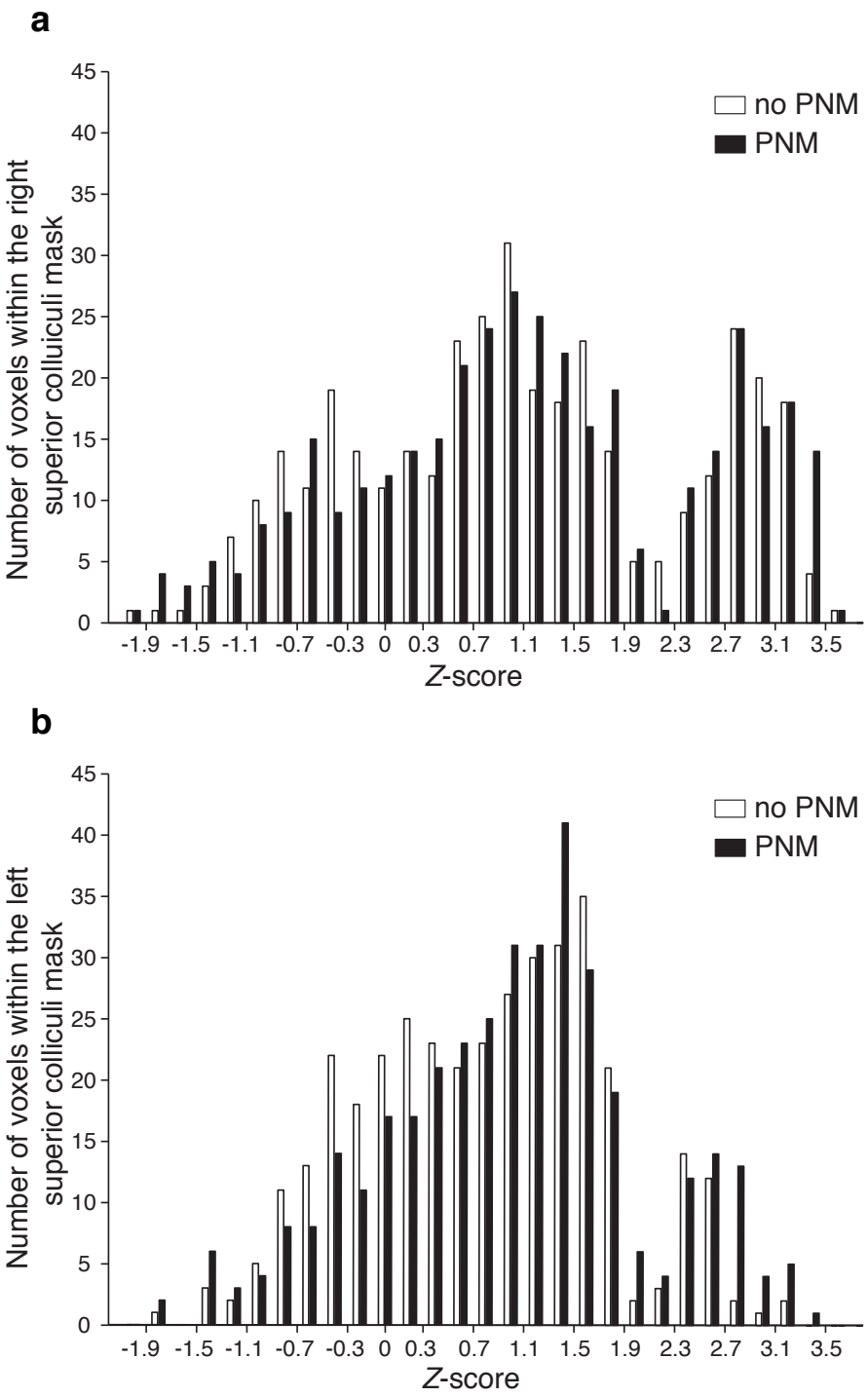

Figure 7*: The distribution of Z-statistics in the superior colliculi revealed with the traditional and the PNM analysis. Histogram showing the Z-score distribution of voxels within the right (a) and left (b) superior colliculi for both analyses (white = conventional analysis, black = PNM analysis).*

To check that the PNM did not lead to further false positives outside of the colliculi, and to investigate the signal blurring that had occurred in the left inferior colliculus for the PNM analysis, we repeated the analysis using a mask that covered the entire midbrain. Using this larger mask we found clusters of activity adjacent to the left superior colliculus with both the conventional and the PNM analysis. In the case of the conventional analysis this cluster was adjacent to the left superior colliculus and extended across 56 voxels. For the PNM analysis this cluster extended from the left superior colliculus, but also included 46 voxels outside the superior colliculi. Thus, when compared to the conventional analysis, the PNM revealed biologically plausible and expected areas of activity in the left superior colliculus, and reduced the number of voxels outside the superior colliculi marked as active. Activity in the right superior colliculus was well localised for both the conventional and PNM analysis, with only six and thirteen voxels within the midbrain that were not within the superior colliculus boundary respectively. No other clusters were revealed outside of the superior colliculi, which is consistent with our hypothesis.

4.5. Discussion

Modelling and removing noise with the PNM significantly improved the ability to measure a BOLD signal from the human midbrain. Including cardiac, respiratory, interaction, and heart rate regressors in the GLM removed structured physiological noise from the data and led to an increased number of voxels that were demonstrated to be significantly active in response to the visual stimulus. Activity in the left superior colliculus, which had been masked by physiological noise, was revealed by the PNM analysis. The number of false positive voxels was also reduced in the PNM analysis, compared to the conventional analysis. This result is consistent with electrophysiological recordings from the superior colliculi in awake primates, which show that each colliculus holds a representation of the contralateral visual field (Goldberg and Wurtz, 1972). The visual stimulus used in this study covered both sides of the visual field, and so would have resulted in activity in both the left and right superior colliculus.

Unlike RETROICOR, the PNM has been specifically optimised for the spinal cord and brainstem (Harvey et al., 2008). Due to the noise characteristics in these regions, higher harmonics of the physiological cycles explain significant noise in the data, so are included in the PNM. This is the first time the PNM has been tested with such high-resolution scans. It is essential to use such small voxels in midbrain fMRI, as it allows accurate localisation of activity to specific nuclei, and reduces partial volume effects. However, as voxel size decreases, so does the SNR of the fMRI data, making it more difficult to detect real signal (Edelstein et al., 1986). This study has shown that it is possible to measure a midbrain signal at high resolution, and that using the PNM increases the effective temporal SNR (Cohen-Adad et al., 2010; Hutton et al., 2011), and permits detection of significant effects in a relatively small group size of ten subjects. We demonstrate that the PNM is effective within the superior colliculi, and the PNM has previously been shown to be effective within the spine (Brooks et al., 2008; Cohen-Adad et al., 2010) and the motor areas of the brainstem (Harvey et al., 2008). In addition, it has been shown that physiological noise in the brainstem is widespread and spatially non-specific (Harvey et al., 2008). Thus, it is likely that the PNM will be effective in other areas of the midbrain, although this will require further investigation.

Recently, an alternative method has been developed to remove physiological noise from fMRI data using reference voxels that are assumed to contain signal unrelated to stimulation to model noise in the time series data (de Zwart et al., 2008). This method has been applied to superior colliculi data (Wall et al., 2009), using an area of the cerebellum as a reference region. However this method carries the risk of removing “functional” signal from the data, or conversely not removing all the physiological noise. If the noise properties vary between the reference and task regions, noise removal will not be optimal. Whilst it may be safe to assume the physiological noise is similar between the dorsal midbrain and the adjacent ventral cerebellum, this assumption would be less valid in more ventral portions of the midbrain. Thus, a single reference region cannot adequately model noise throughout the whole midbrain. The PNM, however, models noise on a voxel by voxel basis, and therefore accounts for local variations.

The methods presented here use a limited FOV. Whilst it is necessary to do this to allow higher resolution scanning at a reasonable temporal resolution, this does limit the number of regions that can be investigated. This is further restricted by the optimised registration, which focuses on the midbrain, potentially at the expense of regions outside this area. This means that subcortical and cortical regions that the midbrain is interacting with at a network level cannot be investigated. The PNM has previously been tested in the brain and spinal cord (Cohen-Adad et al., 2010) and shown to effectively increase the temporal SNR in both regions. Thus it may be possible to investigate cortical and midbrain networks using the PNM. However this would not be optimised for the midbrain to the same extent as the methods presented here, as the larger voxels required for whole-brain coverage would be less reliable at assigning activity to a specific midbrain nucleus, due to their small size and tightly packed arrangement.

Finally, the sample size used here was small, and although this was sufficient for these purposes, a larger sample size may be required for future studies, particularly if more complex tasks are administered that might evoke more subtle neuronal responses.

The methodology presented here improves on previous techniques used to measure BOLD responses in the superior colliculi. Earlier studies did not attempt to optimise midbrain registration, and either used an ROI approach to extract signal (DuBois and Cohen, 2000; Kennerley and Wallis, 2009; Schneider and Kastner, 2005, 2009; Sylvester et al., 2007), or relied on standard registration techniques (Krebs et al., 2010). Many studies have not attempted to reduce the effect of physiological noise (DuBois and Cohen, 2000; Krebs et al., 2010; Schneider and Kastner, 2005, 2009), whilst others have only corrected for cardiac effects (Sylvester et al., 2007) or applied corrections that are specific to only one area of the midbrain (Wall et al., 2009).

The methods outlined here can be used to further investigate properties of the superior colliculi, such as the functional difference between the superficial and deep layers and retinotopic organisation (Cynader and Berman, 1972). However the purpose of the developments of the methods here is to apply these optimised methods to the measurements of reward systems in the human midbrain. Previous

attempts to image these dopaminergic nuclei have either used cardiac gating (D'Ardenne et al., 2008), RETROICOR (Guitart-Masip et al., 2011), or conventional fMRI (Aron et al., 2004; Chase and Clark, 2010; Murray et al., 2008; Waltz et al., 2009; Wittmann et al., 2005). The PNM must also be tested in the dopaminergic midbrain to see if it reduces the impact of physiological noise. It is not known, for example, how similar the vasculature and noise properties of the VTA and SNc are to the superior colliculi, and it is likely that there are some differences due to their differential anatomical location. The next chapter of this thesis will address these issues.

5. Reward and punishment prediction errors (PEs) in the dopaminergic midbrain

5.1. Summary

In this chapter, I present the results from my investigation of the role of the dopaminergic midbrain system in positive and negative PEs. I used the optimised fMRI methods presented in the previous chapters. A financial gain and loss task was used to elicit positive and negative PEs, and these were compared to a zero PE baseline. The medial dopaminergic midbrain system showed an increase in BOLD to both positive PEs and negative PEs.

I also present the results into an investigation of the value of the PNM in the study of dopaminergic midbrain system using fMRI. This includes quantifying the noise that is explained by the PNM regressors, and a comparison of the GLM analysis with and without the PNM. I demonstrate that the PNM does explain noise in the midbrain, including regions of the dopaminergic midbrain system, and by including the PNM in the analysis I revealed a more extensive cluster of activity than was seen without the PNM.

5.2. Introduction

Dopamine neurons in the VTA and SNc are involved in the processing of appetitive, rewarding events. In particular they code for when outcomes are better than expected: a positive PE signal. This has been demonstrated in the monkey (Fiorillo et al., 2003; Schultz et al., 1997; Tobler et al., 2005), rodent (Wang and Tsien, 2011), and human (D'Ardenne et al., 2008; Zaghloul et al., 2009). However, as reviewed in Chapter 1, non-human evidence suggests they may also code for aversive, punishing events (Brischoux et al., 2009; Guarraci and Kapp, 1999; Joshua et al., 2008; Mantz et al., 1989; Matsumoto and Hikosaka, 2009; Mileykovskiy and Morales, 2011; Valenti et al., 2011; Wang and Tsien, 2011), and thus code for negative PEs (i.e., when an outcome is worse than expected).

Relatively little is known about how such theories of midbrain function, based on non-human research, apply to the human. A positive PE signal has been observed in the human using midbrain optimized fMRI (D'Ardenne et al., 2008), but no BOLD response was detected for negative PEs. This is inconsistent with the non-human literature on punishments, and punishment predicting stimuli. In addition, D'Ardenne and colleagues (2008) report no response was observed in the SNc, which is inconsistent with non-human recordings of positive PEs (Bayer and Glimcher, 2005; Fiorillo et al., 2008; Fiorillo et al., 2003; Schultz et al., 1997). I hypothesised that there were two reasons for the absence of a negative PE signal.

The first is that the overall context of the task used by D'Ardenne and colleages (2008) may have been rewarding. There is evidence to suggest that the context of the PE may influence the response of the neurons (Nakahara et al., 2004). For example, if the environment is overall a rewarding one, the individual negative PEs may not be processed as expected, as the final outcome will be rewarding. This is relevant for fMRI experiments, as each participant expects to win in the end. If the participant begins a game with no money, they implicitly know they will not be leaving the experiment with an overall loss (otherwise, once the word gets out, the experimenter will have trouble recruiting further participants). Thus, such a design may bias against the detection of negative PEs. This problem was highlighted by Seymour and colleagues (2007) in their discussion of negative PEs in the striatum.

The second possible reason for the absence of a negative PE signal in the results of D'Ardenne and colleagues (2008) is due to the methodology that was used to minimise physiological noise. Cardiac gating was used during acquisition to reduce the influence of cardiac related noise in the fMRI data. However no attempt was made to remove the respiratory related noise, or the noise that results from the interaction of the two noise sources (Brooks et al., 2008; Harvey et al., 2008), or indeed the slower changes in heart rate over time that explain noise in the data (Chang et al., 2009).

Here I used a Pavlovian conditioning task that has been shown to evoke BOLD responses to negative PEs, as well as positive PEs, in the ventral striatum (Seymour et al., 2007). The participant was paid £20 for participation in the experiment. This is a standard amount to be paid for participation in an fMRI experiment that takes approximately two hours. During the task, the participant could win money to add to this £20, or lose money that would be taken away. Thus, although the participant implicitly knew they would be leaving with a financial gain, the losses were more 'ecologically valid', as they were losing money they had already been given.

In Chapter 4, I demonstrated that the PNM improves the sensitivity of fMRI to a midbrain signal by reducing the impact of the physiological noise on the statistics. However, just one midbrain region was tested: the superior colliculi. The colliculi are on the dorsal wall of the midbrain, adjacent to the fourth ventricle. In contrast, the dopaminergic midbrain neurons lie more ventrally. Some regions (such as parts of the SNc) are embedded amongst other brain tissue, relatively remote from CSF. Other regions, such as the VTA, medial SNc, and very lateral portions of the SNc, have components that are close to the CSF of the basal cistern. Thus, it is important to establish the value of PNM when studying the dopaminergic midbrain system with fMRI, as this region is likely to have different noise properties compared to the colliculi.

A strength of the PNM is that it models the noise on a voxel-wise basis. Therefore, if there is cardiac and respiratory noise in the dopaminergic nuclei, the PNM will adapt to the different noise properties of the region. However, it cannot be assumed that the PNM will be as effective for the dopaminergic midbrain system as it proved to be

in the proof-of-principle investigation of the signal in the superior colliculi (Chapter 4). First, the basic properties of the noise may differ, and may not be as well explained by the regressors of the PNM. Second, the magnitude of this noise in comparison to the noise present in the colliculi was not known. If the noise were to prove to be greater than in dorsal midbrain, recovery of task-related signal might not have proved possible. To exacerbate this, the task-related change in the BOLD signal may be of a lesser magnitude for reward-related activity in comparison to a primary visual response of the colliculi.

The effect of the PNM on the midbrain as a whole has been investigated (Harvey et al., 2008), and it was demonstrated that the PNM reduces the variance across the region. They produced a map showing the change in variance across a sagittal view of the midbrain, but differences within particular sub-regions of the midbrain were not explicitly investigated. The noise properties of the dopaminergic midbrain system have recently been characterised in a *whole-brain* study using RETROICOR, without the additional regressors included in the PNM (Klein-Flügge et al., 2011). In this case, whole-brain maps of the noise in the data were created before and after correction. They found that the dopaminergic midbrain system was prone to physiological noise, as there was a relatively large change in the variance of the data. This was particularly true for regions adjacent to CSF. However, in both the above studies, no statistical analysis of the variance reduction was presented. Additionally, larger voxel sizes were used than are presented here. With large voxels there is a greater influence of partial volume effects. The midbrain is particularly prone to partial volume effects in terms of CSF signal being combined with tissue signal, and this is exacerbated by the use of larger voxels. Thus there is likely to be less influence of physiological noise if smaller voxels are used (Bodurka et al., 2007).

To investigate the use of the PNM within the dopaminergic midbrain system, I analysed these data with and without the inclusion of the PNM. In addition, I quantified the amount of variance that was explained by the PNM across all individuals, and created an image of voxels where significant physiological noise was explained by the PNM. This is the first time that midbrain noise properties with high-resolution fMRI scans has been investigated in this way.

Here I show that the dopaminergic midbrain system returned an increase in BOLD signal in response to both positive and negative PEs. There was considerable overlap between the two patterns of activation. Furthermore, inclusion of the PNM revealed a more extensive pattern (extending into lateral SNc) of activity than was observed without reduction of the physiological noise.

5.3. Methods

5.3.1. Subjects

Approval for this study was granted by the Imperial College Research Ethics Committee. 42 healthy subjects participated in this experiment (22 female; mean age, 26.4yrs). Eleven participants were excluded leaving 31 participants (16 female, mean age, 26.6yrs). One participant was excluded due to a brain abnormality, three due to excess motion (over 2mm), and a further seven that did not learn the task contingencies whilst in the scanner (see section 5.4.1, Behavioural results).

5.3.2. fMRI task

The task was a passive Pavlovian learning experiment, where participants observed cue-outcome contingencies. Visual cues were abstract fractal images (www.fractaldomains.com). Each cue was presented for 3s, and was followed by an actual financial outcome that was presented for 1.5s. This outcome was either nil (represented as an empty circle), a financial gain (represented as a photograph of the amount won), or a financial loss (represented as a photograph of the amount lost, with a red line running through it). The amount was also written under the image, along with a tally of current total winnings. See Figure 8 for the cues, their associated outcomes, and their mean expected values. Cue A reliably led to a nil outcome, whereas cues B, C, D, and E led to two equally probable outcomes each. Participants were naïve to the cues and their outcomes prior to the fMRI scan, so the initial expected value of each cue was nil. After repeated presentations, according to the temporal difference model of learning, the cues had an expected value that was equal to the mean of the two outcomes. On each trial, the expected value of each

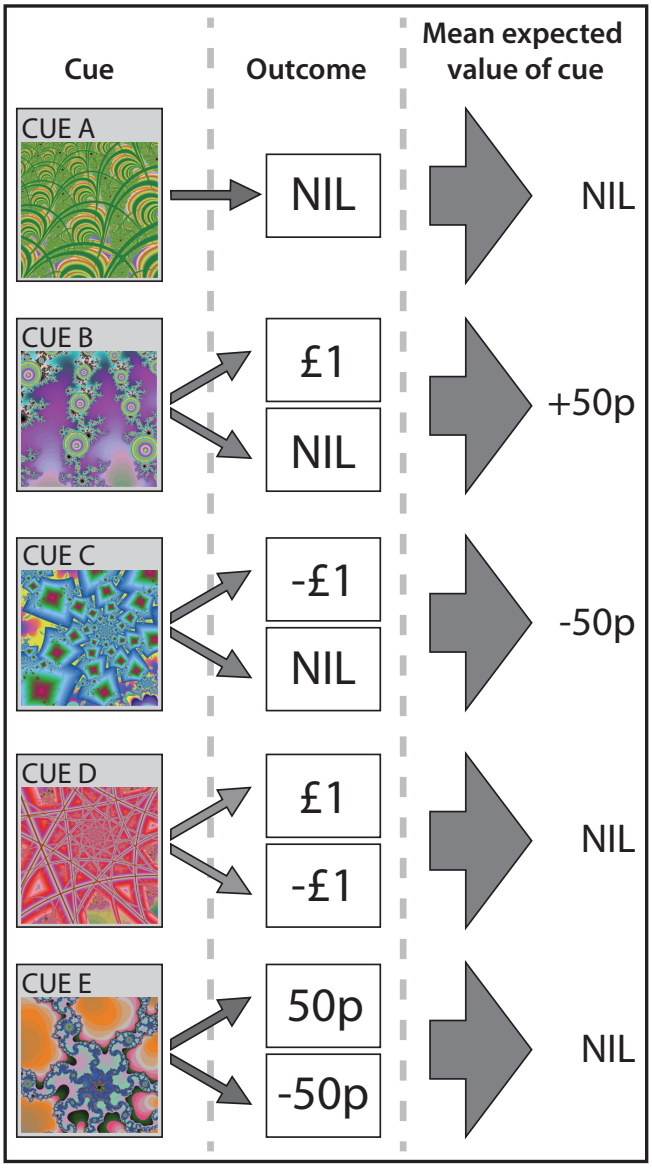

Figure 8: *Experimental design: the cue-outcome contingencies. Cue A reliably led to a nil outcome, cues B to E led to one of two outcomes at equal probability. According to the temporal difference model of learning, the mean expected value of each cue B to E is the mean of the two possible outcomes, as the two outcomes occur with equal probability.*

cue, v, was updated based on the outcome. This is represented by the following formula:

$$v \leftarrow v + \alpha\delta$$

where α is the learning rate, and δ the error term.

Thus, if two outcomes appear with equal probability, the mean expected value of all trials will be the mean of the two values. This is the mechanism by which predictions are modified to more accurately represent future outcomes, based on the error terms previously experienced.

The error term is calculated as the difference between the actual outcome (r) and the expected value of the cue:

$$\delta = r - v$$

Thus, according to the temporal difference model, the gain outcomes, and the nil outcomes of cue C, elicit positive PEs. The loss outcomes, and the nil outcomes of cue B, elicit negative PEs.

Cues were presented in a pseudo-random order with a variable inter-trial interval (0.5 - 4 s) with jitter relative to the TR. Stimulus order was optimised using the optseq2 algorithm. Stimuli were presented using the Psychophysics Toolbox extension for MATLAB. There were three ten-minute functional runs in the scanner, with each run containing a mean of ten trials of each cue-outcome contingency. Participants were paid £20 for participating in the study, and any gains or losses they received whilst in the scanner were added to or taken away from this initial total. There were four functional runs of this task, each lasting 623s.

5.3.3. Behavioural task

In order to ensure that participants paid attention during the passive task, they were told prior to scanning that they would be tested on what they had learnt, and if they performed well they could win a £5 bonus. In addition, this ascertained which participants had learnt the contingencies during the task. The test took the form of a preference task. Pairs of visual cues were presented on a laptop screen outside of the scanner, and participants had to choose which cue they would prefer with a button press. Each cue was paired with every other cue, and each pairing was presented ten times. If the participants correctly chose the cue with the higher expected value over 50% of the time, they received immediate feedback that they had earned the financial bonus. Choices they made when cues had equal expected value were not included in this scoring.

5.3.4. MRI acquisition

MR scanning was performed on the same scanner as previously described, and physiological measures again collected. Functional MR images were obtained using a T2*-weighted, EPI sequence with a field-of-view that covered the long axis of the brainstem (TE = 44ms, TR = 1900ms, flip angle = 90°; resolution, 1.7 × 1.7mm; matrix size, 200 × 200 x 36mm; slice thickness, 1.7mm; 21 coronal slices; no slice gap; interleaved slice order; SENSE, 2). There were four functional runs, each containing 322 scans, and lasting 623s. A matching whole-brain EPI (141 slices; TE = 44ms; TR = 12640s; matrix size, 200 × 200 x 240mm) was also collected. In addition to the T1-weighted and T2-weighted structural images that have previously been described, a dual-echo structural image was collected along the long axis of the brainstem with a T2 and PD contrast to visualise midbrain nuclei (TE of 16ms and 80ms respectively, TR = 4000ms, resolution, 1.3 x 1.3mm; slice thickness, 1.3mm; 32 coronal slices; matrix size, 240 x 180 x 42mm).

5.3.5. Analysis

Pre-processing was carried out in an identical manner to the procedures described in Chapters 3 and 4, with the exception of the spatial smoothing, which had a slightly increased FWHM of 3mm. This was because the region of interest was larger than the colliculi that I had previously investigated, and the prediction was that the SNR would be less for a reward response than a visual sensory response. Midbrain optimised registration, as described in Chapter 3, was used. A GLM approach identical to Chapter 4 was used for the statistical analysis, but a slightly longer HRF of 4.5s was used. The physiological data were processed in an identical manner to that previously described, and 33 physiological noise regressors were created for each individual. At the first-level of the analysis a GLM was created for each individual, for each run of the experiment. A fixed effects analysis was carried out at this level. The second-level of the analysis combined the runs of each individual, again a fixed-effects analysis as it was within-subject. At the final level the results of all individuals from the second-level, were combined. This analysis was mixed-effects.

5.3.5.1. Main effects analysis

Using the above methods two separate analyses were carried out, one without the PNM and one with the PNM. In both analyses, the regressors entered into the model included:

- The first that represented the onset of the cues.
- The second that represented outcomes that elicited a positive PE (all the financial gain outcomes, and the better than expected nil outcome).
- The third that represented outcomes that elicited a negative PE (all the financial loss outcomes, and the worse than expected nil outcome)
- The fourth that represented outcomes that did not elicit a PE (the expected nil outcomes).

In the first analysis the noise regressors consisted of six head motion parameters, and in the second analysis the 33 physiological noise regressors were also included.

Prior to thresholding, a hand-drawn mask was applied to the functional data to include only voxels within the midbrain. This was defined on a standard brain by using anatomical boundaries:

- The dorsal edge of the midbrain was defined by the borders of the colliculi.
- The ventral boundary was defined by the border of the cerebral peduncles with the basal cistern.
- The caudal edge was defined by the cessation of the high intensity region representing the SN.
- The rostral edge was defined by a line drawn from the rostral edge of the superior colliculi and the cerebral peduncles.

The statistical maps were again thresholded using RANDOMISE, with a nominal *t*-value of 2.3 ($p < 0.05$).

5.3.5.2. The utility of the PNM

In addition to comparing the resulting statistical maps from the two analyses to test the value of the PNM when investigating the dopaminergic midbrain system, further

analysis was required. This was because it was not immediately obvious from the results if the PNM was improving the statistics (unlike the results from the superior colliculi, where the inclusion of the PNM led to an improvement in *t*-scores of voxels within this region).

To further investigate the PNM, I used an *F*-test to reveal the amount of variance that was being explained by the 33 physiological regressors at each voxel. For each individual the resulting maps were thresholded ($F_{(33,197)}$=1.45, $p < 0.05$, uncorrected) and binarised, to create a map for each individual representing significance as a binary value. These individual maps were added together to create a group overlap image of significant voxels. This overlay image was analysed using the binomial probability distribution function to calculate a probability value for each voxel in the overlap mask. The binomial probability density function can be used to calculate the probability of an observation occurring by chance when there are two possible outcomes. In this case it calculated, for each voxel, the probability of the observation (the number of participants who show significant activation), taking into account the size of the group and the error rate of the *F*-test.

This probability map was then thresholded at $p < 0.05$ using a false discovery rate (FDR) (Genovese et al., 2002) to correct for multiple comparisons. The analysis was repeated with a more conservative threshold ($p < 0.001$) for the *F*-test and FDR correction, and the same pattern of results was observed.

FDR correction was selected to correct for multiple comparisons, as traditional cluster correction is inappropriate for unsmoothed data, and voxel-wise correction would have been too conservative. Instead of controlling the Type I error rate (false positives) for all voxels in the overlap image, FDR correction controls for the Type I error rate for the voxels that are positive, and ignores voxels that accept the null hypothesis. Thus FDR correction adapts to the dataset in question, and is less conservative than voxel-wise correction.

5.3.5.3. PE responses elicited in the absence of financial outcomes

A second model of the experimental variables was analysed. In this model the regressors entered into the GLM were identical to the PNM analysis (see section **Error! Reference source not found.**), but the PE regressors were further subdivided. Rather than all positive PEs being represented as one variable, they were split into positive PEs that were elicited by a financial gain, and positive PEs that were elicited by a better than expected nil outcome. Similarly, negative PEs were split into PEs elicited by a financial loss, and PEs elicited by a worse than expected nil outcome. This analysis allowed the investigation of the nil outcomes to see if PE responses could be elicited in the absence of financial outcomes. The following four following contrasts were modelled:

1. Positive PE (elicited by a gain outcome) > zero PE
2. Positive PE (elicited by a nil outcome) > zero PE
3. Negative PE (elicited by a loss outcome) > zero PE
4. Negative PE (elicited by a nil outcome) > zero PE

The first step of this analysis was to analyse the responses to these contrasts on a voxelwise basis, using an identical method to that presented for the main effects analysis above. The outputs of contrasts three and four were assessed to see if there was a midbrain response to PEs in the absence of financial outcomes. The voxelwise results of the first two contrasts were binarised to create a binary map of regions that showed a significant BOLD response to positive PEs elicited by gain outcomes, and positive PEs elicited by loss outcomes. These binary maps were then used for an ROI analysis using Featquery. The ROIs were defined using the gain and loss contrasts to avoid using the nil PE outcomes in the creation of the ROI, which would be a circular analysis.

5.3.5.4. Parametric analysis: the temporal difference model

The final analysis made use of the temporal difference model outlined in section 5.3.2. This model represents the learning of the participants throughout the task.

There was no learning phase prior to the scanner task, so the EV of each cue could be modelled as zero at the start of the task. According to the temporal difference model, as the participant's experienced cue-outcome contingencies, their expected value of each cue would be updated on a trial-by-trial basis. This varying EV associated with each cue would modulate the PE associated with each outcome.

Custom Matlab scripts were utilised to update the EV on a trial-by-trial basis. As the order of trials was different for each participant, this was carried out for each individual. A learning rate of 0.5 was chosen for each participant, as I had no measure of individual learning rate during the task.

To create a GLM using this model, each trial was categorised according to its relative level of PE. For each subject the positive PE outcomes were listed by magnitude, this list was then subdivided equally into six bins, varying from low PE, to high PE. The same was done for the negative PEs. This method of categorisation was chosen over and above the categorisation by a fixed level of PE, as the range of PEs experienced by each individual varied considerably due the trial order differences.

These 12 regressors were then entered into the GLM, along with cue onset, the PNM regressors, and motion regressors. The 12 regressors themselves were not parametrically modulated; instead a parametric analysis could be compared by looking for a BOLD signal that correlated with increasing level of PE. To do this the six level of positive PEs (from low positive PE to high positive PE) were contrasted using the following demeaned weightings:

-5 -3 -1 1 3 5

Any voxels that showed a significant positive response to this contrast would increase their BOLD response in a linear manner with the level of positive PE. The same contrast was constructed for the negative PEs, from low negative PE (near zero), to high negative PE (far from zero). In addition, each level of PE was contrasted against the zero PE baseline, and these contrasts were used fro an ROI analysis. The regions used for the ROI analysis were binarised masks of the

midbrain clusters that were associated with positive PE and negative PE from the main effects analysis (Figure 13).

5.4. Results

5.4.1. Behavioural results

If participants chose cue C (which had an expected value of -50p) more frequently than cue B (which had an expected value of +50p), they had not learnt the contingencies whilst in the scanner, and so they were excluded from the analysis. Seven participants fitted this criterion and were removed, and data from the remaining thirty-one participants is presented here.

A preference score was calculated for each cue, based on the number of times it was selected in the preference task. Figure 9 shows the mean preference score for the included participants.

At the group level, a one-way repeated measures ANOVA revealed a significant effect of cue $F_{(4,120)}=35.43$, $p < 0.01$. Planned contrasts revealed participants chose Cue B (expected value= +50p) significantly more than Cue A (EV = nil), $F_{(1,30)}=75.07$, $p < 0.01$, and Cue A significantly more than cue C (expected value = -50p), $F_{(1,30)}=10.13$, $p < 0.05$. These results show that, for cues A, B, and C, the preference score reflects the expected value of these cues. Therefore PEs should be elicited by the outcomes of these cues. Planned contrasts are not reported for cues D and E, as these cues have bivalent outcomes with a nil expected value, and so there are further factors involved in the decision making process for these cues, such as risk behaviour. It is not a simple expected value comparison, as the cues have an equal expected value as cue A.

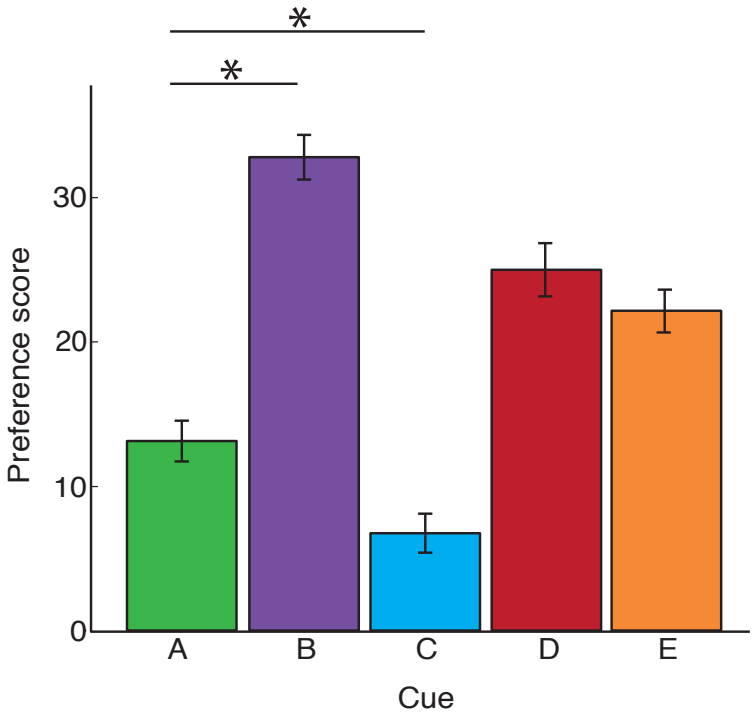

Figure 9: *Results from the preference task. Error bars represent standard error. * represents significant differences (p < 0.01) as reported in the text.*

5.4.2. Localising the dopaminergic midbrain

The location of the midbrain relative to the whole brain can be seen in Figure 10. Whilst there are slices where there is considerable overlap between the SN as defined on PD (Figure 10c) and T2 images (Figure 10d), the are also considerable disparities between the two definitions. At the transverse plane of *z* = -12mm, there is considerable disparity between the region of high intensity on the PD images used to define the SN, and the region of low intensity used to define the SN on the T2 image. The low intensity region of the T2 image also includes portions of the cerebral peduncles. In addition the full extent of the SN is better represented on the PD scan, as a region of high intensity on the PD image represents the caudal section (*z* = -20) of the SN, whereas this same region is of uniform intensity on the T2-weighted scan. This disparity is in line with previous investigations of the SN on MRI images, and from this point forward all images are represented on the group average PD image. However to ensure that the definitions I used represented the underlying anatomy as accurately as possible, histology slices (Figure 10b) (adapted from Naidich et al., 2009) were used to inform the definitions. The boundaries of the dopaminergic midbrain system shown in Figure 10 were defined using a combination of the

anatomical landmarks visible on the histology slices and the regions of high intensity on the PD image. The SNc was defined at the dorsal portion of the SN, and the VTA as the region bordering the medial edge of the SNc and the red nuclei. However anatomical subdivisions within the human SN and VTA are not well understood, as discussed in section 1.2.1, so these boundaries are an estimate.

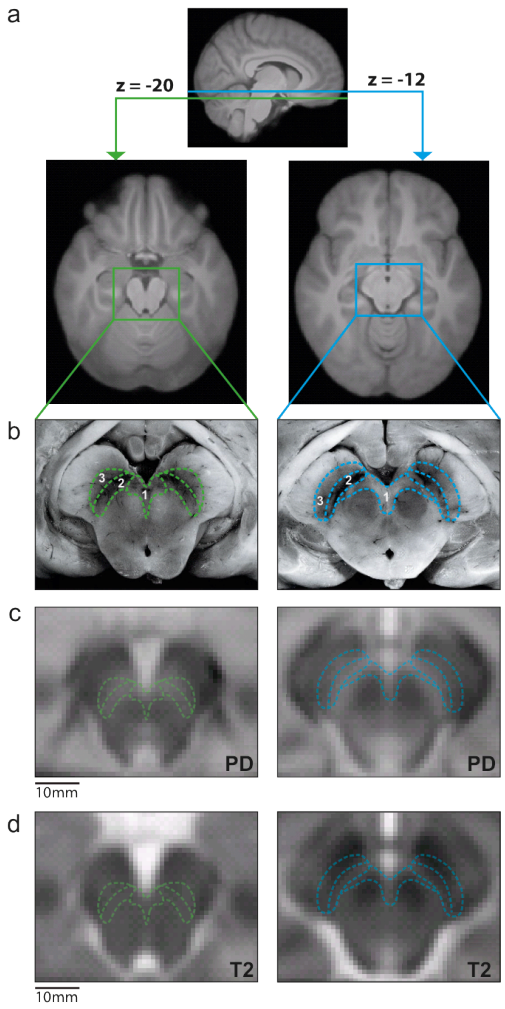

Figure 10: *Localising the dopaminergic midbrain system. (a) The location of the midbrain slices of interest in two z-planes of the whole-brain group average T1 in MNI space. (b) Post mortem histological images of the midbrain used to define boundaries of VTA (1), SNc (2) and SNr (3) shown with green and blue lines, adapted from Naidich et al (2009). (c) PD group average images of the midbrain in MNI space. (d) T2 group average images of the midbrain in MNI space.*

5.4.3. FMRI results

5.4.3.1. Main effects

I investigated the BOLD response in the midbrain during the outcome phase of the trials. It is during the presentation of the outcome that the received outcome is compared to the predicted outcome, and a response to the PE occurs (Schultz et al., 1997). The experimental design allowed both the comparison of positive PEs and negative PEs against a zero PE baseline. The positive PE outcomes included the financial gain outcomes, and the nil outcomes when the alternative was a financial loss. Negative PE outcomes included the financial loss outcomes, and the nil outcomes when the alternative was a financial gain. Figure 11 shows the results of this analysis. The positive PE was associated with activity in the dopaminergic midbrain system, specifically, the caudal VTA and caudomedial SNc. Additionally, I saw a similar area of activity that was associated with negative PE, which extended into the rostromedial SNc on the left.

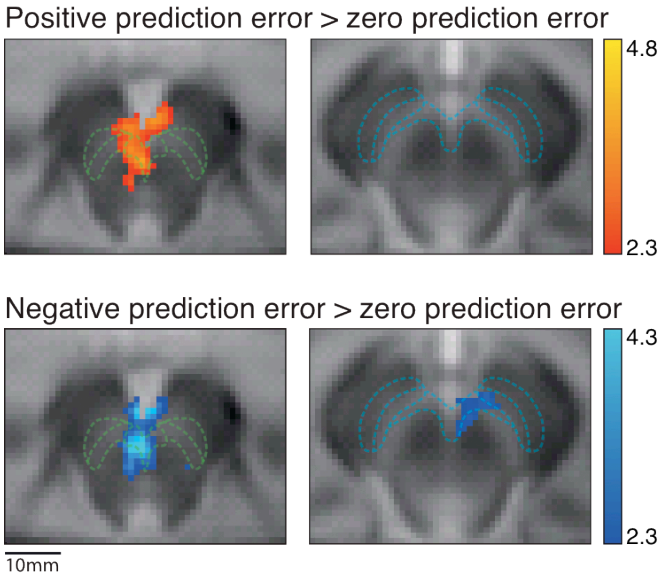

Figure 11: *PE analysis. The VTA responded to the occurrence of a positive PE (top panel) and a negative PE (bottom panel). Both contrasts were against a zero PE baseline (nil outcome of cue A). The statistical maps show significant clusters of voxels (determined using non-parametric permutation testing with a corrected threshold of $p < 0.05$ and a nominal t-value of 2.3). The t-values of the active voxels are indicated by the legends.*

5.4.3.2. The utility of the PNM

When the analysis was rerun with the PNM, I quantified the variance that was explained by the PNM regressors.

Figure 12 shows the voxels where a significant amount of noise was explained by the PNM ($p < 0.05$). When the analysis was repeated with a more conservative threshold ($p < 0.001$) the pattern of significant voxels was similar. This result shows that there is widespread physiological noise that is being explained by the PNM regressors in the midbrain. Voxels near to CSF are particularly prone to noise, and this susceptibility occurs in voxels within the dopaminergic midbrain system. This is particularly true in the rostral regions. Additionally, the right SN contains more significant voxels at $z = 12$ than the left.

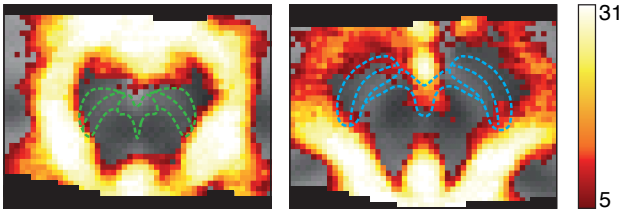

Figure 12: *The location of physiological noise. The overlay image shows how many participants showed significant physiological noise at each voxel. This was created by conducting an F-test at each voxel ($p < 0.05$), which assessed how much noise was explained by the PNM regressors. Such a test was carried out for each individual, and a binary map of each individual's significant voxels were added together to create an overlay image. The binomial probability density function was used to derive p values from the overlap image, which was then thresholded using a false discovery rate ($p < 0.05$) to correct for multiple comparisons. Black voxels are outside the group statistical image.*

The PE contrasts were reanalysed with the inclusion of the PNM (Figure 13). The pattern of activity in the caudomedial dopaminergic midbrain system that had been revealed without the PNM remained. In addition there was a more extensive pattern of activity in the rostral midbrain. For the positive PE contrast the revealed activity was a cluster of medial voxels in a region that had previously shown no activation. For the negative PE activity, the medial region that had previously been apparent was more widespread and extended to the lateral SNc on the left.

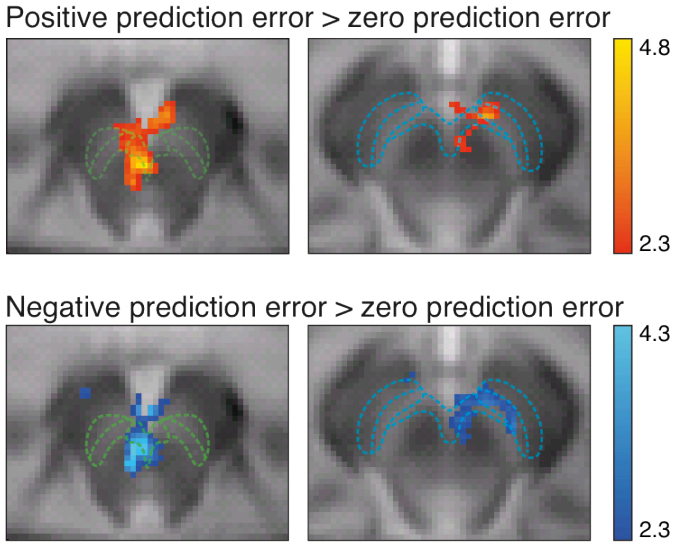

Figure 13: *The positive and negative PEs when PNM is included in the analysis. The activity within the caudal VTA remains the same. For the positive PE contrast, activity is revealed in the rostromedial dopaminergic midbrain system that was previously hidden by physiological noise. In addition, previously hidden activity is revealed in the lateral SNc for negative PEs. The statistical maps show significant clusters of voxels (determined using non-parametric permutation testing with a corrected threshold of $p < 0.05$ and a nominal t-value of 2.3). The t-values of the active voxels are indicated by the legends.*

5.4.3.3. PE responses elicited in the absence of financial outcomes

The PE responses were divided into those that were elicited by financial outcomes and those that were elicited by nil outcomes. This analysis allowed the separation of PE responses caused by the receipt of a financial outcome, and those caused by the absence of a financial outcome, to ensure the observed responses were caused by the PEs, not the financial outcomes themselves. The voxelwise analysis of nil PE

outcomes was carried out to investigate if there was a PE response in the absence of a financial outcome. The nil outcomes that elicited a positive PE were compared to nil outcomes that did not elicit a PE. Similarly nil outcomes that elicited a negative PE were compared to nil outcomes that did not elicit a PE. This second contrast (negative PE>zero PE) revealed a significant cluster of voxels localised in the caudal VTA (see Figure 15). However there was no cluster of activity associated with a positive PE in the absence of a financial outcome.

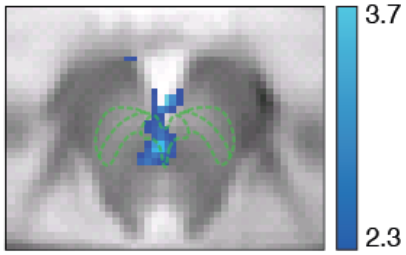

Figure 14: *Negative PE elicited in the absence of a financial loss. Activity associated with a negative PE nil outcome is localised to the caudal VTA. The statistical maps show significant clusters of voxels (determined using non-parametric permutation testing with a corrected threshold of $p < 0.05$ and a nominal t-value of 2.3). The t-values of the active voxels are indicated by the legends.*

The above voxelwise analysis may not be as sensitive to BOLD changes as the original PE analysis as there were far fewer trials associated with the nil PE outcomes compared to the PEs elicited by financial outcomes. To further investigate the nil outcomes, signal associated with PEs elicited by nil outcomes was extracted from the regions of the midbrain that showed a response to PEs elicited by financial outcomes. Figure 15 shows the results of the ROI analysis. There was a significant difference between the positive PE response elicited by the gain outcome, and the positive PE response elicited by a nil outcome ($t_{(30)} = 2.835$, $p < 0.05$). There was no significant difference between the negative PE response elicited by a loss outcome, and a nil outcome ($t_{(30)} = 1.815$), however this was approaching significance ($p = 0.74$). To establish if this test had enough power to detect any possible difference, achieved power was calculated using G*Power (Faul et al., 2007). Power was 0.43, showing that this contrast was indeed underpowered. With the effect size of this *t*-

test, more participants would be required to establish if there was a difference between the two contrasts.

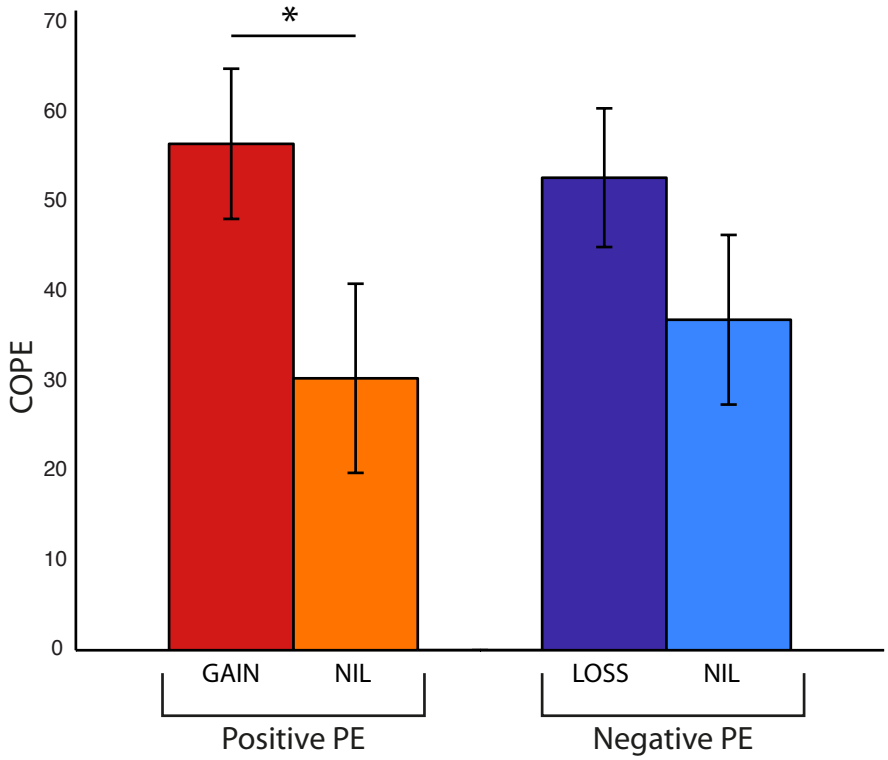

***Figure 15**: Investigating the PEs elicited by nil outcomes. Mean COPE values for different types of PEs. Presented with standard error bars. ROI analysis was used to extract COPE values from within the clusters revealed by the gain positive PE contrast for the positive PE contrasts, and the loss negative PE for the negative PE contrasts. There was a significant difference between the positive PE response elicited by a gain outcome and a nil outcome ($t_{(30)}$=2.835, p<0.05), and no significant difference between the negative PE response elicited by a loss outcome and a nil outcome ($t_{(30)}$=1.815).*

One-sampled *t*-tests were used to see if the signal from the ROIs associated with the nil PEs was different from zero. In this case the zero baseline was the predictable nil outcome. The positive PE elicited by the nil outcome was significantly different from zero ($t_{(30)}$ = 2.875, p < 0.05). The negative PE elicited by the nil outcome was also significantly different from zero ($t_{(30)}$ = 3.897, p < 0.05).

5.4.3.4. Parametric analysis: the temporal difference model

Finally, the temporal difference model was used to model the predicted BOLD response on a trial-by-trial basis. This analysis allowed the investigation of the possibility that the magnitude of the BOLD response scaled with the level of PE. A parametric contrast was constructed that included all six levels of positive PE, with a predicted linear relationship between them. A similar contrast was constructed for the negative PE. Neither contrast revealed activity when analysed on a voxelwise basis.

Constructing such parametric contrasts is limiting, as the only relationship that will lead to a significant result is a linear one. In other words the BOLD response would have to scale linearly with increasing level of PE. To avoid this assumption I carried out an ROI analysis. Each level of positive and negative PE was contrasted with the zero PE baseline. For the positive PE analysis, the region that responded to positive PE (revealed by the main effects contrast) was used as the ROI, for the negative PE analysis, the region that responded to negative PE (revealed by the main effects contrast) was used (see Figure 13 for the results used to create the ROIs).

Figure 16 shows the results of this analysis. To test if the level of positive PE modulated the magnitude of the BOLD response, a repeated measures ANOVA was carried out. The results show that the level of the BOLD response was not significantly affected by the level of positive PE, $F_{(5,150)} = 0.369$, $p > 0.05$). A repeated measures ANOVA was also carried out to investigate if the level of negative PE modulated the BOLD response. Again, the results show that the level of the BOLD response was not significantly affected by the level of negative PE, $F_{(5,150)} = 0.392$, $p > 0.05$).

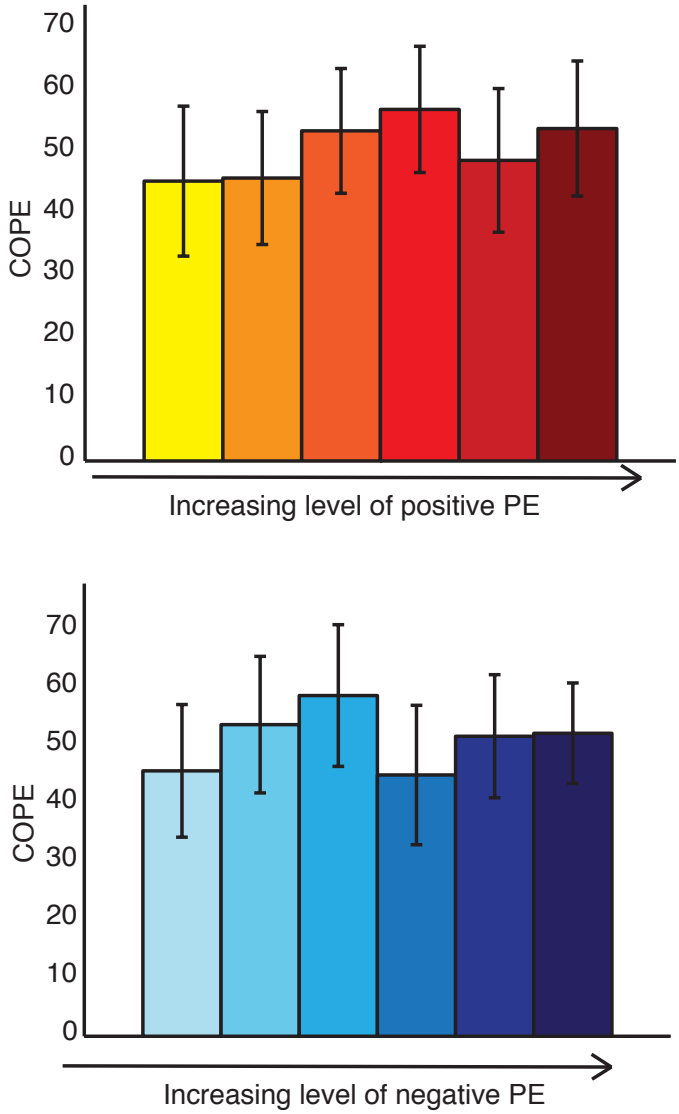

Figure 16: *Temporal difference analysis of PE. Mean COPE values for different levels of PEs. Presented with standard error bars. The top panel shows the BOLD response to increasing level of positive PE, each level compared to the zero PE baseline. The bottom panel shows the BOLD response to increasing levels of negative PE, each level compared to the zero PE baseline.*

5.5. Discussion

5.5.1. Positive and negative prediction errors

Here I have shown that, using financial outcomes to elicit PEs, the human dopaminergic midbrain system codes for positive PEs, as previously reported in non-humans (Fiorillo et al., 2003; Tobler et al., 2005) and humans (D'Ardenne et al., 2008; Zaghloul et al., 2009). In addition the region codes for negative PEs. This is the first time a negative PE signal has been observed in the human dopaminergic

midbrain system. It is in line with the recent non-human research that has found responses to punishing stimuli or cues predicting punishing stimuli (Brischoux et al., 2009; Joshua et al., 2008; Matsumoto and Hikosaka, 2009; Mileykovskiy and Morales, 2011; Wang and Tsien, 2011).

To confirm that the responses I had measured were in fact prediction errors, and were not in response to the financial outcome itself, I compared the BOLD signal in the active region of the midbrain for PEs evoked by a nil outcome to the signal produced by a PE evoked by a financial outcome. I found that the nil outcomes led to an increase BOLD signal (from the nil zero PE baseline), and so the BOLD response occurred in the absence of any unexpected financial outcome. This provides support for the assertion that I have measured PE responses in the dopaminergic midbrain, as unexpected nil outcomes modulated the midbrain signal.

However, for positive PEs, there is a significant difference between the two types of positive PE responses. The BOLD response to an unexpected financial gain is significantly greater than the BOLD response to an unexpected nil outcome that is better than expected. In addition, there is a non-significant difference between the BOLD response to an unexpected financial loss, and the response to a nil outcome that is worse than expected. Although this contrast was non-significant, the contrast is underpowered. More participants would be required to establish if this difference between the two conditions is a genuine effect.

These differences suggest that I am not observing a response that only reflects the level of PE. Electrophysiological findings suggest that the firing rate of dopamine neurons are modulated only by the level of PE, and do not reflect the intrinsic value of the received reward or punishment. However, this result suggests that there is an interaction between the PE response, and the occurrence or absence of financial outcomes. There are several possible interpretations of this result. First, it could be due to the properties of the BOLD signal being measured. Many regions provide inputs to the VTA and SNc, and some of these regions are sensitive to absolute values, such as the amygdala (Paton et al., 2006), and orbito-frontal cortex (Knutson et al., 2005). Inputs to the dopaminergic midbrain may cause a change in the BOLD activity of the dopaminergic midbrain, and modulations of these network level inputs

may cause the additional change in BOLD that is observed when an unexpected finial outcome is received, over and above the PE response. Second, it is possible that the result is a consequence of the use of financial outcomes to create prediction errors. Money is a uniquely human stimulus, with no correlate in the animal. As a secondary reinforcer it may have different properties to primary rewards, and may be processed in a different manner in the midbrain. Despite these unknown factors, it is important to remember that the unexpected nil outcomes did elicit responses in the midbrain, suggesting that I have measured a PE response in the midbrain.

It is of great interest that the BOLD responses I measured did not scale with the level of PE. Previous research into the midbrain (D'Ardenne et al., 2008) has found that the BOLD signal in the VTA increases with the level of positive reward PE. There are three possible reasons to explain this apparent discrepancy. First, it could be due to the power of the experiment. The methods I used, including task design, midbrain optimisation, and high-resolution scanning, may not give me the sensitivity required to detect a parametric modulation in BOLD signal. Second, it may be that the hemodynamic response of the midbrain does not lead to a linear increase in BOLD signal with a linear increase in neural activity. Finally, it may be that the BOLD signal reflects more than the dopaminergic firing rate changes observed in the non-human. As discussed in the introduction, the BOLD signal is more likely to reflect integrative inputs (Logothetis, 2003), at least at the level of the cortex. Therefore, dendrosomatic processes that result from changes in excitatory and inhibitory inputs may modulate the BOLD response at the level of the midbrain. If this is the case, the response would not be expected to scale with the level of PE, as we are measuring more than dopaminergic firing rate.

As fMRI measures activity on a scale of millimetres, it is not possible to elucidate the precise mechanisms at the level of individual neurons, as is possible with single cell recordings, that are causing the changes in BOLD in response to reward and punishment PEs. However, using the extensive research into the non-human dopaminergic midbrain system, it is possible to offer several mechanisms that may be causing the changes in the BOLD signal. There is much overlap between the clusters of activity for both types of PE. This may mean that the same neurons are firing to both types of PE. If this is the case then the neurons are reflecting a saliency

signal, unaffected by the valence of the stimuli (Redgrave et al., 2008). Neurons with such responses have been localised in the non-human (Bromberg-Martin et al., 2010b; Matsumoto and Hikosaka, 2009). However, taken as a whole, the literature suggests a complex model for the neural response to negative PEs, with some neurons increasing their firing rate, others being suppressed, and some showing a rebound excitation at the stimulus offset (Brischoux et al., 2009; Joshua et al., 2008; Matsumoto and Hikosaka, 2009; Valenti et al., 2011; Wang and Tsien, 2011). Therefore it is unlikely that the cluster of activity for the negative PE represents a unitary excitatory response, and instead is a result of the activity of different neuronal types. Co-localisation in fMRI does not mean that the activity is necessarily the result of the same population of neurons, as multiple types of neurons may not be anatomically segregated at a scale that is visible with fMRI, or they may not be anatomically segregated at all.

This result also raises an interesting question regarding projection targets of the dopaminergic neurons. If there are two sub-populations of dopamine neurons that respond to reward and punishment PEs, then this may explain the anatomical segregation that has been observed in the striatum in response to financial gains and losses (Seymour et al., 2007).

5.5.2. Physiological noise

I investigated the physiological noise properties of the dopaminergic midbrain system by identifying voxels that contained a significant amount of variance explained by the PNM regressors. This analysis showed that midbrain tissue bordering the CSF is most prone to physiological noise, and the dopaminergic midbrain system is susceptible due to its proximity to CSF, particularly the rostromedial VTA and SNc complex. More lateral portions of the SNc seem unaffected by the inclusion of the PNM, presumably due to its relative remoteness from CSF. The most lateral portions of the SNc are affected by the inclusion of the PNM, again due to their proximity to CSF. Unfortunately no direct comparison can be made with the previous investigations of the noise properties of the midbrain (Harvey et al., 2008; Klein-Flügge et al., 2011) as no statistical analyses were carried out on the observed variance reductions.

Although PE related activity was observed in the midbrain without the PNM, a more extensive clusters of voxels for both positive and negative PEs were revealed when the PNM was include in the analysis. Activity that was previously hidden by physiological noise was revealed in the medial SNc for positive PE. The medial SNc signal that we had observed in response to negative PE extended laterally with the inclusion of the PNM. Thus, even though the voxels within the lateral SNc were not significantly affected by physiological noise, the inclusion of the PNM does improve signal detection within this region. The lateral SNc is a narrow band of cells, relative to the medial SNc and VTA complex. This may mean that fMRI is relatively insensitive to lateral SNc activations, so is affected by small changes in the level of physiological noise. In addition the SNc cluster extends from the medial to lateral dopaminergic regions, and includes the rostromedial region that is prone to noise. Without the rostromedial cluster the lateral cluster may be too small to reach significance.

Furthermore, the task used here elicits motivationally salient responses, and thus the physiological noise may correlate with task events, which would result in erroneous activations. I have shown that the BOLD activations occur even when physiological data are removed, revealing that the observed BOLD signal reflects task-evoked neuronal activity rather than task-evoked cardiac or respiratory responses.

5.5.3. Limitations

Although this study has provided a novel result that is supported by a large body of non-human experiments, it does have limitations. First, the observed activity in the SNc is localised to the left, with no activity in the right SNc. There has been no suggestion in the animal literature that the function of the SNc is lateralised in this way, so it is likely that the finding is a consequence of the method used. Even with the efforts to optimise fMRI to measure a signal in the midbrain at high-resolution, the power of the experiment is still less than would be expected from a whole-brain study with standard voxel size. This is due to the reduced SNR, which is a consequence of the reduced voxel size, and the relative increase in physiological noise in the midbrain. Even though it is possible to reduce the influence of the physiological noise, it is not possible to completely remove its effects. Thus, the laterality of the

SNc is probably due to the relatively low power of the experiment. The shape of the lateral SNc, which makes it more difficult to obtain an fMRI signal from this region, exacerbates this problem of reliable recovery of signal. In addition, there were more voxels in the left SNc that had a significant amount of variance explained by the PNM, which may mean that this sub-region was more prone to physiological noise.

Another limitation was that the limited FOV used during data acquisition meant that network interactions at the level of the whole-brain could not be investigated. For a full understanding of the reward network, this is required. A potential solution would be to carry out an experiment with a high-resolution technique, such as the one presented here, to elucidate the role of the midbrain nuclei in the human, and then repeat the experiment at the whole-brain level. It could then be inferred, with the optimal level of accuracy, the regions of the midbrain that were involved in the task in question, before investigating network level interactions across the whole brain. An additional advantage would that PNM could be applied to whole-brain data. However, the problem of registration would still remain, as the method presented here achieves optimal midbrain co-registration at the cost of the cortical mantle of the cerebral hemispheres.

5.5.4. What does a signal in the midbrain reflect?

The general consensus within the fMRI community is that the BOLD signal is dominated by integrative inputs and local interneurons (as reflected by the LFP), with a relatively small contribution from action potentials (Logothetis, 2008; Logothetis et al., 2001). This presents a possible problem for the interpretation of the BOLD signal in the dopaminergic midbrain, as the animal models of dopamine neurons are based on measures of output. Although LFP and action potential output often correlate, this is not always the case; there is a report of a change in the BOLD signal occurring without a corresponding increase in the firing rate of neurons (Logothetis and Wandell, 2004).

In addition, no experiments have been carried out to investigate the neural basis of the midbrain BOLD signal. Therefore we can only assume that the BOLD signal reflects the same neural properties in the midbrain as it does in the cortex. However, due to possible differences in vasculature, and differences in the ratio of afferents to

efferents that midbrain neurons receive in comparison to the cortex, this may not necessarily be the case.

Based on what is known about the responses of midbrain dopaminergic neurons to both and positive and negative PEs from the non-human, there are several possibilities as to what the BOLD response could be reflecting. Figure 17 outlines mechanisms by which inputs synapsing directly onto dopamine neurons could be modulating the activity of dopamine neurons. Dopamine neurons could be receiving excitatory input, which causes an increase in dopaminergic output (Figure 17a). In this case the increased metabolic demands that cause a change in the BOLD signal could originate from the dendro-somatic processes of the dopamine neuron (as would be measured by the LFP), or the action potentials themselves. Alternatively, as shown in Figure 17b, these inputs could be sub-threshold and no action potentials could ensue, but the metabolic demands of the dendro-somatic processes could increase the BOLD signal. Alternatively, there could be an increase in the output of the dopamine neurons, due to a decrease in inhibitory inputs (Figure 17c).

Alternatively, the BOLD signal could originate through the modulation of GABAergic interneurons within the dopaminergic midbrain (Figure 18). In the rat, 35% of VTA neurons are GABAergic, and in the SNc this number is 29% (Nair-Roberts et al., 2008). Although the role of these neurons is not known, it is possible that GABAergic interneurons synapse onto dopamine neurons and modulate their activity. These GABA neurons could receive increased inhibition that reduces their inhibitory influence on the dopamine neurons, causing an increase in dopaminergic output (Figure 18a). Finally, these neurons could receive increased excitation, which could lead to a decrease in the dopaminergic firing rate (Figure 18c) or no change in the firing rate (Figure 18d), but an increase in the BOLD signal.

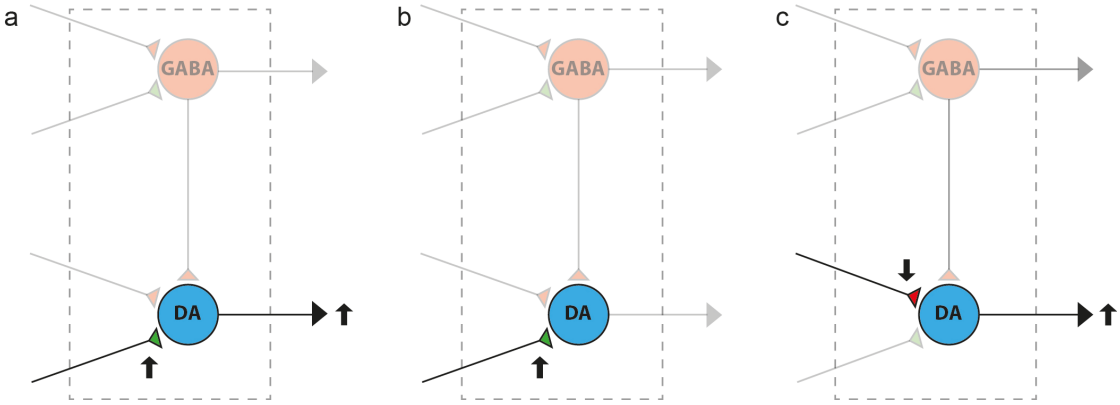

Figure 17: *Possible neural mechanisms underlying the BOLD response in the dopaminergic midbrain. (a) Increased excitatory input to dopamine neurons, resulting in increased firing rate of dopamine neurons, (b) sub-threshold excitatory input to dopamine neurons, with no increase in firing rate, (c) decreased inhibitory input to dopamine neurons, resulting in increased firing rate of dopamine neurons. DA = dopamine (blue), GABA = gamma-aminobutyric acid (red), glutamate = green. Dashed line indicates boundaries of the dopaminergic midbrain.*

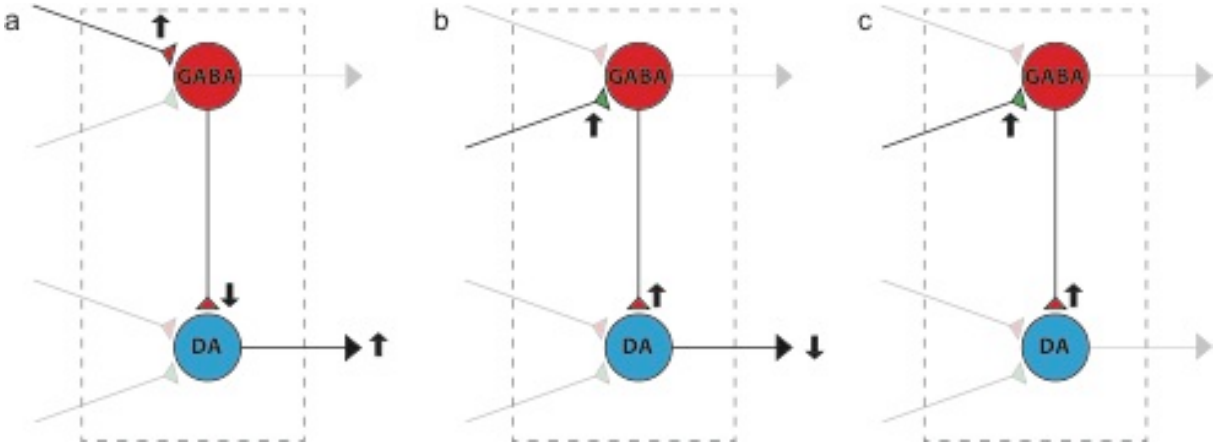

Figure 18: *Possible neural mechanisms via GABAergic interneurons underlying the BOLD response in the dopaminergic midbrain.(a) increased inhibitory input to GABA neurons, leading to decreased inhibition of dopamine neurons, and a resulting increase in dopaminergic firing rate, (b) increased excitation of GABAergic neurons, leading to increased inhibition of dopamine neurons, and a decrease in dopaminergic firing rate, (c) increased excitation of GABAergic neurons, leading to sub-threshold inhibition of dopamine neurons, and no change in the dopaminergic firing rate. DA = dopamine (blue), GABA = gamma-aminobutyric acid (red), glutamate = green. Dashed line indicates boundaries of the dopaminergic midbrain.*

Recent evidence into the role of these midbrain GABA neurons has suggested that they are involved in computing the value of cues, and do not change their firing rate in response to PEs (Cohen et al., 2012). Thus the most parsimonious explanation for the change on BOLD that occurs in response to positive PEs is that dopamine neurons increase their firing rate as a result of increased excitatory, or decreased inhibitory, inputs. For negative PEs, the picture is not as clear, due to the heterogeneous response to these types of PEs within the dopaminergic midbrain. It is possible that there is a network of neurons that fits the model of Figure 18b, that would correspond to the dopaminergic neurons that showing GABA interneuron induced suppression in response to punishment PEs. However it is also likely that there is an increased dopaminergic output, due to the existence of neurons that are excited by punishment PEs.

In addition there is a population of glutamatergic neurons in the VTA that make up 2-3% of the total neuronal population (Nair-Roberts et al., 2008). These neurons form local connections with dopaminergic and non-dopaminergic cells (Dobi et al., 2010). However, as the population of the glutamatergic neurons is relatively small, it is unlikely activity in this population is contributing to the observed BOLD signal.

Taking these possible mechanisms into account, the increase in BOLD signal that was observed for the both positive and negative PE could reflect a number of different neural mechanisms, alone or in combination. In addition, the same change in BOLD signal for these two types of responses could be due to two different underlying neural mechanisms. Clearly, work is needed into the neural basis of a midbrain BOLD signal before such questions can be answered.

5.6. Conclusions

Here I have shown that the BOLD signal of the dopaminergic midbrain system was increased in response to both positive and negative PEs. Moreover, there was a significant amount of physiological nose in the dopaminergic midbrain, which was effectively reduced by the PNM. This the first time that an increase in the BOLD signal in the midbrain has been observed in response to a negative PE.

6. Discussion

6.1. Summary of key findings

The aims of this thesis, as discussed in the introduction, were:

1. To optimise registration to improve the accuracy of localisation of structures at the level of the midbrain;
2. To attempt to reduce the influence of physiological noise in midbrain fMRI data, to improve my ability to measure a signal from the human midbrain;
3. To use the optimised midbrain fMRI methods to measure the BOLD response to positive and negative PEs in the human midbrain, to extend current non-human models of the dopaminergic midbrain to the human.

The first aim was achieved in Chapter 3. I presented a replicable and automated method to improve the localisation of midbrain fMRI signals by improving midbrain registration. Poor registration would greatly reduce the power of a midbrain fMRI experiment, as BOLD signals from a single region across participants would be blurred in standard space. Poor registration could also lead to inaccurate localisation, and the mislabelling of activity. To achieve this improved accuracy, two additional structural scans were used to improve registration between functional and structural T1-weighted images: an EPI that matched the functional data but had whole-brain coverage, and a whole-brain T2-weighted image. This pathway was compared to conventional registration pathways, and was shown to significantly improve midbrain registration. This method used standard analysis tools, and can easily be used by research groups using different protocols and scanners.

In Chapter 4 I achieved the second main aim. A proof-of-principle fMRI study was carried out to test the optimisation methods. A simple visual task was used for this that has previously been shown to activate the superior colliculi bilaterally – both in the human using fMRI, and in the non-human using electrophysiology. Such an experiment had a strongly supported hypothesis, so absence of a measured BOLD signal in this region would indicate that there were methodological problems in obtaining a midbrain signal.

To reduce the physiological artefacts in the functional data, I estimated and removed structured noise using a modified version of the PNM (Brooks et al., 2008; Harvey et al., 2008), which itself is a modification of RETROICOR (Glover et al., 2000). I used the PNM to convert the individual participants cardiac and respiratory measures, which were obtained during the visual fMRI task, into noise regressors. These noise regressors were included in the GLM as regressors of no interest, removing noise from the data and reducing the residual variance, thereby improving the test statistics. The advantage of the method is that noise is removed after acquisition, so the PNM analysis could be compared to a conventional GLM analysis.

Whereas a conventional analysis revealed only unilateral superior colliculi activity, the PNM analysis revealed the predicted bilateral activity. These methods, when used in conjunction with the optimised registration pathway presented in Chapter 3, improve the measurement of a biologically plausible fMRI signal.

The optimised methods presented in Chapters 3 and 4 improved the detection of a BOLD signal in the superior colliculi. There was no reason to suspect that the optimised four-step registration would be more effective at co-registering the superior colliculi over and above any other region of the midbrain so it was likely that it could be used in an experiment investigating the dopaminergic midbrain without further testing or optimisation. The PNM, however, may not have been equally effective throughout all regions of the midbrain. This is because noise properties across the midbrain will differ due to proximity to CSF and large blood vessels. Therefore, in Chapter 5, when the optimised methods were applied to a PE task, the value of the PNM in the dopaminergic midbrain was tested.

In Chapter 5 I presented the results from my investigation of the role of the dopaminergic midbrain system in positive and negative PEs. A financial gain and loss task was used to elicit positive and negative PEs, and these were compared to a zero PE baseline. The medial dopaminergic midbrain system, which included the VTA and medial portions of the SNc, showed an increase in BOLD to both positive and negative PEs. In addition, more lateral portions of the SNc showed an increase in the BOLD response to negative PEs. I also presented the results into an investigation of the value of the PNM in the study of dopaminergic midbrain system

using fMRI. This included quantifying the noise that is explained by the PNM regressors, and a comparison of the GLM analysis with and without the PNM. I demonstrated that the PNM does explain noise in the midbrain, including regions of the dopaminergic midbrain system, and by including the PNM in the analysis I revealed a more extensive cluster of activity than was seen without the PNM.

I then compared PE responses elicited by better or worse than expected financial outcomes to PE responses elicited by better or worse than expected nil outcomes. In the original analysis financial and nil outcomes had been collapsed together. Such a separation of outcomes was necessary to investigate if the BOLD response reflected a genuine PE signal, or was a response to the intrinsic value of the financial outcomes themselves. If there was a BOLD response to the theoretical PEs elicited by better or worse than expected nil outcomes, then I could conclude that the BOLD response did reflect PE.

The results to this analysis showed that the BOLD response reflected both the PE and the intrinsic value of the financial outcome. Whilst the nil outcomes did show a BOLD response that was greater than the expected nil outcome, this response was not as great as the response elicited by unexpected finical outcomes.

Finally, a temporal difference model was applied to the data. The level of the PE did not modulate BOLD signal in the region of the midbrain that had shown a response to PEs. This could be due to a lack of sensitivity to relatively small fluctuations in BOLD, or to the nature of the BOLD signal and what it reflects. Whilst the electrophysiological investigations into the role of midbrain dopamine measures change in firing rates, fMRI measures a wider range of neural processes. Therefore, the BOLD signal could reflect multiple brain signals, including those that are not sensitive to level of PE, such as the coding of expected value, salience, and sensory (visual) processing. When these sources are combined, the mean signal would not scale with the level of PE.

Importantly, the result of this PE study is the first demonstration of a BOLD response to negative PEs in the human dopaminergic midbrain. The result suggests that the non-human experiments that have implicated the dopaminergic midbrain in the

processing of punishing, or punishment predicting, stimuli (Brischoux et al., 2009; Guarraci and Kapp, 1999; Joshua et al., 2008; Mantz et al., 1989; Matsumoto and Hikosaka, 2009; Mileykovskiy and Morales, 2011; Valenti et al., 2011; Wang and Tsien, 2011) are applicable to human midbrain function. Importantly, it is possible that we have measured two different populations of neurons within the same region. The first population may respond to positive PE, and be supressed by negative PE, in line with the original findings in the dopaminergic midbrain (Schultz et al., 1997). The second may respond to both positive and negative PE, and so be insensitive to the valence of the PE. These neurons may be responding to the motivational salience of the stimulus (Berridge and Robinson, 1998; Bromberg-Martin et al., 2010c). Motivational salience, not to be confused with incentive salience, describes the properties of a stimulus is terms of how rewarding or punishing it is. A motivationally salient stimulus is likely to drive behaviours, whether it is exploration and approach to a rewarding stimulus, or fight of flight to a punishing stimulus. Thus these neurons would cause an increased level of attention being paid to the stimuli, resulting in the appropriate behaviour being carried out. This interpretation is in line with those electrophysiological studies that have found neurons that respond to both positive and negative PEs (Bromberg-Martin et al., 2010b; Joshua et al., 2008; Matsumoto and Hikosaka, 2009; Mirenowicz and Schultz, 1996; Wang and Tsien, 2011).

However, a major question remains concerning the BOLD signal I measured. As with any BOLD signal, it is impossible to know precisely which neural mechanisms underlie the observed responses. However this problem is exacerbated in this experiment for two reasons. First, the hypothesis tested was a very specific one, based on precise neural mechanisms that have been measured in-vivo in non-humans. Even using this very specific methodology, this field has been prone to conflicting results. For example, early studies reported electrophysiological identified dopamine neurons that responded to aversive events (e.g. Guarraci and Kapp, 1999; Mantz et al., 1989). However some cells that appear dopaminergic using this method are in fact non-dopaminergic (Ungless et al., 2004). As the mechanisms of interest have been investigated by measuring responses from single neurons, it is problematic to investigate these hypotheses using fMRI, a very non-specific methodology.

Second, there have been no electrophysiological studies into the neural mechanisms that underlie the midbrain BOLD response. Whilst there are examples of cortical studies whereby the BOLD signal has been compared to the underlying electrophysiology (e.g. Logothetis et al., 2001), there have been no such studies of the subcortical regions of the brain. Therefore all modelling and interpretations of the BOLD signal are based on the assumptions that have been derived from cortical electrophysiological studies.

If it is assumed that the neural properties of the BOLD signal are similar to that of the cortex, then there are still many mechanisms that we may be measuring. If we take two types of midbrain neurons: dopamine and GABA, there are multiple neural mechanisms that could cause an increased BOLD signal. In section 5.5.4 I discussed in depth these possible mechanisms, and suggested several possible modifications in excitatory inputs, inhibitory inputs, and output firing that could all plausibly cause an increase in the BOLD signal (see Figure 17 and Figure 18). This simplistic view does not make any predictions about other types of neurons, such as glutamate neurons within the VTA and SNc, and the multiple types of neurons that project to the dopaminergic midbrain.

However, despite these complications, it is reasonable to interpret the observed BOLD changes in Chapter 5 as reflecting changes in the dopaminergic system. There is much non-human evidence that midbrain dopaminergic neurons signal positive PE, and there is an increasing body of evidence that aversive events are also signalled by dopaminergic neurons in the midbrain. Therefore, although the evidence here is not direct evidence for the involvement of dopamine neurons in positive and negative PEs, it is a likely interpretation of the results.

There are tools that may be of use in investigating the neural basis of the BOLD signal in the human. Further characterisation of the response may shed more light on whether the interpretation I have presented is correct. For example, salt appetite has been used in the non-human to investigate changes in the incentive salience of a stimulus. A high concentration saline solution that is aversive becomes appetitive in the unnatural state of induced salt appetite (Tindell et al., 2009). Berridge (2012) predicts that this change will be reflected in the activity of midbrain dopamine

neurons. More work on this topic in the non-human is needed, but if this prediction turns out to be true, this could be investigated in the human. A homologue of this type of experiment is to scan participants in a fed and fasted state, and observe the midbrain response to an outcome that elicits a PE under changing internal states. A similar task as used in Chapter 5 could be used, with a sweet drink as the outcome, instead of monetary outcomes. If the BOLD signal was modulated by the fed or fasted state, it would suggest that the observed signal was dopaminergic.

In addition, non-human experiments suggest an anatomical segregation of functionally different dopamine neurons. Although I have observed a degree of segregation in the SNc for positive and negative PEs, with negative PEs extending more laterally, there was no significant difference between the location of the BOLD signal for positive and negative PEs. It may be that the resolution used here is not high enough to observe potential functional segregation within this region.

As discussed in section 1.2.1.2, the dopaminergic midbrain has a topographical organisation in terms of connectivity with the striatum. In the primate the VTA and the ventral SNc have dense bidirectional connectivity with the ventral striatum (Haber and Knutson, 2010), which is involved in processing of motivational stimuli. Thus, it is logical to assume that the two types of responses I have observed in the VTA are computed in dopaminergic neurons that project to the ventral (or limbic) striatum, hence the observation of both types of PE in the ventral striatum (Seymour et al., 2007). The observation that the two types of PEs are anatomically separable in the ventral striatum suggests that there are two distinct populations of dopamine neurons. One is responding to a positive PE, in a manner described by the reward PE hypothesis (Schultz et al., 1997), and the other responding to a saliency signal that is independent of the outcome valence (Redgrave and Gurney, 2006).

In addition the medial SNc and VTA project to the prefrontal cortex (Fallon, 1981), including the orbito-frontal cortex. The orbito-frontal cortex is involved in coding and representing the expected value of stimuli (Knutson et al., 2005). Therefore, it is logical to expect the orbito-frontal cortex to receive inputs concerning both rewards and punishments, to gain a full representation of expected value. The results presented here suggest that the VTA and medial SNc could provide this region with

information about both rewards and punishments. Similarly the amygdala receives projections from the VTA (Leshan et al., 2010) and is involved in representing expected value.

The lack of activity in the lateral regions of the SNc could be due to several reasons. First, the shape of the SNc is long and thin, in comparison to the relatively compact region of the medial dopaminergic that is equally extensive in all directions. This may make the detection of a signal from this region more challenging, due to increased partial volume effects. Second, the protocol may have been less sensitive to signal within the SNc due to the relatively long TE used during data acquisition. Finally, I may have observed a genuine effect. The medial dopaminergic midbrain projects to regions that are concerned with emotional information, whereas the more lateral portions of the SNc project to motor learning areas, such as the dorsal striatum. The task used in Chapter 5 did not require motor learning, and depended only on Pavlovian conditioning. This may explain why the signal was observed only in the medial portions of the midbrain.

The findings presented here, that the dopaminergic midbrain responds to positive and negative PEs, have interesting implications for disorders that have been associated with a maladaptive dopamine system. Here I will briefly discuss the implications for two such disorders: addiction and schizophrenia.

The common mechanism of all drugs of addiction is that they cause an increase in the dopamine concentration in the regions to which the midbrain dopamine neurons project to (Nestler, 2005). Repeated exposure to such increases lead to the formation of maladaptive memory traces associated with the drug and associated stimuli (Waelti et al., 2001). Thus exposure to drug related stimuli are processed as salient or rewarding, and promote drug consumption (Koob and Volkow, 2010). Additionally, long term exposure to drugs of addiction have been shown to cause an underactive dopamine system (Volkow et al., 2007), which may lead the individual to seek temporary stimulation of this network with drugs of abuse. Thus the finding that the human dopaminergic midbrain shows a response to positive PEs fits with this hypothesis of addiction, as does the possibility that I measured a saliency response, reflected by the region that showed a response to positive and negative PEs.

The negative PE response I observed fits with a different aspect of addiction. Addictive behaviour can be framed in terms of negative reinforcement (Koob and Volkow, 2010). In this model, behaviour that has adverse consequences is preserved by a sense of relief that is felt when adverse feelings, such as drug withdrawal, are relieved by drug taking behaviour. This negative reinforcement could be modulated by the neurons in the dopaminergic midbrain that are coding for punishment PEs.

Schizophrenia, another disorder that has been associated with a maladaptive dopamine system, is characterised by two subsets of symptoms: positive symptoms include hallucinations and delusions, whilst negative symptoms include avolition, anhedonia, and blunted affect. The dopamine hypothesis of schizophrenia was based on evidence that positive symptoms have been associated with increased levels of D2 receptors in the striatum (e.g. Wong et al., 1986). More recently it has been suggested that it is presynaptic dopamine that is affected in schizophrenia. It has been shown that presynaptic dopamine synthesis is increased in drug naïve patients, in comparison to healthy controls (e.g. McGowan et al., 2004). In addition the frontal cortex may actually show a decrease in dopamine function (Grace, 1991). With this evidence in mind, Davis and colleagues (Davis et al., 1991) suggested that the two sets of symptoms in schizophrenia are both caused by a maladaptive dopamine system, but through different mechanisms. The positive symptoms are caused by an increase in the activity of the mesolimbic dopamine projections, whilst the deficit in dopamine projections in the mesocortical projections is responsible for the negative symptoms. The suggestions that there are two distinct dopaminergic populations, one that projects to the striatum and in overactive in schizophrenia, and the other that projects to the frontal cortex and is underactive, would fit with the hypothesis presented here of multiple dopamine populations. In support of a maladaptive PE system, it has been shown that patients with schizophrenia do have an abnormal reward PE response (Murray et al., 2008).

The positive symptoms of schizophrenia have been explained using the saliency hypothesis (see Kapur, 2003 for a review). This hypothesis suggests that stimuli incorrectly are interpreted as novel, surprising, or salient by the dopaminergic midbrain system. This leads to aberrant associations, and positive symptoms. This

hypothesis fits with the results presented here, as one possible interpretation of the data is that I have measured a population of neurons that signal a saliency response. This population of neurons could become dysfunctional in schizophrenia, and allow aberrant associations to form.

6.2. Future directions

The possible future directions of the work in this thesis separate into two themes: first is the application of the methods presented here to further investigate the function of the dopaminergic midbrain, and its network level interactions. Second is the development of the methods themselves.

6.2.1. Applications of the midbrain MRI methods

First, the experiment to investigate PEs in the dopaminergic midbrain could be extended. In the introduction I outlined four potential types of PEs:

1. Positive reward PE: elicited by an event that is more rewarding than expected;
2. Positive punishment PE: elicited by an event that is less punishing than expected;
3. Negative reward PE: elicited by an event that is less rewarding then expected;
4. Negative punishment PE: elicited by an event that is more punishing than expected;

The protocol presented in Chapter 5 investigated positive reward PEs and negative punishment PEs. In addition, outcomes that elicited PEs with the absence of financial outcomes were presented (nil outcomes). However it is not clear how these nil outcomes fit into this terminology, as the outcomes themselves do not have a financial valence. To fully test all types of PEs, a positive punishment PE that it elicited by a financial loss that is less punishing than expected, and a negative reward PE that is elicited by a financial gain that is less than expected, should be included in the experiment. Therefore a future experiment could included these conditions and compare activity elicited by all types of PEs. The results outlined here would suggest that all four types of PEs would elicit an increase in the BOLD signal in the medial dopaminergic midbrain, but there may be differences in the pattern of

activity in the more lateral regions. I have shown that PE responses are elicited in the absence of any financial outcome, so the valence of the outcome should not alter the activity, only whether it is better or worse than expected.

Second, the methods could be used to investigate the midbrain response to primary rewards and punishments, such as food, juice, and pain. Money is a uniquely human stimulus, and has thus not been used in animal research. Instead animal experiments utilise primary rewards, either measuring response to the outcome itself, or to a cue that predicts a primary stimulus. It may be that, with the use of such stimuli in the human, there may be an observable functional segregation within the medial dopaminergic midbrain along the dorsal-ventral dimension (Brischoux et al., 2009), or a medial-lateral subdivision in the VTA and SNc (Matsumoto and Hikosaka, 2009).

Finally, the methods presented here can be used to investigate clinical populations. Dopamine is strongly implicated in the symptoms of Parkinson's disease, as there is substantial dopaminergic cell death as the disease progresses. Parkinson's disease is characterised by cell loss in the dopaminergic midbrain. Motor symptoms include akinesia, rigidity, and tremor. Such symptoms can be relieved by treatment with levodopa, a dopamine replacement therapy. However recent research has focused on the (non-motor) psychiatric symptoms that seem to be induced by dopamine replacement therapy. This includes compulsive use of levodopa (Evans et al., 2010), the development of psychotic symptoms (Kuzuhara, 2001), and impulse control disorders (Evans et al., 2009). Using the methods presented here to characterise the midbrain dopaminergic system in patients presenting with such drug related symptoms, compared to patients without such symptoms, may lead us to better understand the heterogeneity of symptoms associated with Parkinson's, and improve drug therapies. Other disorders that have been hypothesised to be caused by a maladaptive dopaminergic system include drug addiction (Koob and Volkow, 2010; Lüscher and Ungless, 2006), schizophrenia (Moran et al., 2008; Murray et al., 2008), and gambling (Chase and Clark, 2010; Clark et al., 2009). By investigating the PE response in these patients groups, it may help to explain the mechanism that underlies the symptoms of the disorders, which may help improve drug therapies.

6.2.2. Methodological developments

Although the methods presented in this thesis improve detection of the BOLD signal in the human dopaminergic midbrain, further development may allow even more improvement.

In terms of data acquisition, there are several ways in which the protocol could be improved. First, higher field strength magnets could be used for data acquisition. Seven Tesla magnets are becoming increasingly common, and allow scanning at higher resolution than is possible with a three Tesla scanner. Therefore, it may be practical to scan at a resolution where functional subdivisions within the VTA are revealed. Second, structural imaging of the midbrain could be improved. Susceptibility-weighted imaging has been used to image the human midbrain with an improved contrast than is available with T2-weighted images (Manova et al., 2009). Again, high field strengths will also improve the anatomical detail we can obtain from structural scans of the midbrain, and this improve the accuracy with which we can localise midbrain nuclei. If a large body of such structural scans are collected, then it will be possible to create a standard atlas of the midbrain in MNI space. Such an atlas is required to standardise the way in which midbrain fMRI studies are reported, and allow comparison of results across studies.

Finally, the methods presented here could be adapted for use in a whole-brain study with larger voxel sizes. Many researchers want to investigate network level interactions, as the dopaminergic midbrain projects widely to the rest of the brain. Until faster imaging techniques are developed that allow high-resolution scanning of the whole-brain within a reasonable time frame, whole-brain studies must use a relatively low resolution. Although midbrain nuclei cannot be localised as accurately with such voxel sizes, due to increased partial volume effects across nuclei and in increased influence of physiological noise, some of the methods presented here can be applied to the whole-brain studies, improving the accuracy with which we can localise activity to a certain extent. For example, the PNM can be used to reduce the effects of physiological noise. In addition, the optimised registration could be applied to the data. However the analysis would have to be carried out in two steps: the first with accurate cortical registration, the second with accurate subcortical registration.

The next methodological development would be to create a registration pathway that simultaneously achieves good registration at the level of the midbrain, and cortex.

The work presented in this thesis has led to methodological advancements in midbrain fMRI, and provided evidence that the human dopaminergic midbrain is involved in processing both positive and negative PEs. In addition, it leads onto future work that could reveal much about clinical populations, which we are yet to fully understand.

References

Abler, B., Walter, H., Erk, S., Kammerer, H., and Spitzer, M. (2006). Prediction error as a linear function of reward probability is coded in human nucleus accumbens. Neuroimage *31*, 790-795.

Afshar, F., Watkins, E.S., and Yap, J.C. (1978). Stereotaxic atlas of the human brainstem and cerebellar nuclei: a variability study (Raven Press).

Albanese, A., and Minciacchi, D. (1983). Organization of the ascending projections from the ventral tegmental area: a multiple fluorescent retrograde tracer study in the rat. J Comp Neurol *216*, 406-420.

Amiez, C., Joseph, J.-P., and Procyk, E. (2005). Anterior cingulate error-related activity is modulated by predicted reward. Eur J Neurosci *21*, 3447-3452.

Amiez, C., Joseph, J.P., and Procyk, E. (2006). Reward encoding in the monkey anterior cingulate cortex. Cereb Cortex *16*, 1040-1055.

Aron, A.R., Shohamy, D., Clark, J., Myers, C., Gluck, M.A., and Poldrack, R.A. (2004). Human midbrain sensitivity to cognitive feedback and uncertainty during classification learning. J Neurophysiol *92*, 1144-1152.

Balcita-Pedicino, J.J., Omelchenko, N., Bell, R., and Sesack, S.R. (2011). The Inhibitory Influence of the Lateral Habenula on Midbrain Dopamine Cells: Ultrastructural Evidence for Indirect Mediation via the Rostromedial Mesopontine Tegmental Nucleus. J Comp Neurol *519*, 1143-1164.

Bayer, H.M., and Glimcher, P.W. (2005). Midbrain dopamine neurons encode a quantitative reward prediction error signal. Neuron *47*, 129-141.

Beckmann, C.F., Jenkinson, M., and Smith, S.M. (2003). General multilevel linear modeling for group analysis in FMRI. Neuroimage *20*, 1052-1063.

Beckstead, R.M., Domesick, V.B., and Nauta, W.J. (1979). Efferent connections of the substantia nigra and ventral tegmental area in the rat. Brain Res *175*, 191-217.

Berendse, H.W., Groenewegen, H.J., and Lohman, A.H. (1992). Compartmental distribution of ventral striatal neurons projecting to the mesencephalon in the rat. J Neurosci *12*, 2079-2103.

Berridge, K.C. (2012). From prediction error to incentive salience: mesolimbic computation of reward motivation. The European journal of neuroscience *35*, 1124-1143.

Berridge, K.C., and Kringelbach, M.L. (2008). Affective neuroscience of pleasure: reward in humans and animals. Psychopharmacology (Berl) *199*, 457-480.

Berridge, K.C., and Robinson, T.E. (1998). What is the role of dopamine in reward: hedonic impact, reward learning, or incentive salience? Brain research reviews *28*, 309-369.

Berridge, K.C., and Robinson, T.E. (2003). Parsing reward. Trends Neurosci *26*, 507-513.

Bodurka, J., Ye, F., Petridou, N., Murphy, K., and Bandettini, P.A. (2007). Mapping the MRI voxel volume in which thermal noise matches physiological noise-implications for fMRI. Neuroimage *34*, 542-549.

Boehler, C.N., Hopf, J.-M., Krebs, R.M., Stoppel, C.M., Schoenfeld, M.A., Heinze, H.-J., and Noesselt, T. (2011). Task-load-dependent activation of dopaminergic midbrain areas in the absence of reward. J Neurosci *31*, 4955-4961.

Boynton, G.M., Engel, S.A., Glover, G.H., and Heeger, D.J. (1996). Linear systems analysis of functional magnetic resonance imaging in human V1. J Neurosci *16*, 4207-4221.

Brainard, D.H. (1997). The Psychophysics Toolbox. Spat Vis *10*, 433-436.

Brinschwitz, K., Dittgen, A., Madai, V.I., Lommel, R., Geisler, S., and Veh, R.W. (2010). Glutamatergic axons from the lateral habenula mainly trminate on GABAergic neurons of the ventral midbrain. Neuroscience *168*, 463-476.

Brischoux, F., Chakraborty, S., Brierley, D.I., and Ungless, M.A. (2009). Phasic excitation of dopamine neurons in ventral VTA by noxious stimuli. Proc Natl Acad Sci U S A *106*, 4894-4899.

Brog, J.S., Salyapongse, A., Deutch, A.Y., and Zahm, D.S. (1993). The patterns of afferent innervation of the core and shell in the "accumbens" part of the rat ventral striatum: immunohistochemical detection of retrogradely transported fluoro-gold. J Comp Neurol *338*, 255-278.

Bromberg-Martin, E.S., Hikosaka, O., and Nakamura, K. (2010a). Coding of task reward value in the dorsal raphe nucleus. J Neurosci *30*, 6262-6272.

Bromberg-Martin, E.S., Matsumoto, M., and Hikosaka, O. (2010b). Distinct tonic and phasic anticipatory activity in lateral habenula and dopamine neurons. Neuron *67*, 144-155.

Bromberg-Martin, E.S., Matsumoto, M., and Hikosaka, O. (2010c). Dopamine in motivational control: rewarding, aversive, and alerting. Neuron *68*, 815-834.

Brooks, J.C.W., Beckmann, C.F., Miller, K.L., Wise, R.G., Porro, C.A., Tracey, I., and Jenkinson, M. (2008). Physiological noise modelling for spinal functional magnetic resonance imaging studies. Neuroimage *39*, 680-692.

Caplin, A., and Dean, M. (2008). Dopamine, Reward Prediction Error, and Economics. Q J Econ *123*, 663-701.

Chang, C., Cunningham, J.P., and Glover, G.H. (2009). Influence of heart rate on the BOLD signal: the cardiac response function. Neuroimage *44*, 857-869.

Chase, H.W., and Clark, L. (2010). Gambling severity predicts midbrain response to near-miss outcomes. J Neurosci *30*, 6180-6187.

Christoph, G.R., Leonzio, R.J., and Wilcox, K.S. (1986). Stimulation of the lateral habenula inhibits dopamine-containing neurons in the substantia nigra and ventral tegmental area of the rat. J Neurosci *6*, 613-619.

Clark, L., Lawrence, A.J., Astley-Jones, F., and Gray, N. (2009). Gambling near-misses enhance motivation to gamble and recruit win-related brain circuitry. Neuron *61*, 481-490.

Cohen, J.Y., Haesler, S., Vong, L., Lowell, B.B., and Uchida, N. (2012). Neuron-type-specific signals for reward and punishment in the ventral tegmental area. Nature.

Cohen-Adad, J., Gauthier, C.J., Brooks, J.C.W., Slessarev, M., Han, J., Fisher, J.A., Rossignol, S., and Hoge, R.D. (2010). BOLD signal responses to controlled hypercapnia in human spinal cord. Neuroimage *50*, 1074-1084.

Cynader, M., and Berman, N. (1972). Receptive-field organization of monkey superior colliculus. J Neurophysiol *35*, 187-201.

D'Ardenne, K., McClure, S.M., Nystrom, L.E., and Cohen, J.D. (2008). BOLD responses reflecting dopaminergic signals in the human ventral tegmental area. Science *319*, 1264-1267.

Dagli, M.S., Ingeholm, J.E., and Haxby, J.V. (1999). Localization of cardiac-induced signal change in fMRI. Neuroimage *9*, 407-415.

Dahlstroem, A., and Fuxe, K. (1964). Evidence for the existence of monoamine-containing neurons in the central nervous system. I. Demonstration of monoamines in the cell bodies of brain stem neurons. Acta Physiol Scand Suppl, SUPPL 232:231-255.

Davis, K.L., Kahn, R.S., Ko, G., and Davidson, M. (1991). Dopamine in schizophrenia: a review and reconceptualisation. A J Psychiatry *148*, 1474-1486.

Daw, N.D., Kakade, S., and Dayan, P. (2002). Opponent interactions between serotonin and dopamine. Neural Networks *15*, 603-616.

Dayan, P., and Balleine, B.W. (2002). Reward, motivation, and reinforcement learning. Neuron *36*, 285-298.

de Zwart, J.A., van Gelderen, P., Fukunaga, M., and Duyn, J.H. (2008). Reducing correlated noise in fMRI data. Magn Reson Med *59*, 939-945.

Deutch, A.Y., Goldstein, M., and Roth, R.H. (1986). The ascending projections of the dopaminergic neurons of the substantia nigra, zona reticulata: a combined retrograde tracer-immunohistochemical study. Neurosci Lett *71*, 257-263.

Disbrow, E.A., Slutsky, D.A., Roberts, T.P., and Krubitzer, L.A. (2000). Functional MRI at 1.5 tesla: a comparison of the blood oxygenation level-dependent signal and electrophysiology. Proc Natl Acad Sci U S A *97*, 9718-9723.

Dobi, A., Margolis, E.B., Wang, H.-L., Harvey, B.K., and Morales, M. (2010). Glutamatergic and nonglutamatergic neurons of the ventral tegmental area establish local synaptic contacts with dopaminergic and nondopaminergic neurons. J Neurosci *30*, 218-229.

Drayer, B., Burger, P., Darwin, R., Riederer, S., Herfkens, R., and Johnson, G.A. (1986). MRI of brain iron. Am J Roentgenol *147*, 103-110.

DuBois, R.M., and Cohen, M.S. (2000). Spatiotopic organization in human superior colliculus observed with fMRI. Neuroimage *12*, 63-70.

Dunckley, P., Wise, R.G., Fairhurst, M., Hobden, P., Aziz, Q., Chang, L., and Tracey, I. (2005). A comparison of visceral and somatic pain processing in the human brainstem using functional magnetic resonance imaging. J Neurosci *25*, 7333-7341.

Düzel, E., Bunzeck, N., Guitart-Masip, M., Wittmann, B., Schott, B., and Tobler, P. (2009). Functional imaging of the human dopaminergic midbrain. Trends Neurosci.

Eapen, M., Zald, D.H., Gatenby, J.C., Ding, Z., and Gore, J.C. (2011). Using high-resolution MR imaging at 7T to evaluate the anatomy of the midbrain dopaminergic system. Am J Neuroradiol *32*, 688-694.

Edelstein, W.A., Glover, G.H., Hardy, C.J., and Redington, R.W. (1986). The intrinsic signal-to-noise ratio in NMR imaging. Magn Reson Med *3*, 604-618.

Evans, A.H., Lawrence, A.D., Cresswell, S.A., Katzenschlager, R., and Lees, A.J. (2010). Compulsive use of dopaminergic drug therapy in Parkinson's disease: reward and anti-reward. Movement Disord *25*, 867-876.

Evans, A.H., Strafella, A.P., Weintraub, D., and Stacy, M. (2009). Impulsive and compulsive behaviors in Parkinson's disease. Movement Disord *24*, 1561-1570.

Fallon, J.H. (1981). Collateralization of monoamine neurons: mesotelencephalic dopamine projections to caudate, septum, and frontal cortex. J Neurosci *1*, 1361-1368.

Faul, F., Erdfelder, E., Lang, A.G., and Buchner, A. (2007). G*Power 3: a flexible statistical power analysis program for the social, behavioral, and biomedical sciences. Behav Res Methods *39*, 175-191.

Fiorillo, C., Newsome, W., and Schultz, W. (2008). The temporal precision of reward prediction in dopamine neurons. Nat Neurosci *11*, 966-973.

Fiorillo, C.D., Tobler, P.N., and Schultz, W. (2003). Discrete coding of reward probability and uncertainty by dopamine neurons. Science *299*, 1898-1902.

François, C., Yelnik, J., Tandé, D., Agid, Y., and Hirsch, E.C. (1999). Dopaminergic cell group A8 in the monkey: anatomical organization and projections to the striatum. J Comp Neurol *414*, 334-347.

Friese, S., Hamhaber, U., Erb, M., Kueker, W., and Klose, U. (2004). The influence of pulse and respiration on spinal cerebrospinal fluid pulsation. Invest Radiol *39*, 120-130.

Genovese, C.R., Lazar, N.A., and Nichols, T. (2002). Thresholding of statistical maps in functional neuroimaging using the false discovery rate. Neuroimage *15*, 870-878.

German, D.C., and Manaye, K.F. (1993). Midbrain dopaminergic neurons (nuclei A8, A9, and A10): three-dimensional reconstruction in the rat. J Comp Neurol *331*, 297-309.

German, D.C., Schlusselberg, D.S., and Woodward, D.J. (1983). Three-dimensional computer reconstruction of midbrain dopaminergic neuronal populations: from mouse to man. J Neural Transm *57*, 243-254.

Glover, G.H., Li, T.Q., and Ress, D. (2000). Image-based method for retrospective correction of physiological motion effects in fMRI: RETROICOR. Magn Reson Med *44*, 162-167.

Goldberg, M.E., and Wurtz, R.H. (1972). Activity of superior colliculus in behaving monkey. I. Visual receptive fields of single neurons. J Neurophysiol *35*, 542-559.

Grace, A.A. (1991). Phasic versus tonic dopamine release and the modulation of dopamine system responsivity: a hypothesis for the etiology of shizophrenia. Neuroscience *41*, 1-24.

Greitz, D., Wirestam, R., Franck, A., Nordell, B., Thomsen, C., and Ståhlberg, F. (1992). Pulsatile brain movement and associated hydrodynamics studied by magnetic resonance phase imaging. The Monro-Kellie doctrine revisited. Neuroradiology *34*, 370-380.

Groenewegen, H.J., Berendse, H.W., and Haber, S.N. (1993). Organization of the output of the ventral striatopallidal system in the rat: ventral pallidal efferents. Neuroscience *57*, 113-142.

Guarraci, F.A., and Kapp, B.S. (1999). An electrophysiological characterization of ventral tegmental area dopaminergic neurons during differential pavlovian fear conditioning in the awake rabbit. Behav Brain Res *99*, 169-179.

Guimaraes, A.R., Melcher, J.R., Talavage, T.M., Baker, J.R., Ledden, P., Rosen, B.R., Kiang, N.Y., Fullerton, B.C., and Weisskoff, R.M. (1998). Imaging subcortical auditory activity in humans. Hum Brain Mapp *6*, 33-41.

Guitart-Masip, M., Fuentemilla, L., Bach, D.R., Huys, Q.J.M., Dayan, P., Dolan, R.J., and Duzel, E. (2011). Action dominates valence in anticipatory representations in the human striatum and dopaminergic midbrain. J Neurosci *31*, 7867-7875.

Haber, S.N., and Fudge, J.L. (1997). The primate substantia nigra and VTA: integrative circuitry and function. Crit Rev Neurobiol *11*, 323-342.

Haber, S.N., and Knutson, B. (2010). The reward circuit: linking primate anatomy and human imaging. Neuropsychopharmacology *35*, 4-26.

Haber, S.N., Lynd, E., Klein, C., and Groenewegen, H.J. (1990). Topographic organization of the ventral striatal efferent projections in the rhesus monkey: an anterograde tracing study. J Comp Neurol *293*, 282-298.

Halliday, G.M., and Törk, I. (1986). Comparative anatomy of the ventromedial mesencephalic tegmentum in the rat, cat, monkey and human. J Comp Neurol *252*, 423-445.

Harvey, A.K., Pattinson, K.T.S., Brooks, J.C.W., Mayhew, S.D., Jenkinson, M., and Wise, R.G. (2008). Brainstem functional magnetic resonance imaging: Disentangling signal from physiological noise. J Magn Reson Imaging *28*, 1337-1344.

Hawley, M.L., Melcher, J.R., and Fullerton, B.C. (2005). Effects of sound bandwidth on fMRI activation in human auditory brainstem nuclei. Hear Res *204*, 101-110.

Hirsch, E., Graybiel, A.M., and Agid, Y.A. (1988). Melanized dopaminergic neurons are differentially susceptible to degeneration in Parkinson's disease. Nature *334*, 345-348.

Holroyd, C.B., and Coles, M.G.H. (2008). Dorsal anterior cingulate cortex integrates reinforcement history to guide voluntary behavior. Cortex *44*, 548-559.

Hu, X., Le, T.H., Parrish, T., and Erhard, P. (1995). Retrospective estimation and correction of physiological fluctuation in functional MRI. Magn Reson Med *34*, 201-212.

Hutton, C., Josephs, O., Stadler, J., Featherstone, E., Reid, A., Speck, O., Bernarding, J., and Weiskopf, N. (2011). The impact of physiological noise correction on fMRI at 7 T. Neuroimage *57*, 101-112.

Jenkinson, M., Bannister, P., Brady, M., and Smith, S. (2002). Improved optimization for the robust and accurate linear registration and motion correction of brain images. Neuroimage *17*, 825-841.

Jenkinson, M., and Smith, S. (2001). A global optimisation method for robust affine registration of brain images. Med Image Anal *5*, 143-156.

Joel, D., and Weiner, I. (2000). The connections of the dopaminergic system with the striatum in rats and primates: an analysis with respect to the functional and compartmental organization of the striatum. Neuroscience *96*, 451-474.

Joshua, M., Adler, A., Mitelman, R., Vaadia, E., and Bergman, H. (2008). Midbrain dopaminergic neurons and striatal cholinergic interneurons encode the difference between reward and aversive events at different epochs of probabilistic classical conditioning trials. J Neurosci *28*, 11673-11684.

Kapur, S. (2003). Psychosis as a state of aberrant salience: a framework linking biology, phenomenology, and pharmacology in schizophrenia. American J Psychiat *160*, 13-23.

Kennerley, S.W., and Wallis, J.D. (2009). Evaluating choices by single neurons in the frontal lobe: outcome value encoded across multiple decision variables. Eur J Neurosci *29*, 2061-2073.

Kitahama, K., Nagatsu, I., and Pearson, J. (1994). Catecholamine systems in mammalian midbrain and hindbrain: theme and variations. In Phylogeny and development of catecholamine systems in the CNS of vertebrates, W.J.A.J. Smeets, and A. Reiner, eds. (Cambridge University Press), pp. 183-206.

Klein, A., Andersson, J., Ardekani, B.A., Ashburner, J., Avants, B., Chiang, M.-C., Christensen, G.E., Collins, D.L., Gee, J., Hellier, P.*, et al.* (2009). Evaluation of 14 nonlinear deformation algorithms applied to human brain MRI registration. Neuroimage *46*, 786-802.

Klein-Flügge, M.C., Hunt, L.T., Bach, D.R., Dolan, R.J., and Behrens, T.E.J. (2011). Dissociable reward and timing signals in human midbrain and ventral striatum. Neuron *72*, 654-664.

Klose, U., Strik, C., Kiefer, C., and Grodd, W. (2000). Detection of a relation between respiration and CSF pulsation with an echoplanar technique. J Magn Reson Imaging *11*, 438-444.

Knutson, B., Taylor, J., Kaufman, M., Peterson, R., and Glover, G. (2005). Distributed neural representation of expected value. J Neurosci *25*, 4806-4812.

Koob, G., and Volkow, N. (2010). Neurocircuitry of Addiction. Neuropsychopharmacol *35*, 217-238.

Krebs, R.M., Heipertz, D., Schuetze, H., and Düzel, E. (2011). Novelty increases the mesolimbic functional connectivity of the substantia nigra/ventral tegmental area (SN/VTA) during reward anticipation: Evidence from high-resolution fMRI. Neuroimage *58*, 647-655.

Krebs, R.M., Woldorff, M.G., Tempelmann, C., Bodammer, N., Noesselt, T., Boehler, C.N., Scheich, H., Hopf, J.-M., Düzel, E., Heinze, H.-J.*, et al.* (2010). High-field FMRI reveals brain activation patterns underlying saccade execution in the human superior colliculus. PloS one *5*, e8691.

Kuzuhara, S. (2001). Drug-induced psychotic symptoms in Parkinson's disease. Problems, management and dilemma. J Neurol *248 Suppl 3*, III28-31.

Kwong, K.K., Belliveau, J.W., Chesler, D.A., Goldberg, I.E., Weisskoff, R.M., Poncelet, B.P., Kennedy, D.N., Hoppel, B.E., Cohen, M.S., Turner, R.*, et al.* (1992). Dynamic magnetic resonance imaging of human brain activity during primary sensory stimulation. Proc Natl Acad Sci U S A *89*, 5675-5679.

Leshan, R.L., Opland, D.M., Louis, G.W., Leinninger, G.M., Patterson, C.M., Rhodes, C.J., Munzberg, H., and Myers, M.G., Jr. (2010). Ventral tegmental area leptin

receptor neurons specifically project to and regulate cocaine- and amphetamine-regulated transcript neurons of the extended central amygdala. J Neurosci *30*, 5713-5723.

Limbrick-Oldfield, E.H., Brooks, J.C., Wise, R.J., Padormo, F., Hajnal, J.V., Beckmann, C.F., and Ungless, M.A. (2012). Identification and characterisation of midbrain nuclei using optimised functional magnetic resonance imaging. Neuroimage *59*, 1230-1238.

Liston, A.D., Lund, T.E., Salek-Haddadi, A., Hamandi, K., Friston, K.J., and Lemieux, L. (2006). Modelling cardiac signal as a confound in EEG-fMRI and its application in focal epilepsy studies. Neuroimage *30*, 827-834.

Logothetis, N.K. (2003). The underpinnings of the BOLD functional magnetic resonance imaging signal. J Neurosci *23*, 3963-3971.

Logothetis, N.K. (2008). What we can do and what we cannot do with fMRI. Nature *453*, 869-878.

Logothetis, N.K., Guggenberger, H., Peled, S., and Pauls, J. (1999). Functional imaging of the monkey brain. Nat Neurosci *2*, 555-562.

Logothetis, N.K., Pauls, J., Augath, M., Trinath, T., and Oeltermann, A. (2001). Neurophysiological investigation of the basis of the fMRI signal. Nature *412*, 150-157.

Logothetis, N.K., and Wandell, B.A. (2004). Interpreting the BOLD signal. Annu Rev Physiol *66*, 735-769.

Lüscher, C., and Ungless, M.A. (2006). The mechanistic classification of addictive drugs. PLoS Medicine *3*, e437.

Lynd-Balta, E., and Haber, S.N. (1994). The organization of midbrain projections to the ventral striatum in the primate. Neuroscience *59*, 609-623.

Manova, E.S., Habib, C.A., Boikov, A.S., Ayaz, M., Khan, A., Kirsch, W.M., Kido, D.K., and Haacke, E.M. (2009). Characterizing the mesencephalon using susceptibility-weighted imaging. Am J Neuroradiol *30*, 569-574.

Mantz, J., Thierry, A.M., and Glowinski, J. (1989). Effect of noxious tail pinch on the discharge rate of mesocortical and mesolimbic dopamine neurons: selective activation of the mesocortical system. Brain Res *476*, 377-381.

Matsumoto, M., and Hikosaka, O. (2007). Lateral habenula as a source of negative reward signals in dopamine neurons. Nature *447*, 1111-1115.

Matsumoto, M., and Hikosaka, O. (2009). Two types of dopamine neuron distinctly convey positive and negative motivational signals. Nature *459*, 837-841.

McClure, S.M., Berns, G.S., and Montague, P.R. (2003). Temporal prediction errors in a passive learning task activate human striatum. Neuron *38*, 339-346.

McGowan, S., Lawrence, A.D., Sales, T., Quested, D., and Grasby, P. (2004). Presynaptic dopaminergic dysfunction in schizophrenia: a positron emission tomographic [18F] fluorodopa study. Arch Gen Psychiatry *61*, 134-142.

McRitchie, D.A., Cartwright, H., Pond, S.M., van der Schyf, C.J., Castagnoli, N., van der Nest, D.G., and Halliday, G.M. (1998). The midbrain dopaminergic cell groups in the baboon Papio ursinus. Brain Res Bull *47*, 611-623.

McRitchie, D.A., Hardman, C.D., and Halliday, G.M. (1996). Cytoarchitectural distribution of calcium binding proteins in midbrain dopaminergic regions of rats and humans. J Comp Neurol *364*, 121-150.

Menke, R.A., Jbabdi, S., Miller, K.L., Matthews, P.M., and Zarei, M. (2010). Connectivity-based segmentation of the substantia nigra in human and its implications in Parkinson's disease. Neuroimage *52*, 1175-1180.

Mileykovskiy, B., and Morales, M. (2011). Duration of inhibition of ventral tegmental area dopamine neurons encodes a level of conditioned fear. J Neurosci *31*, 7471-7476.

Mirenowicz, J., and Schultz, W. (1996). Preferential activation of midbrain dopamine neurons by appetitive rather than aversive stimuli. Nature *379*, 449-451.

Moran, P.M., Owen, L., Crookes, A.E., Al-Uzri, M.M., and Reveley, M.A. (2008). Abnormal prediction error is associated with negative and depressive symptoms in schizophrenia. Prog Neuropsychopharmacol Biol Psychiatry *32*, 116-123.

Muresan, L., Renken, R., Roerdink, J.B., and Duifhuis, H. (2005). Automated correction of spin-history related motion artefacts in fMRI: simulated and phantom data. IEEE T Bio-Med Eng *52*, 1450-1460.

Murray, G.K., Corlett, P.R., Clark, L., Pessiglione, M., Blackwell, A.D., Honey, G., Jones, P.B., Bullmore, E.T., Robbins, T.W., and Fletcher, P.C. (2008). Substantia nigra/ventral tegmental reward prediction error disruption in psychosis. Mol Psychiatry *13*, 239, 267-276.

Naidich, T.P., Duvernoy, H.M., Delman, B.N., Sorensen, A.G., Kollias, S.S., and Haacke, E.M. (2009). Duvernoy's Atlas of the Human Brain Stem and Cerebellum: High-Field MRI, Surface Anatomy, Internal Structure, Vascularization and 3 D Sectional Anatomy (Springer).

Nair-Roberts, R.G., Chatelain-Badie, S.D., Benson, E., White-Cooper, H., Bolam, J.P., and Ungless, M.A. (2008). Stereological estimates of dopaminergic, GABAergic and glutamatergic neurons in the ventral tegmental area, substantia nigra and retrorubral field in the rat. Neuroscience *152*, 1024-1031.

Nakahara, H., Itoh, H., Kawagoe, R., Takikawa, Y., and Hikosaka, O. (2004). Dopamine neurons can represent context-dependent prediction error. Neuron *41*, 269-280.

Napadow, V., Dhond, R., Kennedy, D., Hui, K.K.S., and Makris, N. (2006). Automated brainstem co-registration (ABC) for MRI. Neuroimage *32*, 1113-1119.

Napadow, V., Dhond, R., Park, K., Kim, J., Makris, N., Kwong, K.K., Harris, R.E., Purdon, P.L., Kettner, N., and Hui, K.K. (2009). Time-variant fMRI activity in the brainstem and higher structures in response to acupuncture. Neuroimage *47*, 289-301.

Nestler, E.J. (2005). Is there a common molecular pathway for addiction? Nat Neurosci *8*, 1445-1449.

Nichols, T.E., and Holmes, A.P. (2002). Nonparametric permutation tests for functional neuroimaging: a primer with examples. Hum Brain Mapp *15*, 1-25.

O'Doherty, J., Dayan, P., Schultz, J., Deichmann, R., Friston, K., and Dolan, R.J. (2004). Dissociable roles of ventral and dorsal striatum in instrumental conditioning. Science *304*, 452-454.

O'Doherty, J.P., Dayan, P., Friston, K., Critchley, H., and Dolan, R.J. (2003). Temporal difference models and reward-related learning in the human brain. Neuron *38*, 329-337.

Oikawa, H., Sasaki, M., Tamakawa, Y., Ehara, S., and Tohyama, K. (2002). The substantia nigra in Parkinson disease: proton density-weighted spin-echo and fast short inversion time inversion-recovery MR findings. Am J Neuroradiol *23*, 1747-1756.

Omelchenko, N., Bell, R., and Sesack, S.R. (2009). Lateral habenula projections to dopamine and GABA neurons in the rat ventral tegmental area. Eur J Neurosci *30*, 1239-1250.

Pagnoni, G., Zink, C.F., Montague, P.R., and Berns, G.S. (2002). Activity in human ventral striatum locked to errors of reward prediction. Nat Neurosci *5*, 97-98.

Parent, A. (1990). Extrinsic connections of the basal ganglia. Trends Neurosci *13*, 254-258.

Paton, J.J., Belova, M.A., Morrison, S.E., and Salzman, C.D. (2006). The primate amygdala represents the positive and negative value of visual stimuli during learning. Nature *439*, 865-870.

Pattinson, K.T., Governo, R.J., MacIntosh, B.J., Russell, E.C., Corfield, D.R., Tracey, I., and Wise, R.G. (2009a). Opioids depress cortical centers responsible for the volitional control of respiration. J Neurosci *29*, 8177-8186.

Pattinson, K.T., Mitsis, G.D., Harvey, A.K., Jbabdi, S., Dirckx, S., Mayhew, S.D., Rogers, R., Tracey, I., and Wise, R.G. (2009b). Determination of the human brainstem respiratory control network and its cortical connections in vivo using functional and structural imaging. Neuroimage *44*, 295-305.

Pearson, J., Goldstein, M., Markey, K., and Brandeis, L. (1983). Human brainstem catecholamine neuronal anatomy as indicated by immunocytochemistry with antibodies to tyrosine hydroxylase. NSC *8*, 3-32.

Pelli, D.G. (1997). The VideoToolbox software for visual psychophysics: transforming numbers into movies. Spat Vis *10*, 437-442.

Piché, M., Cohen-Adad, J., Nejad, M.K., Perlbarg, V., Xie, G., Beaudoin, G., Benali, H., and Rainville, P. (2009). Characterization of cardiac-related noise in fMRI of the cervical spinal cord. Magn Reson Imaging *27*, 300-310.

Plassmann, H., O'Doherty, J.P., and Rangel, A. (2010). Appetitive and aversive goal values are encoded in the medial orbitofrontal cortex at the time of decision making. J Neurosci *30*, 10799-10808.

Poirier, L.J., Giguère, M., and Marchand, R. (1983). Comparative morphology of the substantia nigra and ventral tegmental area in the monkey, cat and rat. Brain Res Bull *11*, 371-397.

Poncelet, B.P., Wedeen, V.J., Weisskoff, R.M., and Cohen, M.S. (1992). Brain parenchyma motion: measurement with cine echo-planar MR imaging. Radiology *185*, 645-651.

Prensa, L., and Parent, A. (2001). The nigrostriatal pathway in the rat: A single-axon study of the relationship between dorsal and ventral tier nigral neurons and the striosome/matrix striatal compartments. J Neurosci *21*, 7247-7260.

Raj, D., Anderson, A.W., and Gore, J.C. (2001). Respiratory effects in human functional magnetic resonance imaging due to bulk susceptibility changes. Phys Med Biol *46*, 3331-3340.

Ranade, S.P., and Mainen, Z.F. (2009). Transient firing of dorsal raphe neurons encodes diverse and specific sensory, motor, and reward events. J Neurophysiol *102*, 3026-3037.

Redgrave, P., and Gurney, K. (2006). The short-latency dopamine signal: a role in discovering novel actions? Nat Rev Neurosci *7*, 967-975.

Redgrave, P., Gurney, K., and Reynolds, J. (2008). What is reinforced by phasic dopamine signals? Brain Res Rev *58*, 322-339.

Redgrave, P., Prescott, T.J., and Gurney, K. (1999). Is the short-latency dopamine response too short to signal reward error? Trends Neurosci *22*, 146-151.

Rees, G., Friston, K., and Koch, C. (2000). A direct quantitative relationship between the functional properties of human and macaque V5. Nat Neurosci *3*, 716-723.

Rutledge, R.B., Dean, M., Caplin, A., and Glimcher, P.W. (2010). Testing the reward prediction error hypothesis with an axiomatic model. J Neurosci *30*, 13525-13536.

Schneider, K.A., and Kastner, S. (2005). Visual responses of the human superior colliculus: a high-resolution functional magnetic resonance imaging study. J Neurophysiol *94*, 2491-2503.

Schneider, K.A., and Kastner, S. (2009). Effects of sustained spatial attention in the human lateral geniculate nucleus and superior colliculus. J Neurosci *29*, 1784-1795.

Schultz, W. (2000). Multiple reward signals in the brain. Nat Rev Neurosci *1*, 199-207.

Schultz, W. (2002). Getting formal with dopamine and reward. Neuron *36*, 241-263.

Schultz, W., Apicella, P., and Ljungberg, T. (1993). Responses of monkey dopamine neurons to reward and conditioned stimuli during successive steps of learning a delayed response task. J Neurosci *13*, 900-913.

Schultz, W., Dayan, P., and Montague, P.R. (1997). A neural substrate of prediction and reward. Science *275*, 1593-1599.

Seymour, B., Daw, N., Dayan, P., Singer, T., and Dolan, R. (2007). Differential encoding of losses and gains in the human striatum. J Neurosci *27*, 4826-4831.

Seymour, B., O'Doherty, J.P., Dayan, P., Koltzenburg, M., Jones, A.K., Dolan, R.J., Friston, K.J., and Frackowiak, R.S. (2004). Temporal difference models describe higher-order learning in humans. Nature *429*, 664-667.

Sigalovsky, I.S., and Melcher, J.R. (2006). Effects of sound level on fMRI activation in human brainstem, thalamic and cortical centers. Hear Res *215*, 67-76.

Smith, S.M. (2002). Fast robust automated brain extraction. Hum Brain Mapp *17*, 143-155.

Solomon, R.L., and Corbit, J.D. (1974). An opponent-process theory of motivation. I. Temporal dynamics of affect. Psychol Rev *81*, 119-145.

Sutton, R.S., and Barto, A.G. (1987). A temporal-difference model of classical conditioning (Seattle, WA, Lawrence Erlbaum).

Swanson, L.W. (1982). The projections of the ventral tegmental area and adjacent regions: a combined fluorescent retrograde tracer and immunofluorescence study in the rat. Brain Res Bull *9*, 321-353.

Sylvester, R., Josephs, O., Driver, J., and Rees, G. (2007). Visual FMRI responses in human superior colliculus show a temporal-nasal asymmetry that is absent in lateral geniculate and visual cortex. J Neurophysiol *97*, 1495-1502.

Tindell, A.J., Smith, K.S., Berridge, K.C., and Aldridge, J.W. (2009). Dynamic computation of incentive salience: "wanting" what was never "liked". J Neurosci *29*, 12220-12228.

Tobler, P.N., Fiorillo, C.D., and Schultz, W. (2005). Adaptive coding of reward value by dopamine neurons. Science *307*, 1642-1645.

Topolovec, J.C., Gati, J.S., Menon, R.S., Shoemaker, J.K., and Cechetto, D.F. (2004). Human cardiovascular and gustatory brainstem sites observed by functional magnetic resonance imaging. J Comp Neurol *471*, 446-461.

Tracey, I., Ploghaus, A., Gati, J.S., Clare, S., Smith, S., Menon, R.S., and Matthews, P.M. (2002). Imaging attentional modulation of pain in the periaqueductal gray in humans. J Neurosci *22*, 2748-2752.

Triantafyllou, C., Polimeni, J.R., and Wald, L.L. (2011). Physiological noise and signal-to-noise ratio in fMRI with multi-channel array coils. Neuroimage *55*, 597-606.

Ungless, M.A., Magill, P.J., and Bolam, J.P. (2004). Uniform inhibition of dopamine neurons in the ventral tegmental area by aversive stimuli. Science *303*, 2040-2042.

Valenti, O., Lodge, D.J., and Grace, A.A. (2011). Aversive stimuli alter ventral tegmental area dopamine neuron activity via a common action in the ventral hippocampus. J Neurosci *31*, 4280-4289.

van Duuren, E., van der Plasse, G., Lankelma, J., Joosten, R.N., Feenstra, M.G., and Pennartz, C.M. (2009). Single-cell and population coding of expected reward probability in the orbitofrontal cortex of the rat. J Neurosci *29*, 8965-8976.

Volkow, N., Fowler, J.S., Wang, G.-J., Swanson, J.M., and Telang, F. (2007). Dopamine in drug abuse and addiction: results of imaging studies and treatment implications. Arch Neurol *64*, 1575-1579.

Waelti, P., Dickinson, A., and Schultz, W. (2001). Dopamine responses comply with basic assumptions of formal learning theory. Nature *412*, 43-48.

Wall, M.B., Walker, R., and Smith, A.T. (2009). Functional imaging of the human superior colliculus: an optimised approach. Neuroimage *47*, 1620-1627.

Waltz, J.A., Schweitzer, J.B., Gold, J.M., Kurup, P.K., Ross, T.J., Salmeron, B.J., Rose, E.J., McClure, S.M., and Stein, E.A. (2009). Patients with schizophrenia have a reduced neural response to both unpredictable and predictable primary reinforcers. Neuropsychopharmacology *34*, 1567-1577.

Wang, D.V., and Tsien, J.Z. (2011). Convergent Processing of Both Positive and Negative Motivational Signals by the VTA Dopamine Neuronal Populations. PloS one *6*, e17047.

Wittmann, B.C., Schott, B.H., Guderian, S., Frey, J.U., Heinze, H.-J., and Düzel, E. (2005). Reward-related FMRI activation of dopaminergic midbrain is associated with enhanced hippocampus-dependent long-term memory formation. Neuron *45*, 459-467.

Wong, D.F., Wagner, H.N., Jr., Tune, L.E., Dannals, R.F., Pearlson, G.D., Links, J.M., Tamminga, C.A., Broussolle, E.P., Ravert, H.T., Wilson, A.A.*, et al.* (1986). Positron emission tomography reveals elevated D2 dopamine receptors in drug-naive schizophrenics. Science *234*, 1558-1563.

Woolrich, M.W., Behrens, T.E., Beckmann, C.F., Jenkinson, M., and Smith, S.M. (2004). Multilevel linear modelling for FMRI group analysis using Bayesian inference. Neuroimage *21*, 1732-1747.

Worsley, K.J., Evans, A.C., Marrett, S., and Neelin, P. (1992). A three-dimensional statistical analysis for CBF activation studies in human brain. J Cereb Blood Flow Metab *12*, 900-918.

Yelnik, J. (2002). Functional anatomy of the basal ganglia. Mov Disord *17 Suppl 3*, S15-21.

Yoo, S.S., Guttmann, C.R., Zhao, L., and Panych, L.P. (1999). Real-time adaptive functional MRI. Neuroimage *10*, 596-606.

Zaghloul, K.A., Blanco, J.A., Weidemann, C.T., McGill, K., Jaggi, J.L., Baltuch, G.H., and Kahana, M.J. (2009). Human substantia nigra neurons encode unexpected financial rewards. Science *323*, 1496-1499.

Zhang, W.-T., Mainero, C., Kumar, A., Wiggins, C.J., Benner, T., Purdon, P.L., Bolar, D.S., Kwong, K.K., and Sorensen, A.G. (2006). Strategies for improving the detection of fMRI activation in trigeminal pathways with cardiac gating. Neuroimage *31*, 1506-1512.